Master of Science Thesis

A Hamiltonian Reduction Method for Nonlinear Dynamics

N.K. Singh

Faculty of Aerospace Engineering · Delft University of Technology

TU Delft Delft University of Technology

A Hamiltonian Reduction Method for Nonlinear Dynamics

Master of Science Thesis

For obtaining the degree of Master of Science in Aerospace Engineering
at Delft University of Technology

N.K. Singh

14th December 2015

Faculty of Aerospace Engineering · Delft University of Technology

Delft University of Technology
Faculty of Aerospace Engineering
Department of Aerospace Structures and Materials

GRADUATION COMMITTEE

Dated: 14th December 2015

Chairman of the committee:

Dr. S.R. Turteltaub

Committee members:

Dr. M.M. Abdalla

Dr. F. Alijani

Dr. ir. E. van Kampen

Acknowledgments

This thesis marks the last milestone in the completion of the M.Sc program at the department of Aerospace Structures and Materials, at the faculty of Aerospace Engineering at Delft University of Technology. The work herein has been conducted over the period from the end of January till November 2015.

My interest for dynamics started during an internship during the summer holiday of 2013, at the end of the B.Sc program. After having followed many courses on composite materials, I decided that I wanted to do something slightly different and recalled that dynamics seemed like an interesting topic. Although knowing that it was going to be challenging, I pursued a thesis with the title: A Hamiltonian Reduction Method for Nonlinear Dynamics.

I would like to thank my supervisor Dr. M.M. Abdalla for his assistance and dedication during the writing of this thesis. I have spent many hours in his office and he was always wanting to help. With his many stories and enthusiasm he managed to motivate me and he ensured me that things would always work out in the end. Furthermore, I would like to thank Dr. S.R. Turteltaub, Dr. F. Alijani and Dr. ir. E. van Kampen for being on my committee. Lastly, I would like to thank my family for having supported me, as well as my friends and girlfriend who cheered me up and heard me out during the more difficult moments.

Delft, University of Technology — N.K. Singh
14th December 2015

Abstract

Nonlinear analysis of dynamic problems has become important for modern industrial design applications. The increasing pressure on airlines to decrease fuel costs demands the design of more efficient aircraft. This requires aircraft manufacturing companies to design lighter structural components. Additionally, certifying agencies set strict requirements on the design of aircraft. The result is the need for more realistic and accurate modelling of critical structural components. Over the years, more powerful finite element discretization methods and improved numerical methods and programming techniques for dynamic analyses of structures have been introduced. Despite these advances and the increase in available computer power, the analysis of nonlinear dynamic problems is yet a computationally demanding task, implying it is very expensive. To reduce the computational time of nonlinear finite element analyses, reduction methods have been developed. These methods have as aim to reduce the number of degrees of freedom, while retaining sufficient accuracy of the solution.

Recently, a new reduction method, applicable to nonlinear static stability problems, has been developed at Delft University of Technology. The aim of this thesis is to extend the reduction method for statics to nonlinear dynamics. This is achieved by using the Hamiltonian formulation to describe the motion of a system. In this formulation, the motion of the system is described by first order ordinary differential equations, known as Hamilton's equation of motion. These can be integrated to yield the momenta and displacements over time. To reduce the number of degrees of freedom, the momentum is assumed to be a multiplication of a basis matrix and an amplitude vector. This is known as the momentum subspace. In this thesis, the basis vectors are chosen to consist of the eigenmodes of the system. The displacements are expanded through a Taylor series up to second order, in the same way as the static reduction method. By deriving Hamilton's principle in the Hamiltonian setting and taking into account the displacement expansion and the assumption for the momentum subspace, the conditions for a canonical transformation are derived. Ensuring the transformation is canonical, a reduced Hamiltonian can be computed. If the transformation is canonical, the resulting system is still a mechanical system and properties such as energy and momentum are conserved. By imposing the conditions that ensure a canonical transformation, orthogonality conditions are obtained that are of the same form as the ones for the static reduction method. The reduction method for dynamics thus reduces to the static one, which implies that the static reduction method is directly applicable to dynamics.

A reduced order model (ROM) is constructed for free vibrations, forced vibrations and damped vibrations, using Hamilton's equations of motion. These are integrated to obtain the response

of the ROM, in terms of displacements and momenta. The displacements and momenta of the full finite element model are computed by back-substituting the reduced response into the displacement expansion and momentum subspace. The ROM is implemented in a finite element framework for both beam and shell elements by making use of the von-Kármán kinematic model.

The reduced order model is applied to a beam, to both an isotropic and composite plate as well as to an isotropic and composite shell. Verification is performed using Abaqus. For beams, excellent agreement is found between Abaqus and the ROM in terms of displacements. The nonlinear analysis required more basis vectors than the linear case, to be in agreement with Abaqus. It is demonstrated that by adding more basis vectors, the solution of the ROM approaches that of Abaqus. Additionally, the internal forces are compared and good agreement is found. A frequency ratio versus amplitude plot is generated using cases from literature and a very good match with the ROM is observed. The response of a simply supported plate shows reasonably good agreement with Abaqus in terms of displacements, whereas peak values of the stress resultants are slightly underestimated by the ROM. A period ratio versus amplitude plot is created using approximate solutions from literature. The ROM shows good agreement with these solutions. Finally, the ROM is applied to shells and is compared to Abaqus in terms of displacements. The agreement is less of quality compared to beams and plates. Attempts have been made to add a relatively large amount of modes to the basis, which showed some improvement of the results. Typically, the first part of the response is in good agreement with Abaqus, however, as time proceeds, the quality of the results lowers. The application of the ROM to shell structures requires more research. The big advantage of the ROM is found when the computational times for beams and plates are compared to that of Abaqus. A drastic reduction in time is observed for the ROM, while still retaining accurate results. The ROM thus saves valuable time.

Table of Contents

Acknowledgments vii

Abstract ix

Nomenclature xix

1 Introduction 1
- 1.1 Background and Motivation . . . 1
- 1.2 Literature Review . . . 2
  - 1.2.1 Modal Superposition Method . . . 3
  - 1.2.2 Ritz-Wilson Method . . . 5
  - 1.2.3 Proper Orthogonal Decomposition . . . 5
  - 1.2.4 Membrane Basis Vectors . . . 6
  - 1.2.5 Perturbation Approach . . . 7
  - 1.2.6 Modal Derivatives Method . . . 12
  - 1.2.7 Koiter-Newton Method . . . 13
- 1.3 Research Objective and Thesis Layout . . . 15

2 Review of the Static Reduction Method 17
- 2.1 Governing equations and asymptotic expansions . . . 18
- 2.2 Derivation of the reduced order model . . . 20
- 2.3 Conclusion . . . 25

3 Lagrangian and Hamiltonian Mechanics and Canonical Transformations 27
- 3.1 Constraints and generalised coordinates . . . 27
- 3.2 D'Alembert's principle . . . 28
- 3.3 Lagrangian mechanics . . . 29
  - 3.3.1 Lagrange's equations . . . 29

3.3.2 Hamilton's Principle . . . 30
3.4 Hamiltonian mechanics . . . 31
3.4.1 The Hamiltonian formulation . . . 31
3.4.2 Hamilton's principle in Hamiltonian setting . . . 32
3.5 Canonical transformations . . . 33
3.6 Conclusion . . . 34

4 Reduction Method for Dynamics 37
4.1 Nonlinear dynamics and momentum subspace . . . 37
4.2 Reduced number of degrees of freedom . . . 39
4.3 Reducing dynamics to statics . . . 40
4.4 Hamiltonian of the reduced order model . . . 40
4.5 The reduced order model for dynamics . . . 41
4.5.1 Free vibrations . . . 42
4.5.2 Forced vibrations . . . 42
4.5.3 Damped vibrations . . . 42
4.5.4 Time integration . . . 43
4.6 Von-Kármán kinematic model . . . 44
4.7 Finite element implementation . . . 45
4.7.1 Beam element . . . 45
4.7.2 Shell element . . . 48
4.8 Conclusion . . . 51

5 Applications of the Reduced Order Model 53
5.1 Beams . . . 53
5.1.1 Comparison to Abaqus . . . 53
5.1.2 Comparison to literature . . . 58
5.2 Plates . . . 58
5.2.1 Comparison to Abaqus . . . 59
5.2.2 Comparison to literature . . . 66
5.3 Shells . . . 67
5.3.1 Comparison to Abaqus . . . 68
5.4 Conclusion . . . 71

6 Conclusion 73

7 Recommendations 75

References 76

References 77

A Derivations 81
A.1 Hamilton's principle . . . 81
A.2 Conditions for a canonical transformation . . . 82

B Finite Element Expressions **85**

B.1 Beam element 85
B.1.1 Shape functions 85
B.1.2 Strain and curvature expressions 85
B.1.3 Derivatives of axial strain 86
B.2 Shell element 86
B.2.1 Geometric coordinates and element area 86
B.2.2 Linear strain-displacement matrix 86
B.2.3 Isoparametric coordinates 87
B.2.4 Shape functions 88
B.2.5 Constant matrices 88

List of Figures

1.1 Aerospace applications . . . 3
1.2 Response curve Koiter-Newton method [1] . . . 14

2.1 Mapping displacement space to force space [1] . . . 18

3.1 Path in configuration space . . . 30

4.1 Vibration of a hinged-hinged beam . . . 38
4.2 Two-node planar beam element [2] . . . 45
4.3 Three-node flat shell element, membrane (left) and bending (right) degrees of freedom [2] . . . 48

5.1 Free undamped response of the hinged-hinged beam . . . 54
5.2 Forced undamped response of the hinged-hinged beam . . . 55
5.3 Forced damped response of the hinged-hinged beam . . . 55
5.4 Influence of the number of modes in basis on response . . . 56
5.5 Axial force of the hinged-hinged beam, forced undamped vibration . . . 57
5.6 Internal moments of the hinged-hinged beam, forced undamped vibration . . . 57
5.7 Influence of the number of modes in basis on the internal moment . . . 58
5.8 Frequency ratio versus amplitude for a hinged-hinged beam . . . 59
5.9 Plate with length, width and mesh structure . . . 59
5.10 First five symmetric modes . . . 60
5.11 Forced undamped vibration of a simply supported plate . . . 61
5.12 Comparison of the stress resultant N_x . . . 62
5.13 Comparison of the stress resultant N_y . . . 62
5.14 Stress resultants for the nonlinear forced undamped response at the center of the plate . . . 63

5.15 Comparison of the moment M_x 64
5.16 Comparison of the moment M_y 64
5.17 Moments for the nonlinear forced undamped response at the center of the plate . 65
5.18 Forced undamped vibration of a simply supported composite plate 66
5.19 Nonlinear dynamic response 67
5.20 Period ratio versus amplitude for a square plate 68
5.21 Shell with length, width and mesh structure 68
5.22 Forced undamped vibration of a simply supported shallow shell 1 mm thick . . . 69
5.23 Forced undamped vibration of a simply supported shallow shell 1 mm thick . . . 70
5.24 Forced undamped vibration of a simply supported shallow shell 4 mm thick . . . 70
5.25 Forced undamped vibration of a simply supported composite shallow shell 71

List of Tables

5.1 Comparison of the noninlinear response of the reduced order model and Abaqus . 56
5.2 Comparison frequency analysis 60
5.3 Computational time and error percentage 61

Nomenclature

Acronyms

MAC	Modal assurance criterion
POD	Proper orthogonal decomposition
POM	Proper orthogonal mode
POV	Proper orthogonal value
ROM	Reduced order model

Symbols

a	Post-buckling coefficient
A	Cross-sectional area
A_r	Cubic stiffness term in the nonlinear stiffness function
A_m	Material matrix
b	Post-buckling coefficient
B_r	Quadratic stiffness term in the nonlinear stiffness function
B	Strain-displacement matrix
C	Constant
C	Four-dimensional tensor
$\bar{\mathsf{C}}$	Reduced four-dimensional tensor
D	Quadratic dissipation function
D_b	Material matrix
E	Young's modulus
f	Force
F	Force
F	Load matrix
h	Thickness
H	Linear functional, Hamiltonian
$\bar{H}$	Reduced Hamiltonian

I	Action
K_t	Tangential stiffness matrix
L	Length, Lagrangian
L_1	Linear functional operator
L_2	Quadratic functional operator
L_{11}	Bilinear functional operator
L	Two-dimensional tensor
$\bar{\mathsf{L}}$	Reduced two-dimensional tensor
m	Mass
M	Linear inertial operator
n	Sampling rate
N	Shape function
p	Generalised momentum, pressure load
P	New generalised momentum
P	Basis matrix
q	Generalised coordinate, displacement
Q	Applied load, new generalised coordinate
Q	Three-dimensional tensor
$\bar{\mathsf{Q}}$	Reduced three-dimensional tensor
t	Time
T	Kinetic energy
$\bar{T}$	Reduced kinetic energy
u	Axial, in-plane degree of freedom
U	Strain energy
v	Cumulative participation, in-plane degree of freedom
V	Potential energy
$\bar{V}$	Reduced potential energy
w	Lateral, out-of-plane degree of freedom
δ	Kronecker delta
ϵ	Strain
θ	Rotational degree of freedom
λ	Scalar multiplier, load parameter, proper orthogonal value
λ_c	Classical buckling load
ν	Poisson's ratio
ρ	Density
τ	Modified time variable
ξ	Damping coefficient, amplitude parameter, generalised displacement
χ	Measure of contribution, curvature
ω	Frequency
ω_0	Natural frequency

ω_1	Natural frequency
$\mathcal{A}$	Area triangular element
$\mathcal{L}$	Linear operator
$\bar{\mathcal{L}}$	Reduced linear operator
$\mathcal{C}$	Cubic operator
$\bar{\mathcal{C}}$	Reduced cubic operator
$\mathcal{Q}$	Quadratic operator
$\bar{\mathcal{Q}}$	Reduced quadratic operator
$\mathbf{C}$	Damping Matrix
$\bar{\mathbf{C}}$	Reduced damping matrix
$\mathbf{e}$	Linear strain
$\mathbf{E}$	Unit basis vector
$\mathbf{f}$	Nodal force vector, internal force vector
$\mathbf{f}_{ex}$	External force vector
$\mathbf{F}$	Force vector
$\mathbf{K}$	Stiffness matrix
$\mathbf{K}_1$	Linear operator of nodal displacements
$\mathbf{K}_2$	Quadratic operator of nodal displacements
$\bar{\mathbf{K}}$	Reduced stiffness matrix
$\mathbf{M}$	Mass matrix
$\bar{\mathbf{M}}$	Reduced mass matrix
$\mathbf{N}$	Stress resultant
$\mathbf{p}$	Proper orthogonal mode, nodal response, momentum vector
$\mathbf{P}$	Force vector
$\mathbf{q}$	Generalised coordinate, applied load, displacement vector
$\mathbf{q}_0$	Displacement vector nominal configuration
$\mathbf{Q}$	Reduced load vector
$\mathbf{r}$	Position vector
$\mathbf{R}$	Correlation matrix
$\mathbf{u}$	Displacement vector
$\mathbf{u}_\alpha$	First order displacement field
$\mathbf{u}_{\alpha\beta}$	Second order displacement field
$\mathbf{u}_{\alpha\beta\gamma}$	Third order displacement field
$\mathbf{v}$	Displacement vector, velocity
$\mathbf{x}$	Displacement vector
$\mathbf{X}$	Ensemble matrix
$\mathbf{Z}$	Vector of generalised coordinates
$\boldsymbol{\gamma}$	Strain
$\boldsymbol{\Gamma}$	Transformation matrix

$\boldsymbol{\varepsilon}$	Strain vector
$\boldsymbol{\theta}$	Nonlinear internal force vector
$\boldsymbol{\lambda}$	Vector of proper orthogonal values
$\boldsymbol{\xi}$	Generalised displacement vector, amplitude vector
$\boldsymbol{\pi}$	Momentum amplitude vector
$\boldsymbol{\sigma}$	Stresses
$\boldsymbol{\phi}$	Normal mode, amplitude vector
$\bar{\boldsymbol{\phi}}$	Reduced force vector
$\boldsymbol{\Phi}$	Modal matrix
$\boldsymbol{\psi}$	Amplitude vector
$\boldsymbol{\omega}$	Vector of eigenfrequencies

Chapter 1

Introduction

1.1 Background and Motivation

In modern industrial design and research applications, the size of finite element models is continuously growing. The need of airlines to decrease fuel costs increases the pressure on aircraft manufacturing companies to design and manufacture more efficient aircraft. This pushes the demand to design lighter structural components. This, together with the strict requirements set by certification agencies, such as the Federal Aviation Administration and its European counter part, the European Aviation Safety Agency, boosts the need of more detailed finite element models and complex analyses. The growing availability of computer power and the maturity of existing finite element packages allows nonlinearity to play a larger role in the design of structural components. These nonlinearities are already taken into account in the early design stages. Key to the early design stages is the need to perform many iterative analyses to see what happens for different load cases. Additionally, the designer may be performing an optimisation for the best design, and also in this case, many analyses are required. However, solving the nonlinear systems in time, generated by a finite element discretisation, remains a computationally demanding task.

From the above description, the need for reduction methods arises. Reduction methods are the techniques to reduce the number of degrees of freedom of a model. They are also known as reduced-basis techniques and condensation methods [3]. The resulting model is called a reduced order model (ROM). In this thesis the terms ROM and reduction methods are used. Over the past, any reduced order model that captured the basic, but essential behaviour of a structure, was a useful tool in structural design. However, in modern design applications all detailed structural behaviour is to be captured by the model, with as aim to eventually obtain the most optimal design. Typically, one model is created for a variety of analyses, such as static analyses, frequency analyses, dynamic analyses or even impact analyses to model bird strikes for example. If the designer requires to perform one of these analyses on a finer mesh, then for the more basic analyses, such as the static analysis, he can either use this same fine mesh or create a coarser mesh. Keeping the fine mesh results in unnecessarily long

computational times, whereas the second option becomes impractical if the designer wishes to go back and forth in doing different types of analyses.

To overcome these issues, reduced order models have been developed in a finite element framework. The aim of these reduced order models is that the flexibility of the finite element method, applied in structural design, is maintained. Additionally, the models capture essential detailed nonlinear structural behaviour at a reduced computational cost compared to the commercial finite element packages. The most profound examples of reduced order models have recently been developed at Delft University of Technology and can be found in [2, 4]. The work in these references is based on perturbation methods. Key to these methods it that the solution to be found is expanded in a Taylor series. Upon substituting the approximate solution in the governing equations, linear systems of equations are obtained, which yields different terms in the expansion of the solution. The work presented in [4] is focused on nonlinear static stability problems, whereas the work in [2] is aimed both at nonlinear static stability problems as well as at nonlinear structural dynamics problems. These works form the basis of the Hamiltonian reduction method for nonlinear dynamics, that is developed in the present thesis.

The reduced order model, in this thesis, is applied to beams, plates and shells. These structural components directly find their way back in aerospace applications. In the aviation industry, beams are used to conveniently model wings [5, 6], whereas plates and shells are used to model thin-walled structures such as wing panels, floor panels or fuselage sections [7]. In space applications, they can be used to model structural components of launchers or even satellite panels. Some examples are given in Figure 1.1. These structural components do not limit themselves to aerospace applications and they are found in various fields such as in the automotive industry, civil engineering, biomedical engineering, etc. Typical aerospace applications of the ROM are for example, acoustic responses of rocket launchers, responses of aircraft wings to gust loads and impact loads during landings, or the response of structures to vibrations of jet and propeller engines. The ROM allows one to quickly analyse different load cases in these types of structural problems, and thus costly time can be saved.

In the next section of this chapter a review of literature is given, after which the research objective and the set-up of the content of the thesis is presented.

1.2 Literature Review

The aim of reduction methods is to condensate a large system into a much smaller one. In this way the computational time can be drastically reduced, while still retaining an accurate solution of a system. In structural analysis, reduction methods typically consist of a two-step discretization. The first step is to discretize the system through finite elements. The second step is to compute basis vectors such that a Ralyleigh-Ritz analysis can be performed [8].

The basic idea of reduction methods is as follows. The generalised coordinates $\mathbf{Z}$, of a system can be described by a large number of degrees of freedom, n. This response can be approximated by a linear combination of basis vectors. In dynamics these basis vectors typically consist of modes of vibrations. The problem can be reformulated in terms of a selected number of discrete variables $\boldsymbol{\psi}$, representing amplitudes. This is done through the transformation as given in Equation 1.1 [3].

(a) Wing upper surface of Airbus A350

(b) Fuselage section of Boeing 787

(c) Artist impression of Ariane 6

(d) Artist impression of MeteoSat-8

Figure 1.1: Aerospace applications

$$\mathbf{Z}_{n,1} = \mathbf{\Gamma}_{n,r}\boldsymbol{\psi}_{r,1} \qquad r \ll n \tag{1.1}$$

In this equation $\mathbf{\Gamma}$ is the transformation matrix, whose columns constitute the basis vectors. This transformation allows one to obtain an accurate response of the system, while the selected number of basis vectors is much smaller than the number of degrees of freedom.

Different reduction methods are available and their difference lays in the selection of these basis vectors. An overview of the methods is given in this section.

1.2.1 Modal Superposition Method

A reduction method traditionally used in linear structural dynamics problems is the mode superposition method. The dynamic equations of motion can be written in matrix format as given in Equation 1.2.

$$\mathbf{M}\ddot{\mathbf{u}} + \mathbf{C}\dot{\mathbf{u}} + \mathbf{K}\mathbf{u} = \mathbf{P}(t) \tag{1.2}$$

This equation can be solved by direct integration or by mode superposition. The idea of the mode superposition method is to reduce the original system of equations by a smaller one through a transformation of the form given by Equation 1.3 [9].

$$\mathbf{u} = \mathbf{\Phi}\mathbf{q} \tag{1.3}$$

in which $\mathbf{\Phi}$ is the modal matrix.

The modal matrix has N columns, containing the mode shapes (eigenvectors) that satisfy the eigenvalue problem given in Equation 1.4. The number of rows of the modal matrix corresponds to the number of generalised coordinates.

$$\mathbf{K\Phi} = \mathbf{M\Phi}\boldsymbol{\omega}^2 \tag{1.4}$$

A transformed equation of motion is obtained:

$$\bar{\mathbf{M}}\ddot{\mathbf{q}} + \bar{\mathbf{C}}\dot{\mathbf{q}} + \bar{\mathbf{K}}\mathbf{q} = \mathbf{Q} \tag{1.5}$$

in which:

$$\bar{\mathbf{M}} = \mathbf{\Phi}^T\mathbf{M\Phi} \qquad \bar{\mathbf{C}} = \mathbf{\Phi}^T\mathbf{C\Phi} \qquad \bar{\mathbf{K}} = \mathbf{\Phi}^T\mathbf{K\Phi} \qquad \mathbf{Q} = \mathbf{\Phi}^T\mathbf{P}(t) \tag{1.6}$$

If proportional damping is used and the modes are normalised with the mass matrix, such that $\mathbf{\Phi}^T\mathbf{M\Phi} = 1$, the original system of equations are transformed to a set of uncoupled equations in the form of Equation 1.7 [10, 11].

$$\ddot{q}_i(t) + 2\xi_i\omega_i\dot{q}_i(t) + \omega_i^2 q_i(t) = Q_i(t) \tag{1.7}$$

The mode superposition method is characterised by selecting the eigenvectors corresponding to the lowest frequency natural modes, such that the number of columns in the modal matrix is much less than the number of rows. Two versions of the method exist. The first being the mode displacement method in which the displacements are computed from modal ones, by solving the first equations of Equation 1.7 and substituting this into Equation 1.3. For a small number of degrees of freedom, sufficient accuracy is obtained through this method. For the determination of internal forces and stresses this method has a deficiency, since they depend on modes with a higher frequency. This is overcome by introducing the mode acceleration method in which effects of truncated modes are considered by static effects only [12]. This comes down to applying a correction factor obtained from a static solution of the non-reduced system.

The mode superposition method has also been applied in nonlinear dynamics in [9] where an incremental-iterative approach is used. The basic difference between a linear and a nonlinear dynamic analysis is that in the nonlinear case the $\bar{\mathbf{K}}$ matrix is not diagonal, thus the non-linearities are included in the stiffness matrix. In this method, the mode shapes and natural frequencies are required to be computed before the response analysis. For larger problems this results in a high computational cost.

In [13] a method is developed based on the modal superposition method. Here the nonlinearities are restricted to a small part of the structure and are included in a pseudo-force vector, which is approximated by a Taylor series. The basis vectors are only computed once and the stiffness is kept constant, resulting in an increase in computational efficiency. The downside of this method is that it can only be applied to structures with local nonlinearities.

1.2.2 Ritz-Wilson Method

Another reduction method typically employed in linear structural dynamics analyses is the Ritz-Wilson method, first introduced in [14]. This method consists of generating Ritz vectors in which the static response to the load is selected as the starting vector. This is followed by an inverse iteration scheme and an orthogonalisation strategy, from which the Ritz vectors are obtained. The Ritz vectors are combinations of the vibration modes excited by the significant part of the harmonic components of the loading. From these vectors the set of coupled equations can be formed as given by Equation 1.5. This method is similar to the mode superposition method, but has the advantage that the computational cost of generating Ritz vectors is smaller than that of generating modes of vibration. Additionally, the mode superposition method does not take into account the information from the loading and thus transformation vectors are generated which do not participate to the response, whereas the Ritz-Wilson method does. Lastly, the Ritz-Wilson method already includes the static correction as discussed for the mode superposition method, since the last vectors of the Ritz basis have higher frequencies than those corresponding to a basis of eigenvectors [15]. In [15] the Ritz-Wilson method has been extended to nonlinear structural dynamics problems by using an incremental-iterative approach. An adaptive integration method is used to avoid the frequent re-evaluations of the transformation matrix (which is a downside of the mode superposition method), which ensures re-evaluations are merely triggered when strictly necessary. Furthermore, this method automatically adjusts the time-step during the analysis.

1.2.3 Proper Orthogonal Decomposition

A method that finds its origin in statistical analysis is the Proper Orthogonal Decomposition (POD) method, also known as Karhunen-Loéve expansion. POD requires information on the nonlinear dynamic response of the system. This may consist either of a displacement, a velocity or an acceleration response field [16]. This information may either follow from tests or from a nonlinear finite element analysis. The POD basis is constructed by taking snapshots of this nonlinear dynamic response at a specified sampling rate, n. In case displacement data of the system is present, one has $\mathbf{x}_i = (x_i(t_1), x_i(t_2), \ldots, x_i(t_n))^T$, for $i = 1, \ldots, N$. The displacement histories are used to create an $n \times N$ ensemble matrix, $\mathbf{X} = [\mathbf{x}_1, \mathbf{x}_2, \ldots, \mathbf{x}_N]$. An $N \times N$ correlation matrix is constructed through Equation 1.8 [17, 18].

$$\mathbf{R} = \frac{1}{n}\mathbf{X}^T\mathbf{X} \tag{1.8}$$

The correlation matrix is real and symmetric, implying that its eigenvectors form an orthogonal basis. These eigenvectors, $\mathbf{p}$, are the so-called proper orthogonal modes (POM), whereas the corresponding eigenvalues $\boldsymbol{\lambda}$ are known as the proper orthogonal values (POV).

As described in [19], a measure of the contribution of each POM to the overall dynamic response is given by Equation 1.9.

$$\chi_i = \frac{\lambda_i}{\sum_{j=1}^{M} \lambda_j} \quad i = 1, \ldots, N \tag{1.9}$$

The M modes that contribute the most are selected and a cumulative participation, υ, is calculated through Equation 1.10, in which the sum of all modes is equal to one.

$$\upsilon = \sum_{i=1}^{M} \chi_i \quad 0 < \upsilon \leq 1 \tag{1.10}$$

This reduces the matrix containing the POMs to $m \times M$. The POMs change as the loading condition is changed. For this reason the POMs are not preferred as the modal basis, since for each loading condition a new modal basis must be constructed. To overcome this, a set of normal modes, representing the POMs, is found. One way of doing is by means of the Modal Assurance Criterion (MAC), which is defined through Equation 1.11 [19].

$$MAC(\mathbf{p}_k, \phi_l) = \frac{|\mathbf{p}_k^T \boldsymbol{\phi}_l|^2}{(\mathbf{p}_k^T \mathbf{p}_k)(\boldsymbol{\phi}_l^T \boldsymbol{\phi}_l)} \quad k = 1, \ldots, M, l = 1, \ldots, N \tag{1.11}$$

This criterion allows one to match the POMs with the normal modes, ϕ . The normal modes that resemble the POMs the closest are what forms the modal basis and these are then projected on the equations of motion.

This method is easily implemented. An application of it to a wind turbine is found in [20] and applications to trusses and frames are found in [21]. The downside of this method, however, is that it requires the solution from a full finite element analysis to obtain the snapshots.

1.2.4 Membrane Basis Vectors

When a structure undergoes large out-of-plane (bending) displacements, in-plane (membrane) displacements result. In [22] five different methods are compared for selecting membrane basis vectors. The difference lays in how the stretching is modelled. They start from the discretized equations of motion in functional form given by Equation 1.12.

$$\mathbf{M}\ddot{\mathbf{x}} + [\mathbf{K} + \mathbf{K1}(\mathbf{x}) + \mathbf{K2}(\mathbf{x}, \mathbf{x})]\,\mathbf{x} = \mathbf{f}(t) \tag{1.12}$$

After transforming the displacements to modal space, the following reduced order equation of motion is obtained.

$$\ddot{\mathbf{p}} + \bar{\mathbf{C}}\dot{\mathbf{p}} + \bar{\mathbf{K}}\mathbf{p} + \boldsymbol{\theta}(p_1,\ p_2,\ \ldots\ ,\ p_n) = \boldsymbol{\Phi}^T \mathbf{f} \tag{1.13}$$

in which $\boldsymbol{\theta}$ is the nonlinear function for the rth equation given by Equation 1.14.

$$\boldsymbol{\theta}_r = \sum_{i=1}^{n}\sum_{j=1}^{n} B_r(i,j) p_i p_j + \sum_{i=1}^{n}\sum_{j=1}^{n}\sum_{k=j}^{n} A_r(i,j,k) p_i p_j p_k \tag{1.14}$$

in which the terms B_r and A_r represent quadratic and cubic modal stiffness, respectively.

The first method is called the bending modes method in which stretching is ignored. This method is the easiest to implement, however, in this method the nonlinear (cubic) terms become too large. For this reason the model is too stiff and gives less accurate results.

The second method is the companion modes method. In this method a companion mode for each bending mode is created using a solution from a nonlinear static finite element analysis. This is done by finding a linear force due to an enforced displacement for a chosen bending mode. Applying this force to a finite element model gives a nonlinear deflected shape that contains bending and membrane displacements. Using the Gram-Schmidt process the bending mode's projection on the nonlinear deflected shape is removed, yielding the companion mode. Although this method is an improvement over the bending modes method, it gives inaccurate results in multi-mode problems.

The following three methods give similar results, although stretching is modelled differently among them. First, the physical condensation method includes membrane stretching by using static condensation of the physical membrane degree of freedom into the bending degree of freedom. This method requires one to have the nonlinear stiffness matrices making this a non-practical design tool.

The bending and membranes modes method is based on including normal membrane modes in the basis. For simpler structures such as beams and planar structures such modes can be identified easily. Usage of this method becomes difficult for complicated structures, since it is then impossible to identify which and how many modes to include.

The last method is the implicit condensation method in which membrane modes are not directly included in the nonlinear model. In this method the nonlinear function is restricted to merely the cubic terms and only bending modes are considered. However, membrane stretching is included upon estimating the nonlinear coefficients through the usage of a nonlinear static finite element analysis, such that the stretching effects are included in the model indirectly.

As is concluded in [22], the implicit condensation method is the most accurate and easiest to implement. Yet a downside remains that one requires access to a finite element analysis to obtain the nonlinear static solution to selected load cases.

1.2.5 Perturbation Approach

Recently, a different reduction method based on the so-called perturbation approach has been developed at TU Delft. This approach is based on the theory of initial postbuckling behaviour developed in [23]. The methods described herein result in compact description of a structure after buckling. Reduction methods based on this approach rely on enriching a set of vibration modes with second order modes as is explained in this section.

Buckling

The work on postbuckling behaviour done in [23] by Koiter, was re-derived based on the principle of virtual work in [24]. Starting for the case of static buckling, the principal of virtual work is given by Equation 1.15.

$$\boldsymbol{\sigma} \cdot \delta\boldsymbol{\varepsilon} = \mathbf{q} \cdot \delta\mathbf{u} \tag{1.15}$$

It allows one to obtain the behaviour of the structure during prebuckling, buckling and postbuckling. In this method the displacement field of the structure is expanded in a Taylor series, which for postbuckling is given by Equation 1.16. This expansion is done around a specific configuration, which usually is the bifurcation point. The stress and strain fields are expanded in the same way. To determine prebuckling behaviour only the first term on the right-hand-side is used, whereas for detection of buckling the first and second term on the right-hand-side are used.

$$\mathbf{u} = \lambda\mathbf{u}_0 + \xi\mathbf{u}_1 + \xi^2\mathbf{u}_2 + \xi^3\mathbf{u}_3 + \dots \tag{1.16}$$

The expansion results in a load-displacement curve with post-buckling coefficients that define the stability properties of the structure. These coefficients are the a and b terms in Equation 1.17.

$$\frac{\lambda}{\lambda_c} = 1 + a\xi + b\xi^2 \tag{1.17}$$

The above procedure gives an asymptotic description of the secondary path branching from a critical point and holds for perfect structures. In a similar procedure the buckling behaviour for an imperfection sensitive structure can be obtained. This is done by modifying the strain-displacement relation by incorporating an additional displacement $\bar{\mathbf{u}}$.

The procedure so far concerns only a single buckling mode of a structure. Buckling modes can be clustered. In [25], the interaction of buckling modes in an axially stiffened cylindrical shell is investigated. They expanded the displacement field for a perfect structure in the form given by Equation 1.18.

$$\mathbf{u} = \lambda_0\mathbf{u}_0 + \xi_i\mathbf{u}_i + \xi_i\xi_j\mathbf{u}_{ij} + \dots \tag{1.18}$$

in which $\mathbf{u}_{ij}$ are the second order displacements fields. These take into account the interaction of the buckling modes $\mathbf{u}_i$ and $\mathbf{u}_j$. The indices run from 1 to M and only the buckling modes that are important to the response are retained. Furthermore, they show that for a slightly imperfect structure, the maximum value of the load factor λ is determined through the solution of M nonlinear equations of the form given by Equation 1.19.

$$\xi_I\left(1 - \frac{\lambda}{\lambda_I}\right)\xi_i + \xi_j + a_{ajI} + \xi_i\xi_j\xi_k b_{ijkI} = \frac{\lambda}{\lambda_I}\bar{\xi}_I \tag{1.19}$$

in which the coefficients a and b are postbuckling coefficients.

In [24], the perturbation approach of static buckling is extended to dynamic buckling, by including inertial forces and assuming the variational form given by Equation 1.20.

$$\boldsymbol{\sigma} \cdot \delta\boldsymbol{\varepsilon} = \mathbf{q} \cdot \delta\mathbf{u} - \mathbf{M}(\ddot{\mathbf{u}}) \cdot \delta\mathbf{u} \tag{1.20}$$

A solution to this equation is assumed, of the form given by Equation 1.21 for a quadratic structure and cubic structure.

$$\mathbf{u} = \lambda f(t)\mathbf{u}_0 + \xi(t)\mathbf{u}_1 \tag{1.21a}$$

$$\mathbf{u} = \lambda f(t)\mathbf{u}_0 + \xi(t)\mathbf{u}_1 + \xi^2(t)\mathbf{u}_2 \tag{1.21b}$$

By applying a Galerkin solution he obtained Equation 1.22 for a quadratic and cubic structure.

$$\left(\frac{1}{\omega_1^2}\right)\ddot{\xi} + \left[1 - \frac{\lambda f(t)}{\lambda_c}\right]\xi + a\xi^2 = \left[\frac{\lambda f(t)}{\lambda_c}\right]\bar{\xi} \tag{1.22a}$$

$$\left(\frac{1}{\omega_1^2}\right)\ddot{\xi} + \left[1 - \frac{\lambda f(t)}{\lambda_c}\right]\xi + b\xi^3 = \left[\frac{\lambda f(t)}{\lambda_c}\right]\bar{\xi} \tag{1.22b}$$

These equations can be integrated in time as to obtain the dynamic behaviour of a system. ω_1^2 is defined through Equation 1.23.

$$\omega_1^2 = \frac{\mathbf{M}(\mathbf{u}_1)\cdot\mathbf{u}_1}{\boldsymbol{\sigma_1}\cdot\mathbf{e}_1} \tag{1.23}$$

In this equation, if $\mathbf{u}_1$ turns out to be a natural vibration mode, then its natural frequency is ω_1. In other cases the equation is seen as a Rayleigh quotient based on the buckling mode $\mathbf{u}_1$. Finally, it is concluded in [24] that results found from Equation 1.22 can only be considered as generalised estimates. This is due to the assumptions made in the derivations, with the biggest assumption being the fact that the dynamic response is described in terms of the deformation pattern resulting during static buckling. For cases with multiple buckling modes this limits the validity of the results.

Nonlinear Vibrations

The perturbation approach applied to buckling problems was extended by [26] to nonlinear free vibrations of elastic structures in an analytical framework. In this work the dynamics of a system are derived through the use of Hamilton's principle given by Equation 1.24.

$$\int_0^{2\pi/\omega}\left[\delta\left(\frac{1}{2}M\left(\frac{\partial\mathbf{u}}{\partial t}\right)\cdot\frac{\partial\mathbf{u}}{\partial t}\right) - \boldsymbol{\sigma}\cdot\delta\boldsymbol{\gamma}\right]dt = 0 \tag{1.24}$$

Only periodic motions are considered. After a change of time variable and applying integration by parts they obtain Equation 1.25.

$$\int_0^{2\pi/\omega}\left[\omega_0^2 M(\ddot{\mathbf{u}})\cdot\delta\mathbf{u} + \boldsymbol{\sigma}\cdot\delta\boldsymbol{\gamma}\right]d\tau = 0 \tag{1.25}$$

By applying linearised theory the vibration modes and frequencies are obtained. For this the relations given by Equation 1.26 are used:

$$\mathbf{u} = \xi \mathbf{u}_1 \quad \boldsymbol{\gamma} = \xi \mathbf{e}_1 \quad \boldsymbol{\sigma} = \xi \boldsymbol{\sigma}_1 \tag{1.26}$$

in which ξ is an amplitude parameter associated with the vibration mode $\mathbf{u}_1$. Using the above two relations the following integral is obtained. When this integrand is equated to zero, the following linearised equation of motion is obtained:

$$\int_0^{2\pi} \left[\omega_0^2 M(\ddot{\mathbf{u}}_1) \cdot \delta \mathbf{u} + \boldsymbol{\sigma}_1 \cdot \delta \mathbf{e} \right] d\tau = 0 \tag{1.27}$$

which can be solved for ω_0^2, which is the natural frequency squared. To find how a structure behaves for finite amplitudes, they assume the following fields:

$$\mathbf{u} = \xi \mathbf{u}_1 + \xi^2 \mathbf{u}_2 \tag{1.28a}$$

$$\boldsymbol{\gamma} = \xi \mathbf{e}_1 + \xi^2 (\mathbf{e}_2 + \frac{1}{2} L_2(\mathbf{u}_1)) + ... \tag{1.28b}$$

$$\boldsymbol{\sigma} = \xi \boldsymbol{\sigma}_1 + \xi^2 \boldsymbol{\sigma}_2 \tag{1.28c}$$

From which they find the asymptotic relation given by Equation 1.29. This equation gives the effect of the amplitude of vibration on the frequency. Note that it has a similar format as Equation 1.17, for postbuckling behaviour.

$$\frac{\omega^2}{\omega_0^2} = 1 + A\xi + B\xi^2 + ... \tag{1.29}$$

The coefficients A and B define the characteristics of the structure. Depending on their value this can imply for instance decreasing or increasing frequency.

The work from [26] does not include the effect of initial imperfections and external loading. In [27], the influence of geometrical imperfection on the vibration frequency of a structure at a given conservative load is discussed. In this work the theory is restricted to imperfections that are of the same shape as the vibration mode, since they expect this to be the most interesting case. The deformations are said to consist of a static part with a specific mode shape and amplitude, and a part that harmonically varies with time. Using a perturbation expansion a static state and a vibrating state are found from which the expressions of vibration frequencies for symmetric and nonsymmetric structures are derived. They do this by first determining the non-buckled state of equilibrium of the perfect structure, then the vibration mode and frequency is found. The influence of small imperfections on the static mode amplitude is determined and lastly, the vibration frequency of the imperfect structure is found.

The theories of [26] and [27] are combined in [28]. In this latter work the extension of the theory to forced vibrations, higher order analysis and multi-mode analysis is shown.

Reduction Method

The analytical method from [26] and [27] is generalised to a finite element context in [2, 29]. Second order modes stemming from the perturbation approach are included in the reduction

of a nonlinear dynamical system of equations. These systems of equations follow from a finite element discretisation. In this work the vibration modes are found by starting from the variational form given by Equation 1.20. A periodic motion is assumed and the time variable $\tau = \omega t$ is introduced, and the variational equation of motion can be integrated to give Equation 1.30.

$$\int_0^{2\pi} \left[\boldsymbol{\sigma} \cdot \delta\boldsymbol{\varepsilon} + \mathbf{M}(\ddot{\mathbf{u}}) \cdot \delta\mathbf{u} - \lambda \mathbf{q}_0 \cdot \delta\mathbf{u}\right] d\tau = 0 \tag{1.30}$$

To obtain the modes of vibration, the following fields are assumed:

$$\mathbf{u} = \lambda \mathbf{u}_0 + \xi \mathbf{u}_1 \tag{1.31a}$$
$$\boldsymbol{\varepsilon} = \lambda \boldsymbol{\varepsilon}_0 + \xi \boldsymbol{\varepsilon}_1 \tag{1.31b}$$
$$\boldsymbol{\sigma} = \lambda \boldsymbol{\sigma}_0 + \xi \boldsymbol{\sigma}_1 \tag{1.31c}$$

which when combined with the integrated equation of motion leads to the eigenvalue problem given by Equation 1.32.

$$\int_0^{2\pi} \left[-\omega_0^2 \mathbf{M}(\ddot{\mathbf{u}}_1) \cdot \delta\mathbf{u} + \lambda \boldsymbol{\sigma}_0 \cdot L_{11}(\mathbf{u}_1, \delta\mathbf{u}) + \boldsymbol{\sigma}_1 \cdot \mathbf{e}\right] d\tau = 0 \tag{1.32}$$

The natural frequency is then obtained, by letting $\delta\mathbf{u} = \mathbf{u}_1$, through Equation 1.33.

$$\omega_0^2 = \frac{\int_0^{2\pi} \left[\lambda \boldsymbol{\sigma}_0 \cdot L_2(\mathbf{u}_1) + \sigma_1 \cdot \mathbf{e}_1\right] d\tau}{\int_0^{2\pi} \mathbf{M}_0(\dot{\mathbf{u}}_1) \cdot \dot{\mathbf{u}}_1 d\tau} \tag{1.33}$$

The vibration modes due to finite deflection amplitudes are obtained by assuming fields of the form given by Equation 1.16 and substituting this into Equation 1.29. After orthogonalising higher order fields the second order field $\mathbf{u}_2$ is found from the solution of the linear problem given by Equation 1.34.

$$-\omega^2 \mathbf{M}(\ddot{\mathbf{u}}_2) \cdot \delta\mathbf{u} + \boldsymbol{\sigma}_2 \cdot \delta\mathbf{e} + \lambda \boldsymbol{\sigma}_0 \cdot L_{11}(\mathbf{u}_2, \delta\mathbf{u}) + \boldsymbol{\sigma}_1 \cdot L_{11}(\mathbf{u}_1, \delta\mathbf{u}) = 0 \tag{1.34}$$

When vibration frequencies are closely spaced the above procedure can be modified to consider the interaction between modes. For this, the displacement is expanded in the form as was given by Equation 1.18, which initially was used for interaction of buckling modes [25]. The second order fields are then found from solving the linear problem given by Equation 1.35.

$$-\omega^2 \mathbf{M}(\ddot{\mathbf{u}}_{ij}) \cdot \lambda\sigma_0 \cdot L_{11}(\mathbf{u}_{ij}, \delta\mathbf{u}) + \sigma_{ij} \cdot \delta\mathbf{e} = -\frac{1}{2}\left[\sigma_i \cdot L_{11}(\mathbf{u}_j, \delta\mathbf{u}) + \sigma_j \cdot L_{11}(\mathbf{u}_i, \delta\mathbf{u})\right] = 0 \tag{1.35}$$

The above equations are implemented in a finite element format. The reduction basis is then formed by following the procedure in [2], giving the reduced basis.

First a few vibration modes are extracted. From this an optimal basis of vibration modes is selected that gives sufficient accuracy for a linear dynamic problem. The basis of second order fields corresponding to the selected vibration modes is extracted. The vibration modes and the second order fields together form the reduced basis, given by Equation 1.36, which can then be projected on the full system of equations.

$$\mathbf{\Phi} = [\mathbf{u}_1 \ \mathbf{u}_2] \tag{1.36}$$

Applications of the procedure to planar beam problems are shown in [29]. It is demonstrated how the enrichment of the basis with second order modes results in accurate results compared to a full finite element analysis, whereas the use of merely vibration modes does not yield any good solution at all. Additionally, it is shown that for an imperfection sensitive structure it is required to have vibration modes as well as buckling modes in the basis to obtain accurate results. The method is successfully applied to plates in [30]. In this work, it is shown how for more complicated geometries the inclusion of interaction modes becomes important to obtain accurate responses. Furthermore, for a cantilever beam it is demonstrated that inclusion of modes in the basis at two different equilibrium configurations yields good results.

Although this method has been demonstrated to yield accurate results when second order fields are included, it still becomes computationally expensive for larger systems with a large number of degrees of freedom. If for a system, n modes are included in the basis, then $n(n+1)/2$ second order modes are to be included as well, to give accurate results. As n increases, the number of second order modes drastically increases and the number of second order modes pre-dominates the number of first order modes, as seen from the equation. This increases the computational cost.

1.2.6 Modal Derivatives Method

The use of path derivatives in the reduced basis has been employed in [31] in a computational algorithm. In this work the nonlinear static response of structures is predicted by employing a Rayleigh-Ritz technique to replace the governing finite element equations. Four criteria have been proposed that the basis vectors must adhere to [3, 31].

1. They must be linearly independent and complete;
2. They must have a low computational costs to generate;
3. They must yield an accurate solution when used (meaning they characterise the non-linear response), and,
4. It must be easy to obtain the system response characteristics using the basis vectors.

The basis vectors used in [31] are a nonlinear solution of the nodal displacement and path derivatives. A path derivative is a derivative of the unknown vector of nodal displacements with respect to a loading or displacement parameter. This choice of basis vectors follows from a perturbation analysis in which a power series is used to express the displacement field [32].

To limit the number of path derivatives used in the basis the fact is used that as the order of the path derivative increases, they become less linearly independent and they contribute less to the response.

Based on the selection of basis vectors proposed above, an extension to a reduction method in nonlinear structural dynamics, named the modal derivatives method, is given in [8]. In this method a basis is selected that contains the actual modes with additionally, modal derivatives. By adding these modal derivatives, more information on the nonlinear solution path is obtained and the number of basis updates is reduced. In this work it is demonstrated that the inclusion of modal derivatives yields accurate results and that for most structures the basis must be updated periodically to comply with the local behaviour of the system.

1.2.7 Koiter-Newton Method

In line with perturbation methods, recently a new method called the Koiter-Newton approach is introduced in [1,4], which improves the efficiency of nonlinear static finite element analysis of buckling sensitive structures. A downside of the reduction method based on the perturbation approach given in Section 1.2.5 is that is it only valid in a small range near the bifurcation point. There is no link between the original finite element model and the reduced order model. As a result of this the range of validity of this approach requires checking by comparing it to a full finite element analysis, which imposes limits on this method. The proposed Koiter-Newton approach overcomes this limitation. It combines Koiter's analysis [23] as a predictor and Newton arc-length method as a corrector. The difference lies in that Koiter's asymptotic expansion is used from the beginning and not just once at the bifurcation point.

In this method the reduced order model is constructed such that the equilibrium equations in the neighbourhood of a known equilibrium state can be estimated. They start from the fact that a discretized set of equilibrium equations can be reduced to a set of nonlinear equations of the form given by Equation 1.37.

$$\mathbf{f}(\mathbf{q}) = \lambda \mathbf{f}_{ext} \tag{1.37}$$

This equation can be seen as a mapping from the displacement space to the force space. A force subspace is defined through Equation 1.38.

$$\mathbf{f} = \mathsf{F}\boldsymbol{\phi} \tag{1.38}$$

in which F is the load matrix containing a set of force vectors of which the first one is the external load. The other force vectors are perturbation loads. The coordinates $\boldsymbol{\phi}$ represent the amplitudes of the forces. Finally, the reduced order model is the relation between $\boldsymbol{\phi}$ and $\boldsymbol{\xi}$. To simplify the discretized equations they are expanded with respect to $\mathbf{u}$ and by considering the force subspace, the equations of equilibrium are given by Equation 1.39.

$$\mathcal{L}(\mathbf{u}) + \mathcal{Q}(\mathbf{u}, \mathbf{u}) + \mathcal{C}(\mathbf{u}, \mathbf{u}, \mathbf{u}) = \mathsf{F}\boldsymbol{\phi} \tag{1.39}$$

To find a solution for $\mathbf{u}$, the equilibrium displacement is expanded using a Taylor series of third order, given by Equation 1.40.

$$\mathbf{u} = \mathbf{u}_\alpha \xi_\alpha + \mathbf{u}_{\alpha\beta} \xi_\alpha \xi_\beta + \mathbf{u}_{\alpha\beta\gamma} \xi_\alpha \xi_\beta \xi_\gamma \tag{1.40}$$

Furthermore the load amplitudes are expanded as Equation 1.41. This represents the reduced order model.

$$\phi = \bar{\mathcal{L}}(\boldsymbol{\xi}) + \bar{\mathcal{Q}}(\boldsymbol{\xi}, \boldsymbol{\xi}) + \bar{\mathcal{C}}(\boldsymbol{\xi}, \boldsymbol{\xi}, \boldsymbol{\xi}) \tag{1.41}$$

After substituting the previous two equations in Equation 1.39 and manipulations, two linear systems of the finite element method are obtained, which yield the first and second order displacement fields. Additionally, expressions for the reduced tensors $\bar{\mathsf{L}}$, $\bar{\mathsf{Q}}$ and $\bar{\mathsf{C}}$ are obtained.

The reduced order model is then solved using a path following technique. The proposed method has a larger range of validity, however, there is still a limitation in the range of validity. To this extent the analysis of the range of validity is automated. Using a full finite element model the exact unbalanced force is computed after each solution step. The norm of this residual is then used to determine whether the reduced order model is accurate enough, based on a chosen tolerance. The procedure comes down to constructing a reduced order model based on a Koiter's expansion. To this reduced order model a path following technique is applied giving the estimated response of the full model. This is referred to as a predictor step. After the reduced order model is no longer valid it is corrected to restore equilibrium using a Newton-based arc-length method. The point on the load-displacement curve where the equilibrium is restored is used as the new expansion point. This is graphically shown in Figure 1.2.

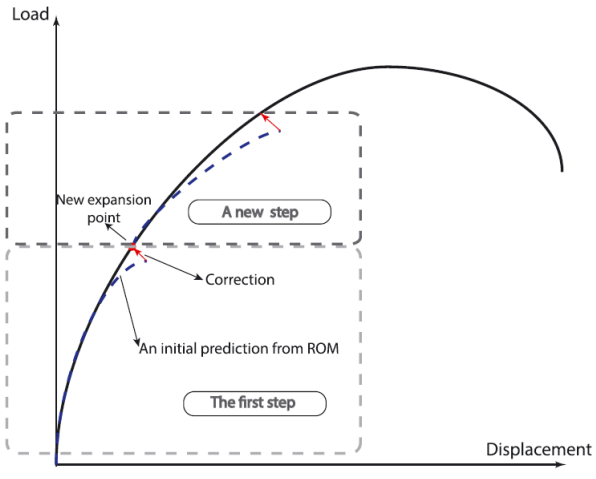

Figure 1.2: Response curve Koiter-Newton method [1]

The procedure has been successfully applied to planar beam problems as well as shell problems. A drastic reduction in the number of linear equations to be solved is observed when comparing the Koiter-Newton method to a full finite element analysis.

1.3 Research Objective and Thesis Layout

The research objective of this thesis is to extend the reduction method, successfully applied to nonlinear static stability problems, presented in [1], to nonlinear dynamics. More specifically, a method is sought that reduces the dynamics to statics, such that the reduced order model for nonlinear static stability problems is directly applicable to nonlinear dynamics. To achieve this, a separate assumption is made for the displacement and the momentum of the system. The assumption consists of assuming that the motion of the system can be described by a linear momentum subspace. The displacement is expanded through a Taylor series expansion of second order. Physically, the nonlinearity of the problem can be explained by considering a hinged-hinged beam that is vibrating with a finite amplitude. The large lateral motion forces the beam to stretch in its longitudinal direction to comply with force equilibrium.

The fact that a separate assumption is made for the displacement and momentum, allows the use of Hamiltonian mechanics. In this formulation the displacement and momentum are treated as independent variables. The dynamics of the problem can thus be conveniently described using this formulation.

The set-up of this thesis is as follows. In Chapter 2, the elements that are needed from the reduction method, applicable to nonlinear static stability problems, are reviewed. The theory of Lagrangian and Hamiltonian mechanics and canonical transformations is introduced in Chapter 3. The Hamiltonian reduction method for nonlinear dynamics is given in Chapter 4, using the theory from the preceding two chapters. In this same chapter the finite element framework is introduced. Examples of applications of the reduced order model are given in Chapter 5. Lastly, the conclusion and recommendations are given in Chapter 6 and Chapter 7, respectively.

Chapter 2

Review of the Static Reduction Method

The Hamiltonian reduction method for nonlinear dynamics, developed in this thesis, is an extension of the static reduction method given in [4]. Therefore, this chapter reviews the parts of the static reduction method that are needed for the extension to dynamics. The static reduction method is referred to as the Koiter-Newton approach. The aim of this method was to find a new analytical approach to nonlinear structural problems in the presence of buckling. Different reduction methods based on Koiter's initial postbuckling theory already exist. These methods model the case of buckling well, however, they have disadvantages. They are not suited to dealing with limit point type buckling. Furthermore, it is difficult to take into account prebuckling nonlinearity using these methods. In the traditional Koiter's postbuckling theory, Koiter's aymptotic expansion is carried out once at the bifurcation point. This limits the range of validity of this method to only near the bifurcation point. The Koiter-Newton method was developed to overcome these limitations. It combines aspects from Koiter's initial postbuckling analysis and Newton arc-length methods to obtain a method that is accurate over the entire equilibrium path and is efficient in the presence of buckling or imperfection sensitivity.

The idea of the reduction method for nonlinear problems is to use the asymptotic technique to replace the governing equations of a structure by a reduced system of equations. This system has less degrees of freedom than the original system. The response of the system is then obtained by solving the reduced order model instead of the full nonlinear finite element model. For the extension to dynamics only the reduced order model from the static reduction method is required and thus this chapter only deals with the reduced order model.

The set-up of this chapter is as follows. The governing equations are discussed in Section 2.1 after which the reduced order model is derived in Section 2.2. Section 2.3 ends the chapter with a brief conclusion.

2.1 Governing equations and asymptotic expansions

In this section the governing equations and their asymptotic expansions are given at a known equilibrium point. The discretized equilibrium equations of a structure can be reduced to a set of nonlinear equations of the form:

$$\mathbf{f}(\mathbf{q}) = \lambda \mathbf{f}_{ex} \tag{2.1}$$

in which $\mathbf{f}$ and $\mathbf{f}_{ex}$ are the internal force vector and external force vector, respectively. λ is the load parameter and $\mathbf{q}$ is the vector containing the degrees of freedom of the model. The vector $\mathbf{q}$ typically describes the current configuration of the structure with respect to a reference configuration.

The system of discrete equilibrium equations, given by Equation 2.1 define a curve in the ($\mathbf{q}$,λ) space as depicted in Figure 2.1. Additionally, these equations can be interpreted as a mapping from displacement space to the force space as shown by the arrow. As a result the equilibrium path can be thought of as the pre-image of the line $\mathbf{f} = \lambda \mathbf{f}_{ex}$ in displacement space.

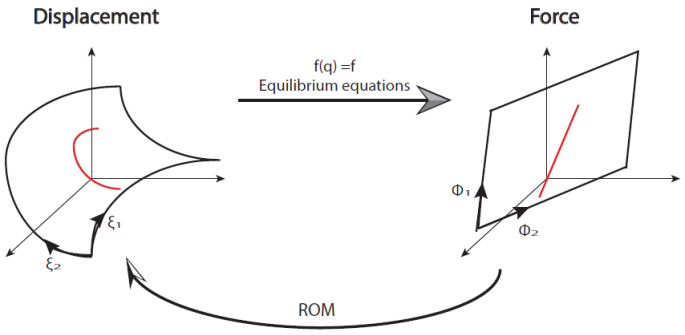

Figure 2.1: Mapping displacement space to force space [1]

This curve is referred to as the equilibrium path. To obtain the relation between the displacement $\mathbf{q}$ and the load parameter λ a path following technique is used. This yields the nonlinear response of the structure.

In the Koiter-Newton approach a reduced order model is constructed to approximate the equilibrium equations in the neighbourhood of a known equilibrium state. This is referred to as ($\mathbf{q}_0$,λ_0). The vector $\mathbf{q}_0$ is the response of the structure at the equilibrium state, which is referred to as the nominal configuration. The current configuration with respect to the nominal configuration is described by $\mathbf{u}$. $\mathbf{q}$ is now the unknown displacement vector near the nominal configuration as expressed by Equation 2.2.

$$\mathbf{q} = \mathbf{q}_0 \circ \mathbf{u} \tag{2.2}$$

The operation between $\mathbf{q}_0$ and $\mathbf{u}$ is not always a simple addition. Translational degrees of freedom are an addition, however, rotational degrees of freedom are not. Therefore, the composition operator is used in Equation 2.2. Physically, the nominal configuration implies

that there could already be some deformation of the structure due to some loading, for example.

In summary, there are two configurations: the nominal configuration described by ($\mathbf{q}_0$,λ_0) and the current configuration (or equilibrium state) described by ($\mathbf{q}$,λ). The current configuration with respect to the nominal configuration is described by ($\mathbf{u}$,$\Delta\lambda$). From this it is derived that the load parameters must satisfy the relation given by Equation 2.3.

$$\Delta\lambda = \lambda - \lambda_0 \tag{2.3}$$

Additionally, the nominal state should statisfy the equilibrium equations given by Equation 2.1, resulting in:

$$\mathbf{f}(\mathbf{q}_0) = \lambda_0 \mathbf{f}_{ex} \tag{2.4}$$

Taking into account Equation 2.2, the equilibrium equations from Equation 2.1 can be rewritten as:

$$\mathbf{f}(\mathbf{q}_0 \circ \mathbf{u}) = \lambda_0 \mathbf{f}_{ex} + \Delta\lambda \mathbf{f}_{ex} \tag{2.5}$$

The Koiter-Newton method is applicable to buckling sensitive structures. When buckling occurs, multiple secondary equilibrium branches that intersect with the primary path at buckling, bifurcation, points exist. For the method to work, specific perturbation loads have to selected that excite these secondary branches. This is achieved by a linear subspace of the force, containing the loading line. The subspace is defined as the span of predefined force vectors. This implies that it can be parametrised by the coordinates ϕ along the predefined force directions. The force subspace is then given by Equation 2.6.

$$\mathbf{f} = \mathsf{F}\boldsymbol{\phi} \tag{2.6}$$

in which F is the load matrix of which the α-th column contains the sub-load vector $\mathbf{f}_\alpha$ and the coordinates ϕ represent the amplitudes of these sub-loads. In the Koiter-Newton method the first sub-load vector is selected to be the external load, whereas the remaining sub-loads are perturbation loads. More details on how to choose the perturbation loads can be found in [4].

The pre-image of the force subspace in the displacement space is in general a nonlinear surface. The back-mapping procedure from the force subspace to the displacement space is indicated by the curved arrow in Figure 2.1. The nonlinear surface is parametrised by a set of coordinates $\boldsymbol{\xi}$. The relation between the coordinates $\boldsymbol{\phi}$ and $\boldsymbol{\xi}$ is the reduced order model.

It is a complex task to construct the pre-image of the force subspace. For this reason an approximation of the nonlinear surface is found using a Taylor series expansion. The equilibrium equations, given by Equation 2.1 are expanded up to third order with respect to $\mathbf{u}$, with as aim to simplify the complicated nonlinearity. Using Equation 2.3 and Equation 2.4, the expansion is obtained as:

$$\mathcal{L}(\mathbf{u}) + \mathcal{Q}(\mathbf{u},\mathbf{u}) + \mathcal{C}(\mathbf{u},\mathbf{u},\mathbf{u}) = \Delta\lambda\mathbf{f}_{ex} \tag{2.7}$$

in which $\mathcal{L}$, $\mathcal{Q}$ and $\mathcal{C}$ are linear, quadratic and cubic operators, respectively. Additionally, they are represented by two-dimensional, three-dimensional and four-dimensional tensors, respectively. The cubic operator $\mathcal{C}(\mathbf{u},\mathbf{v},\mathbf{w})$ can be read as $C_{pijk}u_iv_jw_k$, with u_i, v_j and w_k being components of the vectors $\mathbf{u}$, $\mathbf{v}$ and $\mathbf{w}$, respectively. C_{pijk} is the entry in the four-dimensional tensor C. Note that the Einstein summation convention is applied.

For conservative systems, the internal forces can be derived from a scalar potential. In this case the tensors L, Q and C are symmetric with respect to their subscripts.

Equation 2.7 is extended to take into account the force subspace. This results in:

$$\mathcal{L}(\mathbf{u}) + \mathcal{Q}(\mathbf{u},\mathbf{u}) + \mathcal{C}(\mathbf{u},\mathbf{u},\mathbf{u}) = \mathsf{F}\boldsymbol{\phi} \tag{2.8}$$

2.2 Derivation of the reduced order model

The solution for $\mathbf{u}$ of Equation 2.8 lays on an $m+1$ dimensional surface, where m is the number of perturbation loads. The numerical construction of such a surface would be computationally infeasible. Therefore, an approximate solution is found in terms of a Taylor series expansion. This expansion defines the displacement subspace. The equilibrium surface is parametrised in terms of the generalised displacements $\boldsymbol{\xi}$. The expansion is performed up to third order and is given in Equation 2.9.

$$\mathbf{u} = \mathbf{u}_\alpha\xi_\alpha + \mathbf{u}_{\alpha\beta}\xi_\alpha\xi_\beta + \mathbf{u}_{\alpha\beta\gamma}\xi_\alpha\xi_\beta\xi_\gamma \tag{2.9}$$

in which the subscripts vary from 1,2,...,$m+1$ and the Einstein summation convention is applied. $\mathbf{u}_\alpha$ are the first order displacement fields, and they define the tangent plane to the equilibrium surface at the approximation point. The second order displacement fields $\mathbf{u}_{\alpha\beta}$ describe the interactions among the first and second order displacement fields, respectively.

The equilibrium surface may be parametrised with an infinite number of choices for $\boldsymbol{\xi}$. This parametrisation is fixed by choosing the vector $\boldsymbol{\xi}$ to be work conjugate to the load amplitudes $\boldsymbol{\phi}$, as given by Equation 2.10.

$$(\mathsf{F}\boldsymbol{\phi})^t\,\delta\mathbf{u} \equiv \boldsymbol{\phi}^t\delta\boldsymbol{\xi} \tag{2.10}$$

This equation implies that the virtual work performed in the full model is equal to that in the reduced order model. The displacement expansion is substituted into the left of hand side of Equation 2.10, yielding:

$$\begin{aligned}(\mathsf{F}\boldsymbol{\phi})^t\,\delta\mathbf{u} &= \boldsymbol{\phi}\mathsf{F}^t\left(\mathbf{u}_\alpha\delta\xi_\alpha + \mathbf{u}_{\alpha\beta}\delta\xi_\alpha\xi_\beta + \mathbf{u}_{\alpha\beta}\xi_\alpha\delta\xi_\beta + \dots\right)\\ &= \phi_p\mathbf{f}_p^t\left(\mathbf{u}_\alpha\delta\xi_\alpha + \mathbf{u}_{\alpha\beta}\delta\xi_\alpha\xi_\beta + \mathbf{u}_{\alpha\beta}\xi_\alpha\delta\xi_\beta + \dots\right)\\ &= \left(\mathbf{f}_p^t\mathbf{u}_\alpha\right)\phi_p\delta\xi_\alpha + \left(\mathbf{f}_p^t\mathbf{u}_{\alpha\beta}\right)\phi_p\delta\xi_\alpha\xi_\beta + \left(\mathbf{f}_p^t\mathbf{u}_{\alpha\beta}\right)\phi_p\xi_\alpha\delta\xi_\beta + \dots\\ &\equiv \boldsymbol{\phi}^t\delta\boldsymbol{\xi}\end{aligned} \tag{2.11}$$

To make Equation 2.11 hold for any value of $\boldsymbol{\xi}$, the coefficients of the derivatives must satisfy the constraint equations, or orthogonality constraints given by Equation 2.12.

$$\begin{cases} \mathbf{f}_\alpha^t \mathbf{u}_\beta = \delta_{\alpha\beta} & \text{(2.12a)} \\ \mathbf{f}_\alpha^t \mathbf{u}_{\beta\gamma} = 0 & \text{(2.12b)} \\ \mathbf{f}_\alpha^t \mathbf{u}_{\beta\gamma\delta} = 0 & \text{(2.12c)} \end{cases}$$

with $\delta_{\alpha\beta}$ being the Kronecker delta. The constraint equations imply that the sub-loads $\mathbf{f}_\alpha$ are orthogonal to the second and third order displacement fields. They form the essential ingredient for the extension to dynamics, as will be shown in Chapter 4.

In a similar fashion as the displacement expansion from Equation 2.9, the load amplitudes $\boldsymbol{\phi}$ are expanded as a function of $\boldsymbol{\xi}$:

$$\boldsymbol{\phi} = \bar{\mathcal{L}}(\boldsymbol{\xi}) + \bar{\mathcal{Q}}(\boldsymbol{\xi}, \boldsymbol{\xi}) + \bar{\mathcal{C}}(\boldsymbol{\xi}, \boldsymbol{\xi}, \boldsymbol{\xi}) \tag{2.13}$$

in which $\bar{\mathcal{L}}$, $\bar{\mathcal{Q}}$, $\bar{\mathcal{C}}$ are linear, quadratic and cubic forms. $\bar{\mathsf{L}}$, $\bar{\mathsf{Q}}$ and $\bar{\mathsf{C}}$, are their respective matrix forms.

The displacement expansion from Equation 2.9 and the load expansion from Equation 2.13 are substituted into the equilibrium equations from Equation 2.8.

$$\begin{aligned} &\left\{\mathcal{L}(\mathbf{u}_\alpha) - \mathsf{F}\bar{\mathbf{L}}_\alpha\right\}\xi_\alpha + \left\{\mathcal{L}(\mathbf{u}_{\alpha\beta}) + \mathcal{Q}(\mathbf{u}_\alpha, \mathbf{u}_\beta) - \mathsf{F}\bar{\mathbf{Q}}_{\alpha\beta}\right\}\xi_{\alpha\beta} + \\ &\left\{\mathcal{L}(\mathbf{u}_{\alpha\beta\gamma}) + \frac{2}{3}\left[\mathcal{Q}(\mathbf{u}_{\alpha\beta}, \mathbf{u}_\gamma) + \mathcal{Q}(\mathbf{u}_{\beta\gamma}, \mathbf{u}_\alpha) + \mathcal{Q}(\mathbf{u}_{\gamma\alpha}, \mathbf{u}_\beta)\right] + \right. \\ &\left.\mathcal{C}(\mathbf{u}_\alpha, \mathbf{u}_\beta, \mathbf{u}_\gamma) - \mathsf{F}\bar{\mathbf{C}}_{\alpha\beta\gamma}\right\}\xi_{\alpha\beta\gamma} \\ &= 0 \end{aligned} \tag{2.14}$$

with $\bar{\mathbf{L}}_\alpha$, $\bar{\mathbf{Q}}_{\alpha\beta}$ and $\bar{\mathbf{C}}_{\alpha\beta\gamma}$ being the vector in the multiple dimensional tensors $\bar{\mathsf{L}}$, $\bar{\mathsf{Q}}$ and $\bar{\mathsf{C}}$.

By equating the coefficients of the ξ's in Equation 2.14 to zero, three sets of linear equations are obtained:

$$\mathcal{L}(\mathbf{u}_\alpha) = \mathsf{F}\bar{\mathbf{L}}_\alpha \tag{2.15}$$

$$\mathcal{L}(\mathbf{u}_{\alpha\beta}) + \mathcal{Q}(\mathbf{u}_\alpha, \mathbf{u}_\beta) = \mathsf{F}\bar{\mathbf{Q}}_{\alpha\beta} \tag{2.16}$$

$$\mathcal{L}(\mathbf{u}_{\alpha\beta\gamma}) + \frac{2}{3}\left[\mathcal{Q}(\mathbf{u}_{\alpha\beta}, \mathbf{u}_\gamma) + \mathcal{Q}(\mathbf{u}_{\beta\gamma}, \mathbf{u}_\alpha) + \mathcal{Q}(\mathbf{u}_{\gamma\alpha}, \mathbf{u}_\beta)\right] + \mathcal{C}(\mathbf{u}_\alpha, \mathbf{u}_\beta, \mathbf{u}_\gamma) = \mathsf{F}\bar{\mathbf{C}}_{\alpha\beta\gamma} \tag{2.17}$$

First set of linear systems of equations

Combing Equation 2.15 with the first constraint condition, Equation 2.12a, one can write:

$$\begin{cases} \mathcal{L}(\mathbf{u}_\alpha) = \mathsf{F}\bar{\mathbf{L}}_\alpha \\ \mathbf{f}_\alpha^t \mathbf{u}_\beta = \delta_{\alpha\beta} \end{cases} \tag{2.18}$$

To allow this equation to be implemented in a finite element framework, the notation is altered to a finite element format:

$$\begin{cases} \mathsf{K}_t \mathbf{u}_\alpha = \mathsf{F}\bar{\mathbf{L}}_\alpha \\ \mathsf{F}_\alpha^t \mathbf{u}_\beta = \mathbf{E}_\alpha \end{cases} \tag{2.19}$$

in which $\mathsf{K}_t = \mathsf{L}$, is the tangential stiffness matrix at the nominal configuration. The vectors $\mathbf{E}_\alpha$ are the unit basis vectors, where the α-th entry is equal to unity, and all other entries are zero.

Rewriting Equation 2.19 in a matrix format, the first set of linear systems of equations is obtained:

$$\begin{bmatrix} \mathsf{K}_t & -\mathsf{F} \\ -\mathsf{F}^t & 0 \end{bmatrix} \begin{Bmatrix} \mathbf{u}_\alpha \\ \bar{\mathbf{L}}_\alpha \end{Bmatrix} = \begin{Bmatrix} \mathbf{0} \\ -\mathbf{E}_\alpha \end{Bmatrix} \tag{2.20}$$

This first set of linear systems of equations yields the first order displacement fields as well as the vector $\bar{\mathbf{L}}_\alpha$. The vectors $\bar{\mathbf{L}}_\alpha$ are assembled to form the tensor $\bar{\mathsf{L}}$.

Second set of linear systems of equations

Combining Equation 2.16 with the second constraint condition, Equation 2.12b, gives:

$$\begin{cases} \mathcal{L}(\mathbf{u}_{\alpha\beta}) + \mathcal{Q}(\mathbf{u}_\alpha, \mathbf{u}_\beta) = \mathsf{F}\bar{\mathbf{Q}}_{\alpha\beta} \\ \mathbf{f}_\alpha^t \mathbf{u}_{\beta\gamma} = 0 \end{cases} \tag{2.21}$$

Altering the notation to the finite element notations and rewriting the equations in a matrix format yields the second set of linear systems of equations:

$$\begin{bmatrix} \mathsf{K}_t & -\mathsf{F} \\ -\mathsf{F}^t & 0 \end{bmatrix} \begin{Bmatrix} \mathbf{u}_{\alpha\beta} \\ \bar{\mathbf{Q}}_{\alpha\beta} \end{Bmatrix} = \begin{Bmatrix} -\mathcal{Q}(\mathbf{u}_\alpha, \mathbf{u}_\beta) \\ \mathbf{0} \end{Bmatrix} \tag{2.22}$$

This second set of linear systems of equations yields second order displacement fields together with the vector $\bar{\mathbf{Q}}_{\alpha\beta}$. The vectors $\bar{\mathbf{Q}}_{\alpha\beta}$ are assembled to form the tensor $\bar{\mathsf{Q}}$.

Components of the reduced order model

A simplified way to construct the tensors $\bar{\mathsf{L}}$ and $\bar{\mathsf{Q}}$ of the reduced order model is given below. To obtain the components $\bar{L}_{\alpha\beta}$ of the tensor $\bar{\mathsf{L}}$, Equation 2.15 is multiplied with the transpose of the first order displacement vector $\mathbf{u}_\beta$:

$$\mathbf{u}_\beta^t \mathcal{L}(\mathbf{u}_\alpha) = \mathbf{u}_\beta^t \mathsf{F} \bar{\mathbf{L}}_\alpha \tag{2.23}$$

Using the first constraint equation, which reads $\mathsf{F}^t \mathbf{u}_\beta = \mathbf{E}_\beta$, the above equation is rewritten as:

$$\mathbf{u}_\beta^t \mathsf{F} \bar{\mathbf{L}}_\alpha = (\mathsf{F}^t \mathbf{u}_\beta)^t \bar{\mathbf{L}}_\alpha = \mathbf{E}_\beta^t \bar{\mathbf{L}}_\alpha = \bar{L}_{\beta\alpha} \tag{2.24}$$

The unit basis vectors $\mathbf{E}_\beta$ are such that the β-th entry is unity and other entries are zero. The components of the tensor $\bar{\mathsf{L}}$ are computed through Equation 2.25.

$$\bar{L}_{\beta\alpha} = \mathbf{u}_\beta^t \mathcal{L}(\mathbf{u}_\alpha) \tag{2.25}$$

The tensor L is symmetric in all indices for conservative systems, therefore the tensor $\bar{\mathsf{L}}$ is also symmetric in all indices.

The components $\bar{Q}_{\alpha\beta\gamma}$ of the tensor Q are obtained in a similar fashion. Equation 2.16 is multiplied with the transpose of the first order displacement vector $\mathbf{u}_\gamma$, yielding:

$$\mathbf{u}_\gamma^t \mathcal{L}(\mathbf{u}_{\alpha\beta}) + \mathbf{u}_\gamma^t \mathcal{Q}(\mathbf{u}_\alpha, \mathbf{u}_\beta) = \mathbf{u}_\gamma^t \mathsf{F} \bar{\mathbf{Q}}_{\alpha\beta} \tag{2.26}$$

For conservative systems $\mathbf{u}_\gamma^t \mathcal{L}(\mathbf{u}_{\alpha\beta}) = \mathbf{u}_{\alpha\beta}^t \mathcal{L}(\mathbf{u}_\gamma)$. Using the assumption of conservative systems together with the second orthogonality constraint $\mathsf{F}^t \mathbf{u}_{\alpha\beta}$ from Equation 2.12b and the first set of linear equations from Equation 2.15, which reads $\mathcal{L}(\mathbf{u}_\gamma) = \mathsf{F} \bar{\mathbf{L}}_\gamma$, the left hand side of the above equation is simplified as:

$$\begin{aligned} \mathbf{u}_\gamma^t \mathcal{L}(\mathbf{u}_{\alpha\beta}) + \mathbf{u}_\gamma^t \mathcal{Q}(\mathbf{u}_\alpha, \mathbf{u}_\beta) &= \mathbf{u}_{\alpha\beta}^t \mathcal{L}(\mathbf{u}_\gamma) + \mathbf{u}_\gamma^t \mathcal{Q}(\mathbf{u}_\alpha, \mathbf{u}_\beta) \\ &= (\mathsf{F}^t \mathbf{u}_{\alpha\beta})^t \bar{\mathbf{L}}_\gamma + \mathbf{u}_\gamma^t \mathcal{Q}(\mathbf{u}_\alpha, \mathbf{u}_\beta) \\ &= \mathbf{u}_\gamma^t \mathcal{Q}(\mathbf{u}_\alpha, \mathbf{u}_\beta) \end{aligned} \tag{2.27}$$

The right-hand side of Equation 2.26 is written as:

$$\mathbf{u}_\gamma^t \mathsf{F} \bar{\mathbf{Q}}_{\alpha\beta} = (\mathsf{F} \mathbf{u}_\gamma)^t \, \bar{\mathbf{Q}}_{\alpha\beta} = \mathbf{E}_\gamma^t \bar{\mathbf{Q}}_{\alpha\beta} = \bar{Q}_{\gamma\alpha\beta} \tag{2.28}$$

in which the first constraint equation, $\mathsf{F}^t \mathbf{u}_\gamma = \mathbf{E}_\gamma$, has been used. The unit basis vectors $\mathbf{E}_\gamma$ are such that the γ-th entry is unity and other entries are zero.

Combining Equation 2.26 and Equation 2.28 yields the expression for the components of the tensor $\bar{\mathsf{Q}}$:

$$\bar{Q}_{\gamma\alpha\beta} = \mathbf{u}_\gamma^t \mathcal{Q}(\mathbf{u}_\alpha, \mathbf{u}_\beta) \tag{2.29}$$

Note that the tensor $\bar{\mathsf{Q}}$ is symmetric in all indices due to the assumption for conservative systems.

The remaining term to establish is the four-dimensional tensor $\bar{\mathsf{C}}$. This term is obtained by multiplying both sides of Equation 2.17 by the transpose of $\mathbf{u}_\delta$, yielding:

$$\begin{aligned} &\mathbf{u}_\delta^t \mathcal{L}(\mathbf{u}_{\alpha\beta\gamma}) + \frac{2}{3}\mathbf{u}_\delta^t \left[\mathcal{Q}(\mathbf{u}_{\alpha\beta}, \mathbf{u}_\gamma) + \mathcal{Q}(\mathbf{u}_{\beta\gamma}, \mathbf{u}_\alpha) + \mathcal{Q}(\mathbf{u}_{\gamma\alpha}, \mathbf{u}_\beta)\right] + \\ &\mathbf{u}_\delta^t \mathcal{C}(\mathbf{u}_\alpha, \mathbf{u}_\beta, \mathbf{u}_\gamma) = \left(\mathsf{F}^t \mathbf{u}_\delta\right)^t \bar{\mathbf{C}}_{\alpha\beta\gamma} \end{aligned} \tag{2.30}$$

The subscript δ runs from 1 to $m+1$, and the first term $\mathbf{u}_\delta^t \mathcal{L}(\mathbf{u}_{\alpha\beta\gamma})$, is given by:

$$\mathbf{u}_\delta^t \mathcal{L}(\mathbf{u}_{\alpha\beta\gamma}) = \mathbf{u}_{\alpha\beta\gamma}^t \mathcal{L}(\mathbf{u}_\delta) = \left(\mathsf{F}^t \mathbf{u}_{\alpha\beta\gamma}\right)^t \bar{\mathbf{L}}_\delta = \mathbf{0} \tag{2.31}$$

In this equation use has been made of the fact that $\mathbf{u}_\delta^t \mathcal{L}(\mathbf{u}_{\alpha\beta\gamma}) = \mathbf{u}_{\alpha\beta\gamma}^t \mathcal{L}(\mathbf{u}_\delta)$, which holds for conservative systems. Additionally, use has been made of the third orthogonality constraint, Equation 2.12c.

The right-hand side of Equation 2.30 is rewritten as:

$$\left(\mathsf{F}^t \mathbf{u}_\delta\right)^t \bar{\mathbf{C}}_{\alpha\beta\gamma} = \mathbf{E}_\delta^t \bar{\mathbf{C}}_{\alpha\beta\gamma} = \bar{C}_{\delta\alpha\beta\gamma} \tag{2.32}$$

in which $\mathsf{F}^t \mathbf{u}_\delta = \mathbf{E}_\delta$ follows from the first orthogonality constraint, Equation 2.12a. The unit basis vectors $\mathbf{E}_\delta$ are such that the δ-th entry is unity and the other entries are zero.

Substituting Equation 2.31 and Equation 2.32 into Equation 2.30, gives the expression for the components of the tensor $\bar{\mathsf{C}}$:

$$\begin{aligned} \bar{C}_{\delta\alpha\beta\gamma} = &\frac{2}{3}\mathbf{u}_\delta^t \left[\mathcal{Q}(\mathbf{u}_{\alpha\beta}, \mathbf{u}_\gamma) + \mathcal{Q}(\mathbf{u}_{\beta\gamma}, \mathbf{u}_\alpha) + \mathcal{Q}(\mathbf{u}_{\gamma\alpha}, \mathbf{u}_\beta)\right] + \\ &\mathbf{u}_\delta^t \mathcal{C}(\mathbf{u}_\alpha, \mathbf{u}_\beta, \mathbf{u}_\gamma) \end{aligned} \tag{2.33}$$

For conservative systems a simplified expression for $\bar{C}_{\alpha\beta\gamma\delta}$ is obtained [4]:

$$\bar{C}_{\alpha\beta\gamma\delta} = \mathcal{C}(\mathbf{u}_\alpha, \mathbf{u}_\beta, \mathbf{u}_\gamma, \mathbf{u}_\delta) - \frac{2}{3}\left[\mathbf{u}_{\alpha\beta}^t \mathcal{L}(\mathbf{u}_{\delta\gamma}) + \mathbf{u}_{\beta\gamma}^t \mathcal{L}(\mathbf{u}_{\delta\alpha}) + \mathbf{u}_{\gamma\alpha}^t \mathcal{L}(\mathbf{u}_{\delta\beta})\right] \tag{2.34}$$

The expression for the three tensors $\bar{\mathsf{L}}$, $\bar{\mathsf{Q}}$ and $\bar{\mathsf{C}}$ of the reduced order model and the first and second order displacement fields, $\mathbf{u}_\alpha$ and $\mathbf{u}_{\alpha\beta}$ have been obtained. The expansion of the load amplitudes, as was given by Equation 2.13, represent the reduced order model at the nominal configuration, and is repeated below:

$$\bar{\mathcal{L}}(\boldsymbol{\xi}) + \bar{\mathcal{Q}}(\boldsymbol{\xi}, \boldsymbol{\xi}) + \bar{\mathcal{C}}(\boldsymbol{\xi}, \boldsymbol{\xi}, \boldsymbol{\xi}) = \boldsymbol{\phi} \tag{2.35}$$

The linear and quadratic terms in the left hand side of the reduced order model in Equation 2.35 are found from solving the two sets of linear systems of equations. These systems have the same coefficient matrix. The dimension of this matrix is the addition of the number of degrees of freedom N in the full finite element model and the number $(m+1)$ of the degrees of freedom in the reduced order model. m is the number of load vectors that are chosen in the force subspace F. However, this number is generally very small compared to the number of degrees of freedom in the full finite element model. The components of the linear and quadratic terms of the reduced order model can also be obtained from Equation 2.25 and Equation 2.29, respectively. Lastly, the cubic term is found only through Equation 2.34.

The right-hand side of the reduced order model, which are the load amplitudes $\boldsymbol{\phi}$, is expressed using the load parameter $\Delta\lambda$:

$$\boldsymbol{\phi} = \Delta\lambda \mathbf{E}_1 \tag{2.36}$$

in which the first component of the unit basis vector is one and all others are zero. The first component of $\Delta\lambda$ is the external load, whereas the other components are the load parameters of the perturbation loads. The dimension of $\boldsymbol{\phi}$ is $(m+1)$. The perturbation loads are selected to simulate the response of the structure to actual loads and more information of their selection if found in [4].

The reduced order model is solved using a path following technique, after which the relation between the load parameter $\Delta\lambda$ and the displacement parameter $\boldsymbol{\xi}$ is obtained. The path-following technique is not elaborated upon here. Lastly, to obtain the nonlinear response, Equation 2.2 and Equation 2.3 are used, together with the displacement expansion up to second order given by:

$$\mathbf{u} = \mathbf{u}_\alpha \xi_\alpha + \mathbf{u}_{\alpha\beta}\xi_\alpha\xi_\beta \tag{2.37}$$

2.3 Conclusion

In this chapter the reduction method for the case of statics, called the Koiter-Newton approach, has been reviewed. The method is applicable to elastic nonlinear structural stability problems. For this method a force subspace is defined, which is the product of a load matrix and an amplitude vector. The reduced order model consists of an expansion of these load amplitudes $\boldsymbol{\phi}$ as a function of general displacements $\boldsymbol{\xi}$. In the box below a summary of the reduced order model, together with its associated equations is given.

The reduced order model is represented as:

$$\bar{\mathcal{L}}(\boldsymbol{\xi}) + \bar{\mathcal{Q}}(\boldsymbol{\xi},\boldsymbol{\xi}) + \bar{\mathcal{C}}(\boldsymbol{\xi},\boldsymbol{\xi},\boldsymbol{\xi}) = \boldsymbol{\phi}$$

To obtain the first and second order displacement fields, two sets of linear finite element systems need to be solved:

$$\begin{bmatrix} \mathsf{K}_t & -\mathsf{F} \\ -\mathsf{F}^t & 0 \end{bmatrix} \begin{Bmatrix} \mathbf{u}_\alpha \\ \bar{\mathbf{L}}_\alpha \end{Bmatrix} = \begin{Bmatrix} \mathbf{0} \\ -\mathbf{E}_\alpha \end{Bmatrix}$$

$$\begin{bmatrix} \mathsf{K}_t & -\mathsf{F} \\ -\mathsf{F}^t & 0 \end{bmatrix} \begin{Bmatrix} \mathbf{u}_{\alpha\beta} \\ \bar{\mathbf{Q}}_{\alpha\beta} \end{Bmatrix} = \begin{Bmatrix} -\mathcal{Q}(\mathbf{u}_\alpha, \mathbf{u}_\beta) \\ \mathbf{0} \end{Bmatrix}$$

The side product of solving these systems yields the tensors $\bar{\mathsf{L}}$ and $\bar{\mathsf{Q}}$. Alternatively they are obtained from:

$$\bar{L}_{\alpha\beta} = \mathbf{u}_\alpha^t \mathcal{L}(\mathbf{u}_\beta)$$
$$\bar{Q}_{\alpha\beta\gamma} = \mathbf{u}_\alpha^t \mathcal{Q}(\mathbf{u}_\beta, \mathbf{u}_\gamma)$$

The components of $\bar{\mathsf{C}}$ are obtained from:

$$\bar{C}_{\alpha\beta\gamma\delta} = \mathcal{C}(\mathbf{u}_\alpha, \mathbf{u}_\beta, \mathbf{u}_\gamma, \mathbf{u}_\delta) - \frac{2}{3}\left[\mathbf{u}_{\alpha\beta}^t \mathcal{L}(\mathbf{u}_{\delta\gamma}) + \mathbf{u}_{\beta\gamma}^t \mathcal{L}(\mathbf{u}_{\delta\alpha}) + \mathbf{u}_{\gamma\alpha}^t \mathcal{L}(\mathbf{u}_{\delta\beta})\right]$$

The reduced order model is solved for the displacement parameter $\boldsymbol{\xi}$ using a path following technique. The displacement parameter is used in a displacement expansion of second order to obtained the response of the structure. It is noted that initially a third order Taylor series expansion was used. However, the third order displacement fields are merely used in the derivation of $\bar{\mathsf{C}}$ and are never actually computed, since this is computationally too expensive.

All elements of the reduction method for statics, that are needed for the extension to dynamics, have been discussed. In the next chapter, the theory needed for the derivation of the reduced order model for dynamics is expanded.

Chapter 3

Lagrangian and Hamiltonian Mechanics and Canonical Transformations

In this chapter the theory required for the construction of the Hamiltonian reduction method for nonlinear dynamics is reviewed. The theory bridges the gap between the reduced order model for statics and the one for dynamics. The concepts herein are borrowed from the field of classical mechanics. This is a relatively new term, to distinguish it from, the more recently developed, relativistic and quantum mechanics. Classical mechanics is the field that is concerned with the mathematical description of the motion of everyday objects. The most well-known way to construct the equations of motion of a system is to use Newtonian mechanics. However, in the derivation of the reduction method for nonlinear dynamics, concepts of Lagrangian and Hamiltonian mechanics are needed and this is what the present chapter deals with. Some of the elements presented are not directly used in the reduction method, however they are merely given for clarity and completeness.

The set-up of the chapter is as follows. In Section 3.1 an elaboration is given on constraints and generalised coordinates. In Section 3.2 d'Alembert's principle is explained. In Section 3.3 the basics of Lagrangian mechanics is given followed by Section 3.4, in which Hamiltonian mechanics is introduced. Canonical transformations are explained in Section 3.5 and a short conclusion is given in Section 3.6.

3.1 Constraints and generalised coordinates

Constraints are imposed to limit the motion of a system. Two types of constraints exists. These are termed holonomic constraints and nonholonomic constraints. Constraints are said to be holonomic if they can be represented of the form given by Equation 3.1.

$$f(\mathbf{r}_1, \mathbf{r}_2, \mathbf{r}_3, \ldots, t) = 0 \tag{3.1}$$

where $\mathbf{r}_i$ are the positions of the masses of the system. Constraints that do not satisfy these equations are said to be nonholonomic. This implies that they cannot be described by a closed form or by inequalities [33]. A further distinction is made based on whether the constraints are dependent on time. Constraints that are explicitly dependent on time are called rheonomic, whereas constraints not explicitly dependent on time are called scleronomic [33–35].

Using constraints imposes two difficulties when solving mechanical problems. The first one is that the coordinates $\mathbf{r}_i$ are not independent. The second one is that constraint forces are not known and are to be obtained from the solution of the problem. For holonomic constraints the first problem can be solved through the use of generalised coordinates. In Cartesian coordinates N particles consists of a total of $3N$ degrees of freedom. When there are k holonomic constraints present, then one is left with $3N$-k degrees of freedom. The set of $3N$ independent coordinates involves k dependent coordinates. If these constraints are of the form given by Equation 3.1 one can eliminate the dependent coordinates by using generalised coordinates q_i. This is done by transforming the coordinates $\mathbf{r}_i$ to generalised coordinates of the form:

$$\begin{aligned} \mathbf{r}_1 &= \mathbf{r}_1(q_1, q_2, \ldots, q_{3N-k}, t) \\ &\vdots \\ \mathbf{r}_N &= \mathbf{r}_N(q_1, q_2, \ldots, q_{3N-k}, t) \end{aligned} \tag{3.2}$$

The generalised coordinates implicitly include the constraints and are independent of each other. For nonholonomic constraints this is not possible and there is no general way to eliminate nonholonomic constraints. The second problem is overcome by formulating the mechanics in such a fashion that the constraint forces vanish. The remainder of the thesis only deals with holonomic, scleronomic systems.

3.2 D'Alembert's principle

The principle of virtual work is obtained by subdividing the force into a constraint force and an external force and multiplying this by a virtual displacement $\delta\mathbf{r}_i$. This is an infinitesimal displacement compatible with the constraints. It is assumed that the constraint forces do not perform any work and this thus drops out of the equation. One is left with the principle of virtual work given by Equation 3.3.

$$\sum_i \mathbf{F}_i^{(a)} \cdot \delta\mathbf{r}_i = 0 \tag{3.3}$$

in which $\mathbf{F}_i^{(a)}$ is the applied force.

This equation treats problems of statics. D'Alembert extended this to dynamics by introducing Newton's axiom $\mathbf{F}_i = \dot{\mathbf{p}}_i$ [33]. Note that $\mathbf{p}$ is the momentum. D'Alembert's principle is now defined by Equation 3.4. It states that the sum of the applied loads and the inertial forces perform no virtual work.

$$\sum_i \left(\mathbf{F}_i^{(a)} - \dot{\mathbf{p}}_i\right) \cdot \delta\mathbf{r}_i = 0 \tag{3.4}$$

The term $-\dot{\mathbf{p}}_i$ is known as the inertial force resisting the acceleration of the mass [36]. Overall, the term between brackets can be seen as a system of particles being in equilibrium under a force equal to the actual force plus a "reversed effective force" $-\dot{\mathbf{p}}_i$ [34]. D'Alembert's principle is used for the derivation of Hamilton's principle.

3.3 Lagrangian mechanics

This section gives an overview of concepts of Lagrangian mechanics. Lagrange's equations are introduced together with Hamilton's principle. This section forms the foundation to the extension of the theory to Hamiltonian mechanics.

3.3.1 Lagrange's equations

Lagrange's equations are defined by Equation 3.5.

$$\frac{d}{dt}\left(\frac{\partial L}{\partial \dot{q}_j}\right) - \frac{\partial L}{\partial q_j} = 0 \tag{3.5}$$

in which the Lagrangian is defined by as $L = T - V$. T and V are the kinetic and potential energy, respectively. The generalised momentum associated with a coordinate q_j is defined by Equation 3.6.

$$p_j = \frac{\partial L}{\partial \dot{q}_j} \tag{3.6}$$

This generalised momentum is also referred to as canonical momentum and conjugate momentum. When a Lagrangian of a system does not contain some coordinate q_j, even though it may contain the corresponding velocity $\dot{q}_j$, then this coordinate is called cyclic or ignorable. Lagrange' equation then reduces to Equation 3.7.

$$\frac{d}{dt}\frac{\partial L}{\partial \dot{q}_j} = 0 \tag{3.7}$$

From this it is deduced that p_j is constant and a general conservation theorem follows: *The generalised momentum conjugate to a cyclic coordinate is conserved* [34].

Lagrange's equations allows one to obtain the equations of motion of a system if the potential and kinetic energy are known. The Lagrangian formulation is equivalent to the Newtonian formulation. However, in the Newtonian formulation the forces must be known beforehand, since they directly enter the equations of motion. In the Lagrangian formulation the potential energy implicitly incorporates the forces [33].

3.3.2 Hamilton's Principle

Before presenting Hamiton's principle, two definitions are given. Firstly, the configuration of a system can be described through n generalised coordinates $q_1 \ldots, q_n$. The n-dimensional subspace of the coordinates q_i is known as the configuration space. While time changes from t_1 to t_2, the state of the system changes and it follows a path in this configuration space. A point on this path represents the system configuration at a specific moment in time. Secondly, Hamiton's principle describes the motion of mechanical systems for which all forces, with the exception of constraint forces, can be derived from some generalised scalar potential. These type of systems are referred to as monogenic. Hamiton's principle for monogenic systems is defined as: *The motion of the system from time t_1 to t_2 is such that the action given by Equation 3.8 has a stationary value for the actual path of motion* [34].

$$I = \int_{t_1}^{t_2} L \, dt \tag{3.8}$$

The principle states that from the paths a system point can travel between two instances in time, it will take the path of which Equation 3.8 is stationary. Stationary for a line integral means that the integral along a path has the same value to within first order infinitesimals as those that differ from it by infinitesimal displacements. This is shown in Figure 3.1. It comes down to the time integral of the Lagrangian having an extremum (the variation is zero) and it can be re-expressed as given by Equation 3.9.

$$\delta I = \delta \int_{t_1}^{t_2} L(q_1, \ldots, q_n, \dot{q}_1, \ldots, \dot{q}_n, t) dt = 0 \tag{3.9}$$

This equation represents Hamilton's principle. For its derivation based on d'Alembert's principle, one is referred to Section A.1.

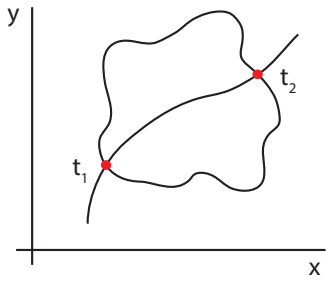

Figure 3.1: Path in configuration space

In [34], some advantages of the variational Hamiton's principle are listed. Firstly, the Lagrangian and Hamiton's principle give a compact way to obtain equations of motions of a system. Furthermore, the principle only involves physical quantities that can be defined without reference to a particular set of generalised coordinates (which are the kinetic and potential energy) and thus it is independent of the chosen coordinate system.

3.4 Hamiltonian mechanics

This section introduces the concepts of Hamiltonian mechanics. The Hamiltonian is introduced as well as Hamilton's equations of motion. Lastly, Hamilton's principle is derived in the Hamiltonian setting in follow-up to Hamilton's principle in Lagrangian mechanics, introduced in the previous section.

3.4.1 The Hamiltonian formulation

In the Lagrangian formulation a system consisting of n degrees of freedom has n second order equations of motion (of the form given by Equation 3.5). The motion of the system is then determined only if $2n$ initial values are specified. In the Hamiltonian formulation the motion is described in terms of first order equations of motion. However, there must still be $2n$ initial conditions to describe $2n$ independent first order equations expressed in terms of $2n$ independent variables. Half of the independent variables are chosen as the q_i generalised coordinates and the other half are the conjugate momenta p_i. The n-dimensional subspace of generalised coordinates q_i is called configuration space, the $2n$-dimensional Cartesian space is called the phase space. Additionally, the n-dimensional subspace of conjugate momenta p_i is called the momentum space [33]. Together the quantities q and p are known as the canonical variables [34]. It is emphasised that in Hamiltonian mechanics the generalised coordinates and the corresponding conjugate momenta are treated as independent variables, they are treated on an equal basis. The Hamiltonian formulation is not necessarily better than the Lagrangian formulation for solving mechanical problems, however it provides the basics for extensions to other areas such as Hamilton-Jacobi theory, perturbation approaches and chaos. Additionally, it gives deeper insight into the formal structure of mechanics [33].

Changing from a Lagrangian formulation consists of changing the variables (q, $\dot{q}$, t) to (q, p, t), which can be done through the Legendre transformation. The Hamiltonian is created by the Legendre transformation and is given by Equation 3.10.

$$H(q, p, t) = \dot{q}_i p_i - L(q, \dot{q}, t) \tag{3.10}$$

Using this equation together with Lagrange's equations and the definition of the generalised momentum, it is possible to derive the canonical equations of Hamilton defined by Equation 3.11.

$$\dot{q}_i = \frac{\partial H}{\partial p_i} \tag{3.11a}$$

$$-\dot{p}_i = \frac{\partial H}{\partial q_i} \tag{3.11b}$$

which constitute $2n$ first order equations of motion instead of the n second order Lagrange equations.

The general conservation theorem from subsection 3.3.1 can be transferred to the Hamiltonian formulation. This is seen from the following equation:

$$\dot{p}_j = \frac{\partial L}{\partial q_j} = -\frac{\partial H}{\partial q_j} \tag{3.12}$$

If a coordinate is cyclic, it will be absent from the Hamiltonian and the conjugate momentum is conserved.

The Hamiltonian, H is a constant of the motion if the Lagrangian, L is not an explicit function of time. This can be seen from differentiating the Hamiltonian with respect to time as given by Equation 3.13.

$$\frac{dH}{dt} = \frac{\partial H}{\partial q_i}\dot{q}_i + \frac{\partial H}{\partial p_i}\dot{p}_i + \frac{\partial H}{\partial t} \tag{3.13}$$

Combining this with the equations of motion from Equation 3.11 gives that:

$$\frac{dH}{dt} = \frac{\partial H}{\partial t} = -\frac{\partial L}{\partial t} \tag{3.14}$$

Thus if time does not explicitly occur in the Lagrangian then it will also not occur in H and H is conserved. The Hamiltonian can also be physically interpreted. If the transformation equations do not explicitly depend on time and the forces are derivable from a potential V that is conservative, then the Hamiltonian represents the total energy $(T + V)$ [33, 34]. This thus implies that in this case the total energy is conserved.

3.4.2 Hamilton's principle in Hamiltonian setting

Hamilton's principle has been introduced in the previous section on Lagrangian mechanics. It is derived using d'Alembert's principle as is shown in Section A.1. Hamilton's principle is now derived in a Hamiltonian setting. It sets the stage for canonical transformations, which are introduced in the next section. The derivation follows the same procedure as the one of Hamilton's principle in Lagrangian setting, which is based on computing the virtual work. To show the similarity, Hamilton's equations can be written in a similar form as d'Alembert's principle, although instead of one equation there are now two:

$$\begin{aligned} \mathbf{p} - m_i\dot{\mathbf{q}}_i &= \mathbf{0} \\ \mathbf{F}_i - \dot{\mathbf{p}}_i &= \mathbf{0} \end{aligned} \tag{3.15}$$

These equations are equivalent to Hamilton's equations of motion, as are given in Equation 3.11. The virtual work is computed by multiplying the first canonical equation of Hamilton by $\delta\mathbf{p}$ and the second one by $\delta\mathbf{q}$:

$$\begin{aligned} \dot{\mathbf{q}}_i \cdot \delta\mathbf{p}_i &= \frac{\partial H}{\partial p_i} \cdot \delta\mathbf{p}_i \\ \dot{\mathbf{p}}_i \cdot \delta\mathbf{q}_i &= -\frac{\partial H}{\partial q_i} \cdot \delta\mathbf{q}_i \end{aligned} \tag{3.16}$$

The second of these equations is subtracted from the first one:

$$\dot{\mathbf{q}}_i \cdot \delta\mathbf{p}_i - \dot{\mathbf{p}}_i \cdot \delta\mathbf{q}_i = \frac{\partial H}{\partial p_i} \cdot \delta\mathbf{p}_i + \frac{\partial H}{\partial q_i} \cdot \delta\mathbf{q}_i \tag{3.17}$$

The right hand side of Equation 3.17 represents the variation of the Hamiltonian δH. Integrating between two time states t_1 and t_2, one obtains:

$$\int_{t_1}^{t_2} (\delta H + \dot{\mathbf{p}}_i \cdot \delta\mathbf{q}_i - \dot{\mathbf{q}}_i \cdot \delta\mathbf{p}_i)\, \mathrm{d}t = 0 \tag{3.18}$$

This result is Hamilton's principle in the Hamiltonian setting. It is used in the next section on canonical transformations. Equation 3.18 is also known as the modified Hamilton's principle [34].

3.5 Canonical transformations

This section introduces canonical transformations. The concept of canonical transformations is to transform one set of canonical variables q_i, p_i to another set Q_i, P_i. Where Q_i and P_i are:

$$Q_i = Q_i(q, p, t) \tag{3.19a}$$

$$P_i = P_i(q, p, t) \tag{3.19b}$$

The requirement for the transformation to be canonical is that the new set of coordinates satisfy Hamilton's equations of motion, with a new Hamiltonian $H'(P_j, Q_j, t)$:

$$\dot{Q}_i = \frac{\partial H'}{\partial P_i} \tag{3.20a}$$

$$\dot{P}_i = -\frac{\partial H'}{\partial Q_i} \tag{3.20b}$$

Canonical transformations are useful in simplifying mechanical systems. This is explained by considering a Hamiltonian given by $H = H(q_j, p_j, t)$. The motion of a system is found through integration of the Hamilton equations given by Equation 3.11. For a cyclic coordinate $\frac{\partial H}{\partial q_i} = 0$, which implies that $\dot{p}_i = 0$. From this it is seen that the conjugate momentum $p_i = \alpha_i$ = constant. If one is to find a transformation of the form given by Equation 3.19, where all coordinates Q_i are cyclic, then all momenta are constant. The new Hamiltonian H' is then merely a function of the constant momenta P_i and this simplifies the problem.

If Q_i and P_i are canonical coordinates, implying that the transformation is canonical, then Hamilton's principle in the Hamiltonian setting, given by Equation 3.18, should also hold for these transformed coordinates. More specifically, a canonical transformation ensures that the form of the term $\dot{\mathbf{p}}_i \cdot \delta\mathbf{q}_i - \dot{\mathbf{q}}_i \cdot \delta\mathbf{p}_i$ is conserved.

A general transformation is performed given by Equation 3.21.

$$\mathbf{q} = \mathbf{q}(\boldsymbol{\xi}, \boldsymbol{\pi}) \tag{3.21a}$$
$$\mathbf{p} = \mathbf{p}(\boldsymbol{\xi}, \boldsymbol{\pi}) \tag{3.21b}$$

Substituting this transformation in the term whose form is to be conserved, the conditions for a canonical transformation are derived, as given by Equation 3.22. The full derivation is given in Section A.2.

$$\begin{aligned}\dot{\mathbf{p}}^t\delta\mathbf{q} - \dot{\mathbf{q}}^t\delta\mathbf{p} = &\left[\left(\frac{\partial\mathbf{p}}{\partial\boldsymbol{\xi}}\right)^t\cdot\left(\frac{\partial\mathbf{q}}{\partial\boldsymbol{\xi}}\right) - \left(\frac{\partial\mathbf{q}}{\partial\boldsymbol{\xi}}\right)^t\cdot\left(\frac{\partial\mathbf{p}}{\partial\boldsymbol{\xi}}\right)\right]\cdot\dot{\boldsymbol{\xi}}^t\delta\boldsymbol{\xi} + \\ &\left[\left(\frac{\partial\mathbf{p}}{\partial\boldsymbol{\pi}}\right)^t\cdot\left(\frac{\partial\mathbf{q}}{\partial\boldsymbol{\pi}}\right) - \left(\frac{\partial\mathbf{q}}{\partial\boldsymbol{\pi}}\right)^t\cdot\left(\frac{\partial\mathbf{p}}{\partial\boldsymbol{\pi}}\right)\right]\cdot\dot{\boldsymbol{\pi}}^t\delta\boldsymbol{\pi} + \\ &\left[\left(\frac{\partial\mathbf{q}}{\partial\boldsymbol{\xi}}\right)^t\cdot\left(\frac{\partial\mathbf{p}}{\partial\boldsymbol{\pi}}\right) - \left(\frac{\partial\mathbf{p}}{\partial\boldsymbol{\xi}}\right)^t\cdot\left(\frac{\partial\mathbf{q}}{\partial\boldsymbol{\pi}}\right)\right]\cdot\left(\dot{\boldsymbol{\pi}}^t\delta\boldsymbol{\xi} - \dot{\boldsymbol{\xi}}^t\delta\boldsymbol{\pi}\right)\end{aligned} \tag{3.22}$$

For the transformation to be canonical, the terms between square brackets should be:

$$\left[\left(\frac{\partial\mathbf{p}}{\partial\boldsymbol{\xi}}\right)^t\cdot\left(\frac{\partial\mathbf{q}}{\partial\boldsymbol{\xi}}\right) - \left(\frac{\partial\mathbf{q}}{\partial\boldsymbol{\xi}}\right)^t\cdot\left(\frac{\partial\mathbf{p}}{\partial\boldsymbol{\xi}}\right)\right] = \mathbf{0} \tag{3.23a}$$
$$\left[\left(\frac{\partial\mathbf{p}}{\partial\boldsymbol{\pi}}\right)^t\cdot\left(\frac{\partial\mathbf{q}}{\partial\boldsymbol{\pi}}\right) - \left(\frac{\partial\mathbf{q}}{\partial\boldsymbol{\pi}}\right)^t\cdot\left(\frac{\partial\mathbf{p}}{\partial\boldsymbol{\pi}}\right)\right] = \mathbf{0} \tag{3.23b}$$
$$\left[\left(\frac{\partial\mathbf{q}}{\partial\boldsymbol{\xi}}\right)^t\cdot\left(\frac{\partial\mathbf{p}}{\partial\boldsymbol{\pi}}\right) - \left(\frac{\partial\mathbf{p}}{\partial\boldsymbol{\xi}}\right)^t\cdot\left(\frac{\partial\mathbf{q}}{\partial\boldsymbol{\pi}}\right)\right] = \mathbf{I} \tag{3.23c}$$

These conditions can be compared to any literature on classical mechanics such as [33,34], in which the same conditions are presented. If these conditions hold, then one obtains:

$$\dot{\mathbf{p}}^t\delta\mathbf{q} - \dot{\mathbf{q}}^t\delta\mathbf{p} = \dot{\boldsymbol{\pi}}^t\delta\boldsymbol{\xi} - \dot{\boldsymbol{\xi}}^t\delta\boldsymbol{\pi} \tag{3.24}$$

from which it is seen that the form of the term in the original system is conserved. The resulting transformed system is thus a Hamiltonian system, implying that Hamilton's equation of motion are applicable. If a canonical transformation is applied to a Hamiltonian, the transformed system is thus also a Hamiltonian system. In such a transformation properties such as energy and momentum are conserved. In light of the Hamiltonian reduction method for nonlinear dynamics, the transformed canonical coordinates $\boldsymbol{\xi}$ and $\boldsymbol{\pi}$ should be less in number than the original canonical coordinates. This is shown in the following chapter.

3.6 Conclusion

In this chapter the theory of Lagrangian and Hamiltonian mechanics have been reviewed. D'Alembert's principle has been introduced together with Lagrange's equation of motion and Hamilton's principle. It has been stated that the Hamiltonian of a system can be derived from

the Lagrangian, from which the canonical equations of Hamilton can be obtained. Additionally, the concept of canonical transformations has been introduced. Canonical transformations allow one to transform a Hamiltonian expressed in terms of one set of independent coordinates and momenta to another set. The essence is that the transformed system is still a Hamiltonian system such that it represents a mechanical system. Through this transformation properties such as energy and momentum are conserved. The set of coordinates and momenta in the transformed Hamiltonian may contain less degrees of freedom than the original model. This fact is made use of in the reduction method for nonlinear dynamics. In the next chapter the theory is applied to establish the reduced order model for nonlinear dynamics.

Chapter 4

Reduction Method for Dynamics

In the previous two chapters the reduction method for statics and the theory of Lagrangian and Hamiltonian mechanics and canonical transformations has been reviewed. Additionally, the conditions that ensure a canonical transformation have been derived. The foundation has been laid to construct the reduced order model for dynamics as is presented in this chapter. It is shown that the reduced order model for dynamics reduces to the one for statics. The theory presented in Chapter 2 is directly applicable to dynamics. The reduction method is implemented in a finite element framework using the von-Kármán kinematic model. This is done for both beam and shell elements.

In Section 4.1 the basics of nonlinear dynamics and the momentum subspace are introduced. Section 4.2 explains how the number of degrees of freedom is reduced and the corresponding conditions that must be satisfied to achieve this. Section 4.3 shows how the reduced order model for dynamics reduces to that of statics. The Hamiltonian of the reduced order model is introduced in Section 4.4. The reduced order model, for different types of vibrations, is presented in Section 4.5. The von-Kármán kinematic model and the finite element implementation for beams and plates are given in Section 4.6 and Section 4.7, respectively. Finally, a brief conclusion is given in Section 4.8.

4.1 Nonlinear dynamics and momentum subspace

The aim is to construct a reduced order model for nonlinear dynamics. The nonlinearity is limited to geometric nonlinearity only. This implies that the material stays within the linear elastic regime, however, the displacements are large enough to induce finite strains. The strain-displacement relationship becomes nonlinear when strains are finite. This type of nonlinearity is typical for structural components used in the field of aerospace, automotive or civil engineering, for example. This thesis is limited to geometric nonlinearities and external loads that are time-dependent.

To understand the source of nonlinearity and the assumptions made, a hinged-hinged beam is considered. If the beam is vibrating, its shape may look as shown in Figure 4.1a. If the

(a) Vibrating beam

(b) Segmented beam

Figure 4.1: Vibration of a hinged-hinged beam

amplitude of the vibration is finite, then nonlinearities come into play. This is explained by turning to Figure 4.1b, where the beam is divided into segments that are equal of length in the undeformed state. During the vibration at a finite amplitude, it is seen that segment a and d are more strained than segment b and c. However, the force equilibrium must be satisfied. The total force thus has to be constant, implying that the total strain must also be constant. To satisfy force equilibrium the beam has to 'adjust' in the axial/longitudinal direction. In Figure 4.1b, node 2 will shift slightly to the left such that the strain in segment a is reduced and the strain in segment b is increased. The same holds for node 4, and segment c and d, only here node 4 must shift to the right. The nonlinearity in the axial direction of the beam, is thus induced by the finite lateral motion. In essence, the beam stretches in the axial direction to satisfy force equilibrium. This in contrary to linear vibrations, where this is assumed to not occur.

The out-of-plane motion is much larger than the in-plane motion and therefore, the inertia of the beam is assumed to be in the lateral direction. An assumption is made for the momentum and is given by Equation 4.1.

$$\mathbf{p} = \mathbf{M}\left[\boldsymbol{\Phi}_1 \;\; \boldsymbol{\Phi}_2 \;\; \boldsymbol{\Phi}_3 \ldots \boldsymbol{\Phi}_n\right]\boldsymbol{\pi} \tag{4.1}$$

where $\boldsymbol{\Phi}_n$ are the eigenmodes, and $\mathbf{M}$ is the mass matrix, and π is the amplitude, to be determined later. The assumption implies that the momentum of the system is assumed to be defined by a linear subspace. Since, $\mathbf{p}$ is defined by a linear subspace, $\dot{\mathbf{p}}$ is in the same subspace. Thus the assumption for the momentum essentially states that the forces are in this same subspace. This is seen by recalling d'Alembert's principle, that says that the forces are proportional to the derivative of the momentum $\dot{\mathbf{p}}$.

Selecting the modes in the momentum subspace is merely one of many options. Alternatively Ritz-Wilson vectors can be used, for example. The more general case for the momentum subspace is therefore written as given by Equation 4.2.

$$\mathbf{p} = \mathsf{P}\boldsymbol{\pi} \tag{4.2}$$

where P is the basis matrix. It is formed from the sub-momentum vectors P_δ. The coordinates π, represent the amplitudes of the sub-momentum vectors.

The overall shape of the motion of the system is thus described by a momentum subspace. The displacement, on the other hand, is expanded in a Taylor series of second order, which follows the procedure of [2, 4], and is repeated for convenience in Equation 4.3.

$$\mathbf{q} = \mathbf{q}_0 + \mathbf{u}_\alpha \xi_\alpha + \mathbf{u}_{\alpha\beta}\xi_\alpha\xi_\beta \tag{4.3}$$

For plane structures in dynamics, such as beams and plates, the first order displacement field $\mathbf{u}_\alpha$ is associated with the out-of-plane motion. This is due to the fact that their stiffness in the out-of-plane direction is much less than the in-plane stiffness. The second order displacement field $\mathbf{u}_{\alpha\beta}$, on the other hand, is associated with the in-plane motion. $\mathbf{q}_0$ is the displacement of the system in the nominal configuration. In this thesis the nominal configuration is assumed to be the undeformed configuration and thus $\mathbf{q}_0$ is zero.

4.2 Reduced number of degrees of freedom

The entire motion of the system is described by a momentum subspace and a displacement expansion. The link between Chapter 3 is now made. In this chapter it was shown that in Hamiltonian mechanics, the motion of a system is defined by two independent variables, being the momentum and position coordinates.

To construct a reduced system, i.e. a system with less degrees of freedom, the number of entries of the amplitude vectors $\boldsymbol{\pi}$ and $\boldsymbol{\xi}$ should be less than the number of degrees of freedom in the original system. This transformation of coordinates is written as given by Equation 4.4.

$$\mathbf{u} = \mathbf{u}(\boldsymbol{\xi}) = \mathbf{u}_\alpha \xi_\alpha + \mathbf{u}_{\alpha\beta}\xi_\alpha\xi_\beta + \mathbf{u}_{\alpha\beta\gamma}\xi_\alpha\xi_\beta\xi_\gamma \tag{4.4a}$$

$$\mathbf{p} = \mathbf{p}(\boldsymbol{\pi}) = \mathsf{P}\boldsymbol{\pi} = \mathsf{P}_\delta\boldsymbol{\pi}_\delta \tag{4.4b}$$

Note that the position is expanded in a Taylor series of third order, in contrary to Equation 4.3, which was of second order. The third order expansion merely has as function to derive the constraint equations, given in the next section as well as deriving the four-dimensional tensor $\bar{\mathsf{C}}$ for the reduced order model. Expanding the actual response of the system to third order would require third order displacement fields. These are too expensive to compute and therefore the expansion is truncated at the second order terms. This is in line with Equation 2.37 of the static reduction method.

The aim is thus to transform one set of canonical conjugate variables to another set, such that this latter set has less degrees of freedom than the original system. This is where the reduced order model arises. From the new set of canonical conjugate variables the Hamiltonian can then be constructed, which allows one to obtain the response of the reduced system. However, as discussed in the previous chapter, the transformed system is only a Hamiltonian system, if the transformation is canonical. The amplitude vectors $\boldsymbol{\xi}$ and $\boldsymbol{\pi}$ then represent the position and momentum of the reduced order model and are the equivalent of $\mathbf{u}$ and $\mathbf{p}$ in the original model. The number of degrees of freedom of the reduced order model is defined by the number of modes (or other basis vectors) selected in the basis matrix. If, for example, two modes are used in the basis, the number of degrees of freedom of the ROM is said to be two.

When comparing Equation 4.4 to Equation 3.21, it is seen that the former is a special case of the general latter case. Note that, however, the symbol $\mathbf{u}$ is used rather than $\mathbf{q}$. To ensure the transformation is canonical, the conditions given by Equation 3.23, restated here for convenience, must be satisfied.

$$\left[\left(\frac{\partial \mathbf{p}}{\partial \boldsymbol{\xi}}\right)^t \cdot \left(\frac{\partial \mathbf{u}}{\partial \boldsymbol{\xi}}\right) - \left(\frac{\partial \mathbf{u}}{\partial \boldsymbol{\xi}}\right)^t \cdot \left(\frac{\partial \mathbf{p}}{\partial \boldsymbol{\xi}}\right)\right] = \mathbf{0} \tag{4.5a}$$

$$\left[\left(\frac{\partial \mathbf{p}}{\partial \boldsymbol{\pi}}\right)^t \cdot \left(\frac{\partial \mathbf{u}}{\partial \boldsymbol{\pi}}\right) - \left(\frac{\partial \mathbf{u}}{\partial \boldsymbol{\pi}}\right)^t \cdot \left(\frac{\partial \mathbf{p}}{\partial \boldsymbol{\pi}}\right)\right] = \mathbf{0} \tag{4.5b}$$

$$\left[\left(\frac{\partial \mathbf{u}}{\partial \boldsymbol{\xi}}\right)^t \cdot \left(\frac{\partial \mathbf{p}}{\partial \boldsymbol{\pi}}\right) - \left(\frac{\partial \mathbf{p}}{\partial \boldsymbol{\xi}}\right)^t \cdot \left(\frac{\partial \mathbf{u}}{\partial \boldsymbol{\pi}}\right)\right] = \mathbf{I} \tag{4.5c}$$

The first of Equation 4.5 does not depend on $\boldsymbol{\pi}$, while the second one does not depend on $\boldsymbol{\xi}$. Therefore, the terms $\frac{\partial \mathbf{p}}{\partial \boldsymbol{\xi}}$ and $\frac{\partial \mathbf{u}}{\partial \boldsymbol{\pi}}$ are zero. The first two conditions of Equation 4.4 are satisfied already, whereas the third condition reduces to:

$$\left(\frac{\partial \mathbf{u}}{\partial \xi_a}\right)^t \cdot \left(\frac{\partial \mathbf{p}}{\partial \pi_b}\right) = \delta_{ab} \tag{4.6}$$

4.3 Reducing dynamics to statics

The conditions of Equation 4.6 is expanded by substituting the expression for the displacement and momentum, from Equation 4.4, and performing the differentiation, which yields:

$$(\mathbf{u}_a + 2\mathbf{u}_{a\beta}\xi_\beta + 3\mathbf{u}_{a\beta\gamma}\xi_\beta\xi_\gamma)^t \cdot \mathsf{P}_b = \delta_{ab} \tag{4.7}$$

This equation is satisfied if the following three constraint equations hold:

$$\begin{cases} \mathsf{P}_\delta^t \mathbf{u}_\alpha = \delta_{\alpha\delta} & (4.8a) \\ \mathsf{P}_\delta^t \mathbf{u}_{\alpha\beta} = 0 & (4.8b) \\ \mathsf{P}_\delta^t \mathbf{u}_{\alpha\beta\gamma} = 0 & (4.8c) \end{cases}$$

At this point the analogy to the reduction method for statics, as discussed in Chapter 2 is made. The constraints given by Equation 4.8 are of the same form as the constraint equations for the reduction method for statics, given by Equation 2.12. The only difference between the two is that the sub-load vectors $\mathbf{f}_\alpha$ are replaced with the sub-momentum vectors P_δ. This convenient analogy reduces the dynamic case to the static case, which implies that the reduced order model for nonlinear dynamics is identical to the one of statics. The reduced order model reviewed in Chapter 2 is therefore directly applicable to dynamics.

4.4 Hamiltonian of the reduced order model

To formulate the equations of motion of the system, use is made of the Hamiltonian. As discussed in Chapter 3, the Hamiltonian is computed from the addition of the total kinetic energy and the potential energy:

$$H(\mathbf{u}, \mathbf{p}) = T(\mathbf{u}, \mathbf{p}) + V(\mathbf{u}) \tag{4.9}$$

Such systems are called natural Hamiltonian systems. In this thesis a constant mass matrix is assumed and the kinetic energy depends on the momentum. The Hamiltonian is calculated through Equation 4.10.

$$H(\mathbf{u}, \mathbf{p}) = \frac{1}{2}\mathbf{p}^t\mathbf{M}^{-1}\mathbf{p} + V(\mathbf{u}) \tag{4.10}$$

For the reduced order model, the Hamiltonian (or reduced Hamiltonian) is a function of $\boldsymbol{\xi}$ and $\boldsymbol{\pi}$. For the computation of the kinetic energy, use is made of the momentum subspace given by Equation 4.1. The potential energy is computed by integrating Equation 2.13 for the load amplitudes. The kinetic and potential energy are given by Equation 4.11.

$$\begin{cases} \bar{T} = \frac{1}{2}\boldsymbol{\pi}^t\left(\mathsf{P}^t\mathbf{M}^{-1}\mathsf{P}\right)\boldsymbol{\pi} & \text{(4.11a)} \\ \bar{V} = \frac{1}{2}\bar{\mathbf{L}}_{\alpha\beta}\xi_\alpha\xi_\beta + \frac{1}{3}\bar{\mathbf{Q}}_{\alpha\beta\gamma}\xi_\alpha\xi_\beta\xi_\gamma + \frac{1}{4}\bar{\mathbf{C}}_{\alpha\beta\gamma\delta}\xi_\alpha\xi_\beta\xi_\gamma\xi_\delta & \text{(4.11b)} \end{cases}$$

If the basis matrix is taken to be $\mathbf{M}\cdot\boldsymbol{\Phi}$, with $\boldsymbol{\Phi}$ being the modal matrix, one can simplify the reduced Hamiltonian and compute a reduced mass matrix. Substituting this expression for P, the kinetic energy simplifies to:

$$\bar{T} = \frac{1}{2}\boldsymbol{\pi}^t\left(\boldsymbol{\Phi}^t\mathbf{M}\boldsymbol{\Phi}\right)\boldsymbol{\pi} \tag{4.12}$$

The reduced mass matrix is identified to be $\bar{\mathbf{M}} = \left(\boldsymbol{\Phi}^t\mathbf{M}\boldsymbol{\Phi}\right)^{-1}$.

Finally, the Hamiltonian of the reduced order model becomes:

$$\bar{H} = \bar{T} + \bar{V} \tag{4.13}$$

This reduced Hamiltonian still represents a mechanical system, since the transformation of the original position and momentum coordinates $\mathbf{u}$ and $\mathbf{p}$ to the new set of coordinates $\boldsymbol{\xi}$ and $\boldsymbol{\pi}$, is canonical.

4.5 The reduced order model for dynamics

At this point the reduced Hamiltonian of the system has been obtained. The equations of motion are to be obtained, such that they can be integrated to yield the response of the system. This section considers three different cases separately. These are free vibrations, forced vibrations and damped vibrations. Lastly, it is described how the equations of motion are solved.

4.5.1 Free vibrations

Hamilton's canonical equations of motion, from Equation 3.21, are applied to obtain $2\bar{n}$ coupled differential equations, of first order for the position and momentum coordinates. It is assumed that a modal basis is used and the basis matrix is $\mathsf{P} = \mathbf{M}\boldsymbol{\Phi}$. The $2\bar{n}$ first order ordinary differential equations can be written as given by Equation 4.14.

$$\dot{\boldsymbol{\xi}} = \frac{\partial \bar{H}}{\partial \boldsymbol{\pi}} = \bar{\mathbf{M}}^{-1}\boldsymbol{\pi} \tag{4.14a}$$

$$\dot{\boldsymbol{\pi}} = -\frac{\partial \bar{H}}{\partial \boldsymbol{\xi}} = -\left\{\bar{\mathcal{L}}(\boldsymbol{\xi}) + \bar{\mathcal{Q}}(\boldsymbol{\xi},\boldsymbol{\xi}) + \bar{\mathcal{C}}(\boldsymbol{\xi},\boldsymbol{\xi},\boldsymbol{\xi})\right\} \tag{4.14b}$$

For the finite element implementation, it is convenient to write the latter of these equations using index notation:

$$\dot{\pi}_\alpha = -\left\{\bar{L}_{\alpha\beta}\xi_\beta + \bar{Q}_{\alpha\beta\gamma}\xi_\beta\xi_\gamma + \bar{C}_{\alpha\beta\gamma\delta}\xi_\beta\xi_\gamma\xi_\delta\right\}$$

where the Einstein summation convention is applied.

After having integrated the equations of motion, the response of the original model, in terms of $\mathbf{u}$ and $\mathbf{p}$, is obtained by applying Equation 4.2 and Equation 4.3. These equations link the response of the reduced order model to the response of the full finite element model.

4.5.2 Forced vibrations

To account for time-varying loads, the equations of motion from the previous section require little modification. The reduced force is computed through Equation 4.15.

$$\bar{\boldsymbol{\phi}}(t) = \mathbf{u}_\alpha^t \mathbf{f}_{ex} \tag{4.15}$$

This force is added as a term to the equation for $\dot{\boldsymbol{\pi}}$, yielding the canonical equations of motion for a forced undamped vibration as given by Equation 4.16.

$$\dot{\boldsymbol{\xi}} = \frac{\partial \bar{H}}{\partial \boldsymbol{\pi}} = \bar{\mathbf{M}}^{-1}\boldsymbol{\pi} \tag{4.16a}$$

$$\dot{\boldsymbol{\pi}} = -\frac{\partial \bar{H}}{\partial \boldsymbol{\xi}} = -\left\{\bar{\mathcal{L}}(\boldsymbol{\xi}) + \bar{\mathcal{Q}}(\boldsymbol{\xi},\boldsymbol{\xi}) + \bar{\mathcal{C}}(\boldsymbol{\xi},\boldsymbol{\xi},\boldsymbol{\xi})\right\} + \bar{\boldsymbol{\phi}}(t) \tag{4.16b}$$

4.5.3 Damped vibrations

To simulate damping, a quadratic dissipation function is used:

$$D = \frac{1}{2}\dot{\mathbf{u}}^t \mathbf{C}\dot{\mathbf{u}} \tag{4.17}$$

For the damping matrix, use is made of Rayleigh damping, as given by Equation 4.18. In anticipation of the following chapter, it is noted that in the case of a linear analysis, this damping model corresponds to the one used in the Abaqus. However, in the nonlinear case the damping in Abaqus does not correspond to Rayleigh damping. In Abaqus the coefficient β is interpreted as defining viscous material damping, which induces a damping stress proportional to the strain rate. To compare Abaqus to the reduced order model in the case of damping, only mass proportional damping can be used.

$$\mathbf{C} = \alpha\mathbf{M} + \beta\mathbf{K} \tag{4.18}$$

For the reduced order model a reduced damping matrix $\bar{\mathbf{C}}$ is obtained defined by:

$$\bar{\mathbf{C}} = \bar{\mathbf{M}} \left(\mathsf{P}^t \mathbf{M}^{-1} \mathbf{C} \mathbf{M}^{-1} \mathsf{P} \right) \bar{\mathbf{M}} \tag{4.19}$$

The canonical equations of motion are slightly modified to incorporate Rayleigh damping. Damping is non-conservative and thus the Hamiltonian is not conserved. A Hamitonian with damping is therefore called a perturbed Hamiltonian as pointed out in [37]. The canonical equations of motion for free vibrations of a damped system are given by Equation 4.20.

$$\dot{\boldsymbol{\xi}} = \frac{\partial \bar{H}}{\partial \boldsymbol{\pi}} = \bar{\mathbf{M}}^{-1} \boldsymbol{\pi} \tag{4.20a}$$

$$\dot{\boldsymbol{\pi}} = -\frac{\partial \bar{H}}{\partial \boldsymbol{\xi}} = -\left\{ \bar{\mathcal{L}}(\boldsymbol{\xi}) + \bar{\mathcal{Q}}(\boldsymbol{\xi}, \boldsymbol{\xi}) + \bar{\mathcal{C}}(\boldsymbol{\xi}, \boldsymbol{\xi}, \boldsymbol{\xi}) \right\} - \bar{\mathbf{C}} \bar{\mathbf{M}}^{-1} \boldsymbol{\pi} \tag{4.20b}$$

The damping can also be applied to a forced vibration, by perturbing the Hamilton equations of motion of the previous system by adding the damping term.

Proof reduced damping matrix:

$$\begin{aligned} D &= \frac{1}{2} \dot{\mathbf{u}}^t \mathbf{C} \dot{\mathbf{u}} \\ &= \frac{1}{2} \mathbf{p}^t \left(\mathbf{M}^{-1} \mathbf{C} \mathbf{M}^{-1} \right) \mathbf{p} \\ &= \frac{1}{2} \boldsymbol{\pi}^t \left(\mathsf{P}^t \mathbf{M}^{-1} \mathbf{C} \mathbf{M}^{-1} \mathsf{P} \right) \boldsymbol{\pi} \\ &= \frac{1}{2} \dot{\boldsymbol{\xi}}^t \bar{\mathbf{M}} \left(\mathsf{P}^t \mathbf{M}^{-1} \mathbf{C} \mathbf{M}^{-1} \mathsf{P} \right) \bar{\mathbf{M}} \dot{\boldsymbol{\xi}} \\ &= \frac{1}{2} \dot{\boldsymbol{\xi}}^t \bar{\mathbf{C}} \dot{\boldsymbol{\xi}} \end{aligned}$$

4.5.4 Time integration

Equation 4.14, Equation 4.16 and Equation 4.20 represent the $2\bar{n}$ equations of motion of the system for free, forced and free damped vibrations, respectively. They can be integrated to obtain the response of the reduced order model, in terms of $\boldsymbol{\xi}$ and $\boldsymbol{\pi}$. Note that damping term can also be added to the equations for the forced vibration, to simulate a damped forced vibration.

This thesis is not focused on the method by which these differential equations can be solved. For this reason the standard solver *ode*45 from Matlab is used. This function allows one to obtain $\boldsymbol{\xi}$ and $\boldsymbol{\pi}$ together with their first order time derivatives.

4.6 Von-Kármán kinematic model

This section introduces the kinematic model used in the thesis for beams and plates. It consists of a simplification of the quadratic kinematic model based on the Green-Lagrange strain tensor. For beams the axial strain ϵ and the curvature χ are given by Equation 4.21.

$$\begin{cases} \epsilon = u_{,x} + \frac{1}{2}(u_{,x}^2 + w_{,x}^2) \\ \chi = w_{,xx} \end{cases} \tag{4.21}$$

Whereas, the von-Kármán kinematic model or simplified Green-Lagrange strain model, for beams is:

$$\begin{cases} \epsilon = u_{,x} + \frac{1}{2}w_{,x}^2 \\ \chi = w_{,xx} \end{cases} \tag{4.22}$$

where the subscript imply partial derivatives. It is observed that the nonlinearity arises from the second term in the expression of the axial strain.

The full Green-Lagrange strain tensor for plates is given by:

$$\begin{cases} \epsilon_x = u_{,x} + \frac{1}{2}(u_{,x}^2 + v_{,x}^2 + w_{,x}^2) \\ \epsilon_y = v_{,y} + \frac{1}{2}(u_{,y}^2 + v_{,y}^2 + w_{,y}^2) \\ \epsilon_{xy} = \frac{1}{2}(u_{,y} + v_{,x}) + \frac{1}{2}(u_{,y}\, xu_{,y} + v_{,x}\, v_{,y} + w_{,x}\, w_{,y}) \end{cases}, \begin{cases} \chi_{xx} = w_{,xx} \\ \chi_{yy} = w_{,xx} \\ \chi_{xy} = w_{,xy} \end{cases} \tag{4.23}$$

The von-Kármán kinematic model is derived from this as:

$$\begin{cases} \epsilon_x = u_{,x} + \frac{1}{2}w_{,x}^2 \\ \epsilon_y = v_{,y} + \frac{1}{2}w_{,y}^2 \\ \epsilon_{xy} = \frac{1}{2}(u_{,y} + v_{,x}) + \frac{1}{2}(w_{,x}\, w_{,y}) \end{cases} \tag{4.24}$$

However, this model entirely neglects the nonlinear in-plane rotation terms. For flat plate situations these terms may be negligible, whereas for assemblies consisting of plate and shell structures, these terms are important [2]. To obtain a more suitable model that accounts for nonlinear in-plane effects, the Green-Lagrange strain tensor from Equation 4.23 is considered. Neglecting the terms $u_{,x}^2$, $v_{,y}^2$ and $u_{,x}\, u_{,y} + v_{,x}\, v_{,y}$, overcomes the issues and one is left with the simplified Green-Lagrange strain tensor, given by Equation 4.25, which still yields accurate results. This is shown in Chapter 5.

$$\begin{cases} \epsilon_x = u_{,x} + \frac{1}{2}(v_{,x}^2 + w_{,x}^2) \\ \epsilon_y = v_{,y} + \frac{1}{2}(u_{,y}^2 + w_{,y}^2) \\ \epsilon_{xy} = \frac{1}{2}(u_{,y} + v_{,x}) + \frac{1}{2}(w_{,x}\, w_{,y}) \end{cases}, \begin{cases} \chi_{xx} = w_{,xx} \\ \chi_{yy} = w_{,xx} \\ \chi_{xy} = w_{,xy} \end{cases} \tag{4.25}$$

In this thesis the kinematic model from Equation 4.22 is used for beams, and the one from Equation 4.25 is used for plates and shells.

4.7 Finite element implementation

This section reviews the finite element formulation from [2,4]. Two types of elements are used. These are a two-node planar beam element, and a triangular three-node flat shell element.

4.7.1 Beam element

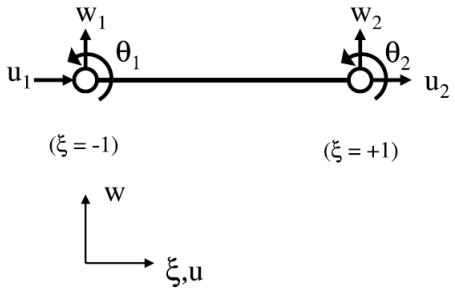

Figure 4.2: Two-node planar beam element [2]

The beam element is shown in Figure 4.2. It has three degrees of freedom per node, which are assembled in the element nodal displacement vector:

$$\mathbf{q} = \begin{bmatrix} u_1 & w_1 & \theta_1 & u_2 & w_2 & \theta_2 \end{bmatrix}^t \tag{4.26}$$

The isoparametric coordinate system is used, with the relation between the isoparametric and Cartesian coordinates system being:

$$\xi = \frac{2}{L}x - 1 \tag{4.27}$$

The in-plane and out-of-plane displacements u and w are interpolated through:

$$\begin{bmatrix} u(\xi) \\ w(\xi) \end{bmatrix} = \begin{bmatrix} N_{u1} & 0 & 0 & N_{u2} & 0 & 0 \\ 0 & N_{w1} & N_{\theta 1} & 0 & N_{w2} & N_{\theta 2} \end{bmatrix} \mathbf{q} \tag{4.28}$$

The expressions for the shape functions are found in Appendix B.

Strain vector and von-Kármán kinematics

A strain vector $\boldsymbol{\varepsilon}$ is introduced that contains the axial strain ϵ and curvature χ. In turn, these are split into a linear and a nonlinear strain component.

$$\boldsymbol{\varepsilon} = \begin{Bmatrix} \epsilon \\ \chi \end{Bmatrix} = \boldsymbol{\varepsilon}_l + \boldsymbol{\varepsilon}_{nl} \tag{4.29}$$

Expressions for the axial strain and curvature are obtained by applying the von-Kármán kinematic model. However, as pointed out in [2] a numerical problem, referred to as locking occurs when in-plane displacement components are interpolated to a lower degree than out-of-plane components. To overcome this, an approach is used by enforcing constant quantities within the element. The axial strain and curvature are computed from Equation 4.30.

$$\begin{cases} \epsilon = \frac{1}{L}\int_0^L \left(u_{,x} + \frac{1}{2}w_{,x}^2\right) \mathrm{d}x \\ \chi = w_{,xx} \end{cases} \tag{4.30}$$

Note that the axial strain is averaged over the element length L.

The curvature χ is linear with respect to the displacements, whereas the axial strain ϵ contains nonlinear terms. This is in agreement with the discussion at the beginning of this chapter where the out-of-plane motion is linear, whereas the in-plane stretching due to the out-of-plane motion, is nonlinear. Expressions for ϵ and χ are found in Appendix B. The linear part of the strain vector only contributes to the linear stiffness matrix and not to third or higher order derivatives of the strain energy. For this reason, the remainder of this section only considers the axial strain to compute the strain energy. The part of the strain energy for bending, resulting from the curvature, can be added.

Axial strain energy and the reduced order model

The axial strain energy for the beam element is computed using Equation 4.31.

$$U = \frac{1}{2}\int_0^L EAL\epsilon^2 \,\mathrm{d}x \tag{4.31}$$

where E is the Young's modulus and A is the cross-sectional area of the beam. The terms in the equilibrium equations Equation 2.8 are determined from derivatives of the strain energy up to fourth order. The internal force vector f, tangential stiffness matrix L, three-dimensional matrix Q and the four-dimensional matrix C are found as given below [4]:

$$f_i = \frac{\partial U}{\partial q_i} = EAL\left(\epsilon\frac{\partial \epsilon}{\partial q_i}\right) \tag{4.32}$$

$$L_{ij} = \frac{\partial^2 U}{\partial q_i \partial q_j} = EAL\left(\frac{\partial \epsilon}{\partial q_i}\frac{\partial \epsilon}{\partial q_j} + \epsilon\frac{\partial^2 \epsilon}{\partial q_i \partial q_j}\right) \tag{4.33}$$

$$Q_{ijk} = \frac{1}{2}\frac{\partial^3 U}{\partial q_i \partial q_j \partial q_k} = \frac{EAL}{2}\left(\frac{\partial \epsilon}{\partial q_j}\frac{\partial^2 \epsilon}{\partial q_i \partial q_k} + \frac{\partial \epsilon}{\partial q_i}\frac{\partial^2 \epsilon}{\partial q_j \partial q_k} + \frac{\partial \epsilon}{\partial q_k}\frac{\partial^2 \epsilon}{\partial q_i \partial q_j}\right) \tag{4.34}$$

$$C_{ijkl} = \frac{1}{6}\frac{\partial^4 U}{\partial q_i \partial q_j \partial q_k \partial q_l} = \frac{EAL}{6}\left(\frac{\partial^2 \epsilon}{\partial q_i \partial q_l}\frac{\partial^2 \epsilon}{\partial q_j \partial q_k} + \frac{\partial^2 \epsilon}{\partial q_j \partial q_l}\frac{\partial^2 \epsilon}{\partial q_i \partial q_k} + \frac{\partial^2 \epsilon}{\partial q_k \partial q_l}\frac{\partial^2 \epsilon}{\partial q_i \partial q_j}\right) \tag{4.35}$$

The subscripts i, j, k, l run from 1 to 18. A compact notation is introduced for the first and second order derivatives of the strain with respect to the degrees of freedom. These are the vector denoted by $\mathbf{b}$ and the matrix denoted by s. Their expression for the beam element are found in Appendix B. The internal force vector $\mathbf{f}$ and the tangential stiffness matrix L can be written in short as:

$$\mathbf{f} = EAL\,(\epsilon \mathbf{b}) \tag{4.36}$$

$$\mathsf{L} = EAL\left(\mathbf{b}\mathbf{b}^t + \epsilon \mathsf{s}\right) \tag{4.37}$$

The tangential stiffness matrix is used to solve the first set of linear systems of Equation 2.20, yielding the first order displacement field and $\bar{\mathcal{L}}$ in the reduced order model. To obtain $\bar{\mathcal{Q}}$ in the reduced order model as well as the second order displacement field, the second system of linear systems of Equation 2.22 has to be solved. To achieve this, the quadratic form $\mathcal{Q}(\mathbf{u}_\alpha, \mathbf{u}_\beta)$ must be computed. It is obtained by multiplying the three-dimensional matrix Q by two first order displacement fields $\mathbf{u}_\alpha$ and $\mathbf{u}_\beta$. Making use of the compact notation, $\mathcal{Q}(\mathbf{u}_\alpha, \mathbf{u}_\beta)$ is written as:

$$\mathcal{Q}(\mathbf{u}_\alpha, \mathbf{u}_\beta) = \frac{EAL}{2}\left[(\mathbf{b}^t\mathbf{u}_\alpha)(\mathsf{s}\mathbf{u}_\beta) + (\mathbf{b}^t\mathbf{u}_\beta)(\mathsf{s}\mathbf{u}_\alpha) + (\mathbf{u}_\alpha^t \mathsf{s}\mathbf{u}_\beta)\mathbf{b}\right] \tag{4.38}$$

To obtain the cubic term $\bar{\mathcal{C}}$ in Equation 2.34 of the reduced order model, the term $\mathcal{C}(\mathbf{u}_\alpha, \mathbf{u}_\beta, \mathbf{u}_\gamma, \mathbf{u}_\delta)$ is to be obtained. This is achieved by multiplying Equation 4.35 by the four first order displacement fields $\mathbf{u}_\alpha$, $\mathbf{u}_\beta$, $\mathbf{u}_\gamma$ and $\mathbf{u}_\delta$. The compact notation is given by Equation 4.39.

$$\begin{aligned}\mathcal{C}(\mathbf{u}_\alpha, \mathbf{u}_\beta, \mathbf{u}_\gamma, \mathbf{u}_\delta) = \frac{EAL}{6}\Big[&\left(\mathbf{u}_\alpha^t \mathsf{s}\mathbf{u}_\delta\right)\left(\mathbf{u}_\beta^t \mathsf{s}\mathbf{u}_\gamma\right) + \left(\mathbf{u}_\beta^t \mathsf{s}\mathbf{u}_\delta\right)\left(\mathbf{u}_\alpha^t \mathsf{s}\mathbf{u}_\gamma\right) \\ &+ \left(\mathbf{u}_\gamma^t \mathsf{s}\mathbf{u}_\delta\right)\left(\mathbf{u}_\alpha^t \mathsf{s}\mathbf{u}_\beta\right)\Big]\end{aligned} \tag{4.39}$$

The expressions $\mathcal{L}$, $\mathcal{Q}$ and $\mathcal{C}$ of the von-Kármán beam element have been obtained. They are directly used to obtain the $\bar{\mathcal{L}}$, $\bar{\mathcal{Q}}$ and $\bar{\mathcal{C}}$ in the reduced order model, which in turn are used in Hamilton's canonical equations of motion. These are integrated to determine the response of the system.

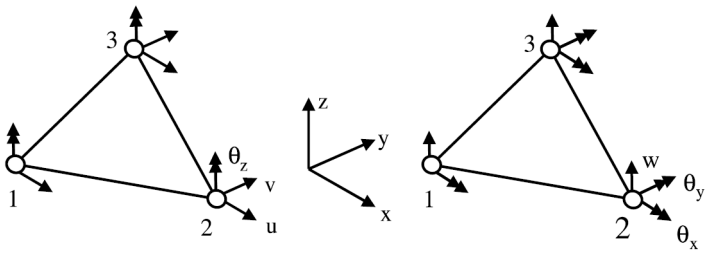

Figure 4.3: Three-node flat shell element, membrane (left) and bending (right) degrees of freedom [2]

4.7.2 Shell element

The triangular three-node flat shell element is a combination of a membrane element and a bending element, as shown in Figure 4.3. The membrane part contains the in-plane degrees of freedom, and the bending part the out-of-plane degrees of freedom. In total it has six degrees of freedom per node as given by:

$$\mathbf{q}_i = \begin{bmatrix} u_i & v_i & w_i & \theta_{x_i} & \theta_{y_i} & \theta_{z_i} \end{bmatrix} \tag{4.40}$$

where $i = 1, 2, 3$, denotes the node numbers. The total degrees of freedom are assembled in a vector:

$$\mathbf{q} = \begin{bmatrix} \mathbf{q}_1 & \mathbf{q}_2 & \mathbf{q}_3 \end{bmatrix}^t \tag{4.41}$$

Strain definitions

Similar as for the beam element, the curvatures are linear with respect to the displacement. For this reason the in-plane strain ϵ will only be considered. The in-plane strain is split into two parts, which is a linear and a nonlinear part. More specifically, it is expressed in the form given by Equation 4.42.

$$\epsilon = \epsilon_l + \epsilon_{nl} = \left(\mathsf{B}_l + \frac{1}{2}\mathsf{B}_{nl}(\mathbf{q}) \right) \mathbf{q} = \mathsf{B}_l \mathbf{q} + \frac{1}{2}\mathbf{q}^t \mathsf{S} \mathbf{q} \tag{4.42}$$

In this thesis the following expression for the total B matrix is adopted:

$$\mathsf{B}(\mathbf{q}) = \mathsf{B}_l + \mathsf{B}_{nl}(\mathbf{q}) \tag{4.43}$$

The B_l matrix is obtained from [38] and it is found in Appendix B.

Linear stiffness matrix

The linear strain-displacement matrix B_l allows one to directly compute the membrane part of the stiffness matrix through Equation 4.44.

$$K_{in-plane} = K_{b_{in-plane}} + K_{h_{in-plane}} = A\mathsf{B}_l^t\mathsf{A}_m\mathsf{B}_l + K_{h_{in-plane}} \tag{4.44}$$

Note that the stiffness matrix is composed of a so-called basic stiffness matrix, and a higher order stiffness matrix. The basic stiffness matrix ensures convergence, whereas the higher order stiffness matrix is for stability. Explicit expressions for the computation of the latter one is found in [38]. The same holds for the bending part of the stiffness matrix of which the derivation is found in [39].

Material matrix

A_m and D_b are the material matrices of an isotropic material for membrane and bending, respectively. The are given by Equation 4.45.

$$\mathsf{A}_m = \frac{Eh}{1-\nu^2}\begin{bmatrix} 1 & \nu & 0 \\ \nu & 1 & 0 \\ 0 & 0 & \frac{1-\nu}{2} \end{bmatrix} \tag{4.45a}$$

$$\mathsf{D}_b = \frac{Eh^3}{12(1-\nu^2)}\begin{bmatrix} 1 & \nu & 0 \\ \nu & 1 & 0 \\ 0 & 0 & \frac{1-\nu}{2} \end{bmatrix} \tag{4.45b}$$

To simulate a symmetric composite laminate, these material matrices can be replaced by the A and D matrix in the ABD-matrix from classical laminate theory.

Nonlinear in-plane strain and stress resultant

Expressions for ϵ_{nl}, $\mathsf{B}_{nl}(\mathbf{q})$ and S are computed by using the matrices K_{xx}, K_{yy} and K_{xy}. These constant matrices are obtained from [2] and expressions for them can be found in Appendix B.

$$\epsilon_{nl}(\mathbf{q},\mathbf{q}) = \frac{1}{2}\begin{bmatrix} \mathbf{q}^t\mathsf{K}_{xx}\mathbf{q} \\ \mathbf{q}^t\mathsf{K}_{yy}\mathbf{q} \\ \mathbf{q}^t\mathsf{K}_{xy}\mathbf{q} \end{bmatrix} \tag{4.46}$$

$$\mathsf{B}_{nl}(\mathbf{q}) = \frac{\partial\epsilon_{nl}}{\partial\mathbf{q}} = \begin{bmatrix} \mathbf{q}^t\mathsf{K}_{xx} \\ \mathbf{q}^t\mathsf{K}_{yy} \\ \mathbf{q}^t\mathsf{K}_{xy} \end{bmatrix} \tag{4.47}$$

$$\mathsf{B}_{nl}(\mathbf{q}) = \frac{\partial^2\epsilon_{nl}}{\partial\mathbf{q}^2} = \begin{bmatrix} \mathsf{S}(1,:,:) = \mathsf{K}_{xx} \\ \mathsf{S}(2,:,:) = \mathsf{K}_{yy} \\ \mathsf{S}(3,:,:) = \mathsf{K}_{xy} \end{bmatrix} \tag{4.48}$$

S is a 3×3×3 matrix, with $\mathsf{S}(a,:,:)$ indicating the a-th two-dimensional matrix in S.

The in-plane stress resultant is obtained by multiplying the strain by the materials matrix. It is split into a linear and nonlinear part:

$$\mathbf{N} = \mathsf{A}_m \left(\mathsf{B}_l + \frac{1}{2}\mathsf{B}_{nl}(\mathbf{q}) \right) \mathbf{q} = \mathsf{A}_m \mathsf{B}_l \mathbf{q} + \frac{1}{2}\mathsf{A}_m \mathsf{B}_{nl}(\mathbf{q})\mathbf{q} = \mathbf{N}_l + \mathbf{N}_{nl} \tag{4.49}$$

In-plane strain energy and the reduced order model

Using the index notation, the in-plane strain energy is computed by Equation 4.50

$$U_{in-plane} = \frac{1}{2}\mathcal{A}\mathsf{A}_{m_{\alpha\beta}}(\epsilon_{l_\alpha} + \epsilon_{nl_\alpha})(\epsilon_{l_\beta} + \epsilon_{nl_\beta}) \tag{4.50}$$

The subscripts $\alpha, \beta = 1, 2, 3$ refer to the components in the tensor and $\mathcal{A}$ is the area of the shell element. Only the nonlinear terms contribute to the quadratic and cubic terms in the equilibrium equations given in Equation 2.8. This nonlinear part of the strain energy is defined by:

$$U = \frac{1}{2}\mathcal{A}\mathsf{A}_{m_{\alpha\beta}}(2\epsilon_{l_\alpha}\epsilon_{nl_\beta} + \epsilon_{nl_\alpha}\epsilon_{nl_\beta}) \tag{4.51}$$

Similar as for the beam element, the internal force vector f_i and the tangential stiffness matrix L_{ij} are found by differentiating the in-plane strain energy up to first and second order, respectively:

$$f_i = \frac{\partial U}{\partial q_i} = \frac{\mathcal{A}\mathsf{A}_{m_{\alpha\beta}}}{2}\left(2\frac{\partial \epsilon_{l_\alpha}}{\partial q_i}\epsilon_{nl_\beta} + \frac{\partial \epsilon_{nl_\beta}}{\partial q_i}\epsilon_{nl_\alpha} + \frac{\partial \epsilon_{nl_\alpha}}{\partial q_i}\epsilon_{nl_\beta} + 2\frac{\partial \epsilon_{nl_\beta}}{\partial q_i}\epsilon_{l_\alpha} \right) \tag{4.52}$$

$$L_{ij} = \frac{\partial^2 U}{\partial q_i \partial q_j} = \mathcal{A}\mathsf{A}_{m_{\alpha\beta}}\left(\frac{\partial \epsilon_{l_\alpha}}{\partial q_i}\frac{\partial \epsilon_{nl_\beta}}{\partial q_j} + \frac{\partial \epsilon_{l_\alpha}}{\partial q_j}\frac{\partial \epsilon_{nl_\beta}}{\partial q_i} + \frac{\partial^2 \epsilon_{nl_\alpha}}{\partial q_i \partial q_j}\epsilon_{nl_\beta} + \frac{\partial^2 \epsilon_{nl_\beta}}{\partial q_i \partial q_j}\epsilon_{l_\alpha} + \frac{\partial \epsilon_{nl_\alpha}}{\partial q_i}\frac{\partial \epsilon_{nl_\beta}}{\partial q_j} \right) \tag{4.53}$$

where the indices are $i, j = 1, \ldots, 18$ and the Einstein summation convention is applied over the indices α and β. With the aid of the expression from the previous sections, a more compact form is obtained:

$$\mathbf{f} = \mathcal{A}\left(\mathsf{B}_l^t \mathbf{N}_{nl} + \mathsf{B}_{nl}^t \mathbf{N} \right) \tag{4.54}$$

$$\mathsf{L} = \mathcal{A}\left(\mathsf{B}_l^t \mathsf{A}_m \mathsf{B}_{nl} + \mathsf{B}_{nl}^t \mathsf{A}_m \mathsf{B}_l + \mathsf{B}_{nl}^t \mathcal{A}_m \mathsf{B}_{nl} + N_x \mathsf{K}_{xx} + N_y \mathsf{K}_{yy} + N_{xy}\mathsf{K}_{xy} \right) \tag{4.55}$$

N_x, N_y and N_{xy} refer to the three components of the stress resultant vector $\mathbf{N}$. Q_{ijk} and C_{ijkl} are obtained by differentiating the in-plane strain energy up to third and fourth order, respectively. However, one is to obtain $\mathcal{Q}(\mathbf{u}_\alpha, \mathbf{u}_\beta)$. A simpler method is to multiply Equation 4.54

by $\mathbf{u}_\alpha^t$ and $\mathbf{u}_\beta$ and then to differentiate with respect to the degrees of freedom. To this extent two compact notations are introduced. The stress resultant related to the displacement $\mathbf{u}_\alpha$, and the stress resultant depending on the first order displacement fields $\mathbf{u}_\alpha$ and $\mathbf{u}_\beta$ are defined as:

$$\begin{cases} \overline{\mathbf{N}}(\mathbf{u}_\alpha) = \mathsf{A}_m \mathsf{B}(\mathbf{u}_\alpha)\mathbf{u}_\alpha \\ \overline{\overline{\mathbf{N}}}(\mathbf{u}_\alpha, \mathbf{u}_\beta) = \mathsf{A}_m \mathsf{B}_{nl}(\mathbf{u}_\alpha)\mathbf{u}_\beta \end{cases} \tag{4.56}$$

The expression of $\mathcal{Q}(\mathbf{u}_\alpha, \mathbf{u}_\beta)$ for the shell element then is:

$$\mathcal{Q}(\mathbf{u}_\alpha, \mathbf{u}_\beta) = \frac{\mathcal{A}}{2}\left(\mathsf{B}_{nl}^t(\mathbf{u}_\beta)\overline{\mathbf{N}}(\mathbf{u}_\alpha) + \mathsf{B}_{nl}^t(\mathbf{u}_\alpha)\overline{\mathbf{N}}(\mathbf{u}_\beta) + \mathsf{B}^t\overline{\overline{\mathbf{N}}}(\mathbf{u}_\alpha, \mathbf{u}_\beta)\right) \tag{4.57}$$

The term $\mathcal{C}(\mathbf{u}_\alpha, \mathbf{u}_\beta, \mathbf{u}_\gamma, \mathbf{u}_\delta)$ in Equation 2.34 is computed by multiplying Equation 4.57 by the first order displacement field $\mathbf{u}_\gamma^t$, then differentiating it with respect to the degrees of freedom, and then multiplying it by $\mathbf{u}_\delta$. Furthermore, the following compact notation is used:

$$\mathbf{m}(\mathbf{u}_\alpha, \mathbf{u}_\beta) = \mathsf{B}_{nl}(\mathbf{u}_\alpha)\mathbf{u}_\beta \tag{4.58}$$

$$\mathcal{C}(\mathbf{u}_\alpha, \mathbf{u}_\beta, \mathbf{u}_\gamma, \mathbf{u}_\delta) = \frac{\mathcal{A}}{6}\left[\overline{\overline{\mathbf{N}}}(\mathbf{u}_\alpha, \mathbf{u}_\delta)\mathbf{m}(\mathbf{u}_\beta, \mathbf{u}_\gamma) + \overline{\overline{\mathbf{N}}}(\mathbf{u}_\beta, \mathbf{u}_\delta)\mathbf{m}(\mathbf{u}_\alpha, \mathbf{u}_\gamma) + \overline{\overline{\mathbf{N}}}(\mathbf{u}_\gamma, \mathbf{u}_\delta)\mathbf{m}(\mathbf{u}_\alpha, \mathbf{u}_\beta)\right] \tag{4.59}$$

Expressions for $\mathcal{L}$ and $\mathcal{Q}(\mathbf{u}_\alpha, \mathbf{u}_\beta)$ have been obtained. They are used in the linear systems of equations to obtain the first and second order displacement fields as well as $\bar{\mathcal{L}}$ and $\bar{\mathcal{Q}}$ in the reduced order model. $\mathcal{C}(\mathbf{u}_\alpha, \mathbf{u}_\beta, \mathbf{u}_\gamma, \mathbf{u}_\delta)$ is used to obtain the $\bar{\mathcal{C}}$.

4.8 Conclusion

In this chapter, the reduced order model for nonlinear dynamics has been presented. It has been explained that the out-of-plane motion of the system induces the nonlinear effects in the axial direction for beams, and in-plane for plates. A momentum subspace has been introduced for the overall motion of the system, whereas the standard displacement expansion, as used in the static reduction method, has been used for the displacements. Using Hamiltonian mechanics and a canonical transformation, three constraint equations have been derived. It was shown that these conditions are similar of form as the constraint equations in the static reduction method. From this, the analogy between dynamics and statics was made, such that the reduced order model from statics is directly applicable to dynamics. The reduced Hamiltonian was constructed, and the Hamilton canonical equations of motion have been used to derive the reduced order model for free vibrations, forced vibrations and damped vibrations. These differential equations can be integrated in time to yield the response of the reduced order model, from which the response of the actual model is obtained. Lastly, the finite element framework was introduced. A planar beam element and a triangular flat shell

element are used in this thesis. Expressions have been obtained that must be used to solve the two sets of linear systems of equations, to obtain the first and second order displacement fields and the linear and quadratic forms of the reduced order model. Furthermore, the expression has been obtained to compute the cubic form of the reduced order model. The reduced order model for nonlinear dynamics thus consists of $2\bar{n}$ first order ordinary differential equations, which are integrated in time to obtain ξ and π. These are substituted back into the displacement expansion and momentum subspace to obtain the response of the full finite element model. The reduced order model can now be applied. This is done in the next chapter.

Chapter 5

Applications of the Reduced Order Model

The reduced order model for nonlinear dynamics has been constructed and the finite element framework has been introduced. In this chapter the reduced order model is applied to beams, plates and shells. The emphasis lays on comparing the results of the reduced order model to a commercial finite element software. The selected software for this purpose is Abaqus. Additionally, the results of the reduced order model are compared to literature. The chapter is divided in four sections. In Section 5.1 the reduced order model is applied to beams. In Section 5.2 the application to plates is shown and in Section 5.3 it is applied to shells. Finally, a brief conclusion is given in Section 5.4.

5.1 Beams

In this section the reduced order model is applied to beams. The response of the reduced order model is compared to the one produced by Abaqus in terms of displacements and internal forces. It is demonstrated for a free undamped vibration, a forced undamped vibration and a forced damped vibration. Following the comparison to Abaqus, the results of the reduced order model are compared to methods from literature.

5.1.1 Comparison to Abaqus

A hinged-hinged beam with a length of 20 m is considered. It has a rectangular cross section with a height of 0.1 m and a width of 0.01 m. The beam has a density of 2480 kg/m^3 and a Young's modulus of 69 GPa.

Free undamped vibrations are considered first. The beam is given an initial displacement, such that the displacement at the center of the beam is 100 mm. The initial displacement for the linear and nonlinear case is set to be the same and is chosen so that the amplitude ratio

(maximum amplitude divided by radius of gyration) is at least $\sqrt{12}$ in the nonlinear case. For a rectangular cross section this ensures that the response is certainly nonlinear. Figure 5.1 shows the displacement-time history of the center of the beam for the free undamped vibration, for both the linear and the nonlinear case. In the computation of the response through the reduced order model, only the first eigenmode is used in the basis for both the analyses. Using one mode is sufficient to obtain excellent agreement between the reduced order model and Abaqus. It is observed that in the same time period, the nonlinear response shows more cycles than the linear response. This displays that the beam stiffens in the nonlinear case, resulting in a higher frequency. Furthermore, it is noted that the mesh in the ROM and Abaqus is chosen so that the response is space converged. Additionally, the time increment in Abaqus is selected such that the response is time converged.

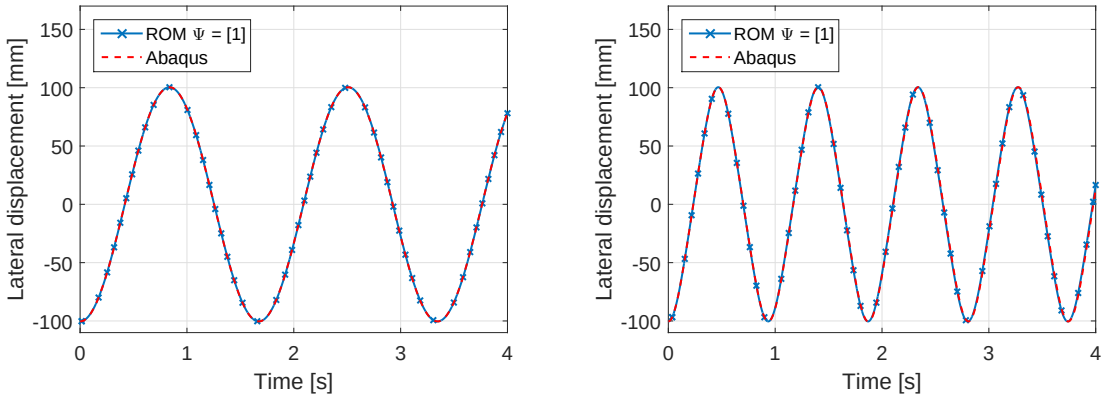

(a) Linear response **(b)** Nonlinear response

Figure 5.1: Free undamped response of the hinged-hinged beam

Figure 5.2 shows the displacement-time history of the center of the beam for a forced undamped vibration with zero initial conditions. The concentrated load applied at the center of the beam is:

$$F = \lambda \cdot \sin(\omega t)$$

where λ is set to 50 N and $\omega = 0.8\omega_1$.

The frequency of the excitation is chosen to be near resonance. The load amplitude is chosen such that the maximum amplitude ratio is at least $\sqrt{12}$ in the nonlinear case. A large difference in behaviour is observed between both cases. It is seen that the lateral displacement in the linear analysis is much larger than in the nonlinear case. Again, this is attributed to the stiffening effect in the nonlinear case. Additionally, the phenomenon of beats is seen in the linear analysis. For the linear analysis, one mode in the basis is sufficient to obtain agreement between the ROM and Abaqus. For the nonlinear case, two modes (the first and third mode) are used in the basis of the ROM to obtain agreement with Abaqus. The agreement between the response of the ROM and the one of Abaqus is excellent. Note that the second mode is not used in the basis, since it does not contribute to the response at the center of the beam. Only symmetric modes are used in the basis matrix.

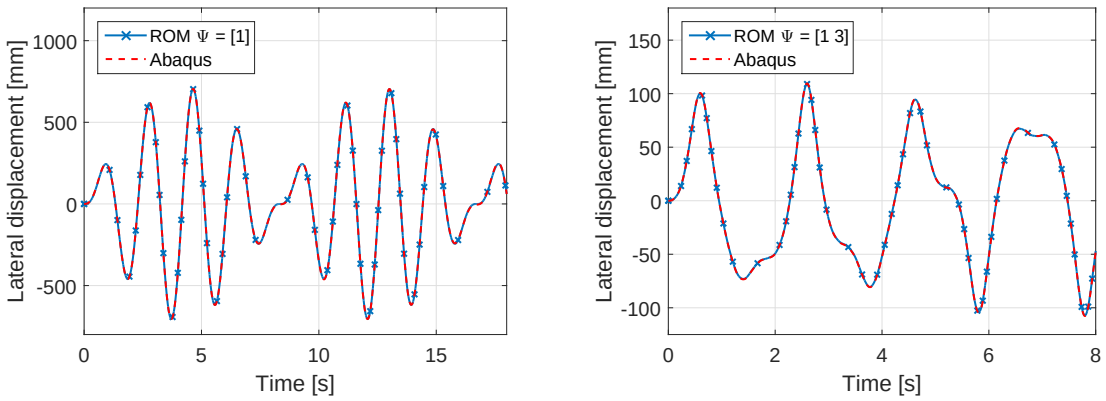

(a) Linear response **(b)** Nonlinear response

Figure 5.2: Forced undamped response of the hinged-hinged beam

The last time-displacement history for the beam is shown in Figure 5.3. This is the same analysis as was done for Figure 5.2, with the difference that mass proportional damping is added. The response of the ROM matches perfectly to the one of Abaqus. The example illustrates that the ROM is able to produce a damped response as well. It is noted, however, that stiffness proportional damping in the nonlinear case does not match to the damping used in Abaqus. This is due to the fact that Abaqus uses a different damping model in the case of geometric nonlinearity, as discussed in Chapter 4.

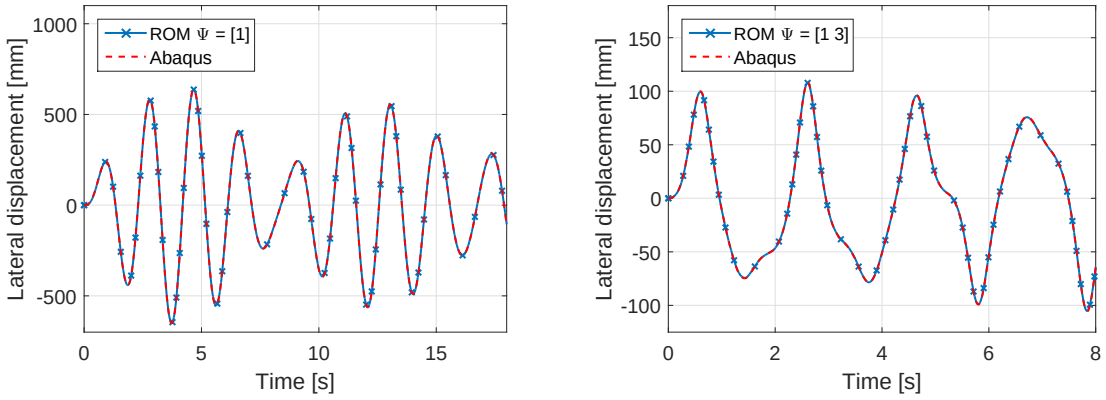

(a) Linear response **(b)** Nonlinear response

Figure 5.3: Forced damped response of the hinged-hinged beam

So far the response has been investigated qualitatively by means of plots. To show the quality of the agreement between the ROM results and the Abaqus results, the error between the two is computed at the maximum displacement amplitude, which is where the stresses are expected to be the highest. The error percentages are given in Table 5.1. The cases correspond to the previously presented plots. It is seen that the error percentages are negligibly small. Additionally, the computational times for both the ROM and Abaqus are given in the same table. The ROM outperforms Abaqus for all the three cases. The ROM does computations

in the order of a few seconds, whereas Abaqus takes minutes. Overall, the ROM is thus many times faster than Abaqus for the tested cases and its accuracy is almost spot on. It is noted however, that the given computational times are estimates, and depend on computer power. The computational time of Abaqus can be decreased by running the analyses on multiple cores, for example. On the contrary, the efficiency of the code of the ROM can be improved and potentially even lower computational times can be achieved.

Table 5.1: Comparison of the noninlinear response of the reduced order model and Abaqus

Case	Error at maximum amplitude [%]	Time ROM [s]	Time Abaqus [s]
Hinged-hinged free undamped	0.0	1.1	128
Hinged-hinged forced undamped	-0.5	2.3	290
Hinged-hinged forced damped	-0.5	2.2	282

In the preceding examples, a maximum of two modes are used in the basis. The results of the ROM can be improved by adding more modes to the basis. In Figure 5.4 it it demonstrated how the number of modes influence the results. The graph is an enlargement of the maximum peak of the response given in Figure 5.2b. A large difference is observed between one mode in the basis or multiple modes in the basis. After adding more modes, the response converges and approaches that of Abaqus. Adding more modes beyond this point has little effect on the response. This is seen for the cases of three and four modes in the basis. It is up to the user of the ROM to decide when results are satisfactory.

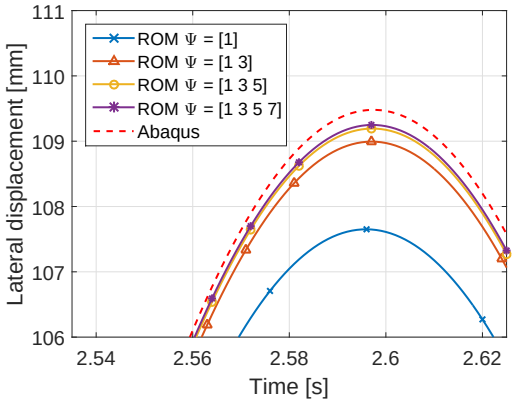

Figure 5.4: Influence of the number of modes in basis on response

So far only displacements have been considered. In the design of structures one is typically interested in the internal forces. From this the stresses can be computed and it can be determined whether a structure fails. For beams the internal forces are the axial force and the bending moment. The axial force and bending moment, for each element are computed by:

$$N = EA\epsilon \tag{5.1a}$$
$$M = EI\chi \tag{5.1b}$$

For a forced undamped vibration of the hinged-hinged beam the axial force is plotted in Figure 5.5. As expected, the axial force for the linear analysis is zero. In the nonlinear analysis two modes have been used and excellent agreement with Abaqus is found.

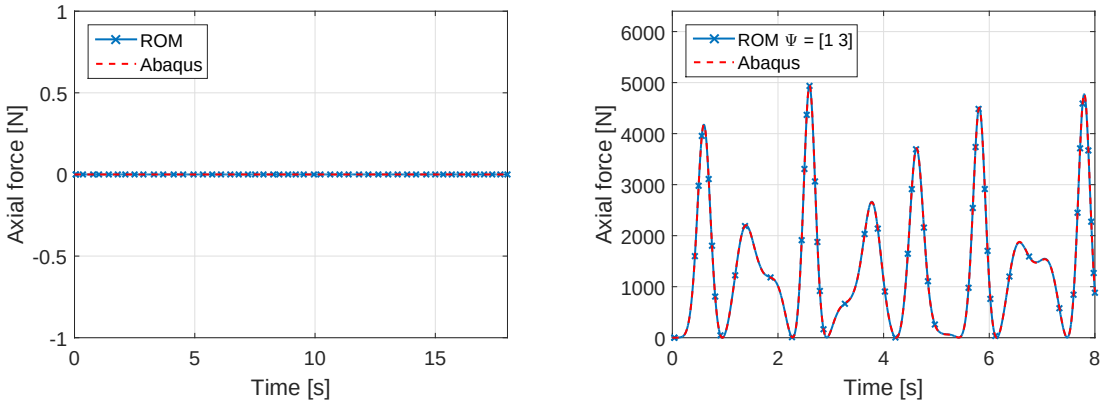

(a) Linear response **(b)** Nonlinear response

Figure 5.5: Axial force of the hinged-hinged beam, forced undamped vibration

The bending moments for the linear and nonlinear analysis are plotted in Figure 5.6. These are the bending moment at the center of the beam. Noteworthy is that for the linear analysis two modes are required to obtain good agreement with Abaqus, whereas in the nonlinear case four modes are needed. This is more than is required for the displacement and axial force. Nevertheless, even in the case of adding more modes to the basis, the computational times of the ROM are still much less than that of Abaqus.

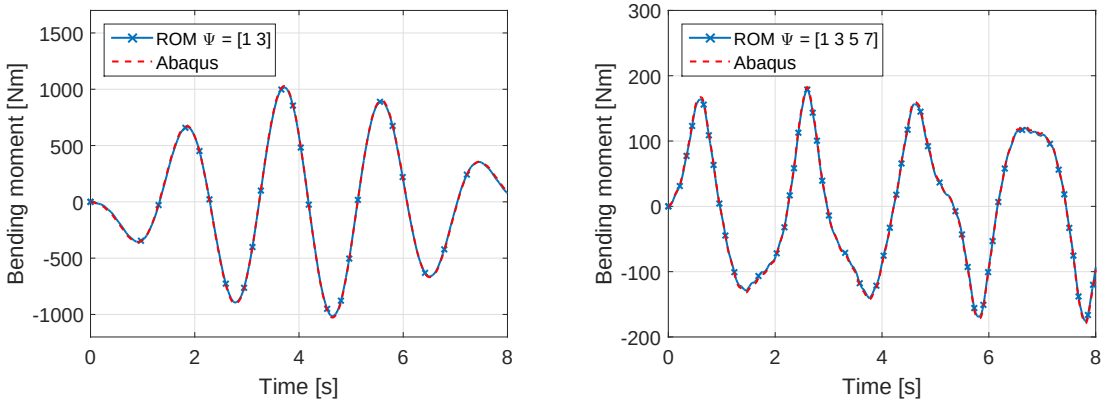

(a) Linear response **(b)** Nonlinear response

Figure 5.6: Internal moments of the hinged-hinged beam, forced undamped vibration

The effect of adding modes to the basis on the bending moment is shown in Figure 5.7. This plot is an enlargement of the highest peak in Figure 5.6b. It demonstrated that by adding

more modes, the response of the ROM approaches that of Abaqus. Furthermore, it shows that the use of only two modes (as was done for the displacement and axial force) still yields reasonable agreement with Abaqus. However, to have error percentages in the same order as for the displacement and axial force, four modes have to be used for the bending moment.

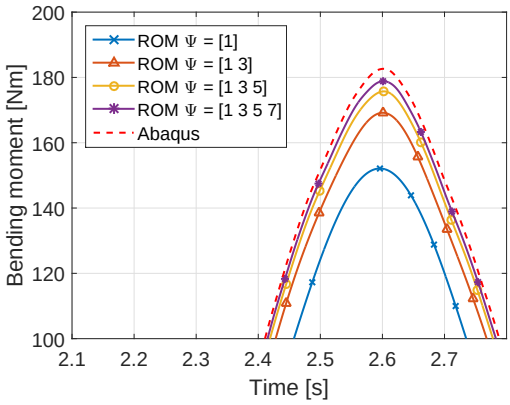

Figure 5.7: Influence of the number of modes in basis on the internal moment

5.1.2 Comparison to literature

In addition to the comparison to Abaqus, a comparison is made to some methods found in literature. The ROM is compared to three other methods. These are the Ritz-Galerkin (RG) solution [40, 41], the Assumed-Time-Mode (ATM) solution [41, 42] and the Assumed-Space-Mode (ASM) solution [41]. The three methods are plotted in Figure 5.8 together with the response of the ROM with one mode in the basis. The plot shows the frequency ratio (nonlinear frequency/linear frequency) versus the nondimensional amplitude. The plot of the ROM was created by running it several times for different initial conditions for the same beam as in the preceding examples. The amplitude is nondimensionalised by dividing it by radius of gyration.

All four methods in Figure 5.8 are in very good agreement. The frequency ratio increases with amplitude, implying that the beam stiffens. Note that only one mode has been used, since it is too complicated to find initial conditions for the ROM with more than one mode in the basis. However, techniques are available in the literature to achieve this.

5.2 Plates

In this section the reduced order model is applied to rectangular plates. It is applied to a plate with isotropic material properties as well as to a composite plate. The displacement responses are presented together with the stress resultants and moments. The results of the ROM are compared to Abaqus. Additionally, a comparison of the ROM to some cases from literature is performed.

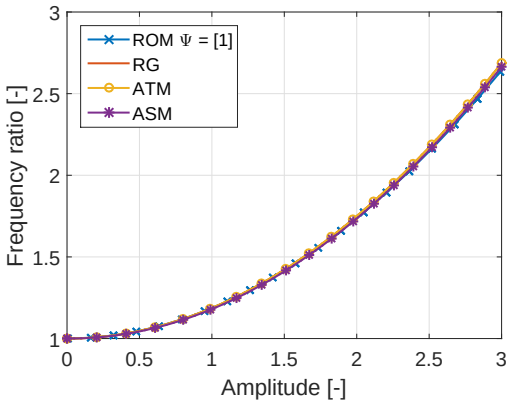

Figure 5.8: Frequency ratio versus amplitude for a hinged-hinged beam

5.2.1 Comparison to Abaqus

Response of an isotropic plate

The isotropic plate is made of the typical aerospace aluminium 7075 alloy. The Young's modulus of this material is 71.7 GPa, the density is 2810 kg/m^3 and the Poisson's ratio is 0.33. The dimensions of the panel that is analysed are a length of 300 mm, a width of 200 mm and a thickness of 0.5 mm. It is simply supported along all of its edges. More specifically, the three translational degrees of freedom are constrained. Triangular elements are used to mesh the panel in a symmetric fashion, as shown in Figure 5.9. The mesh is structured in such a way that it respects the symmetry of the plate.

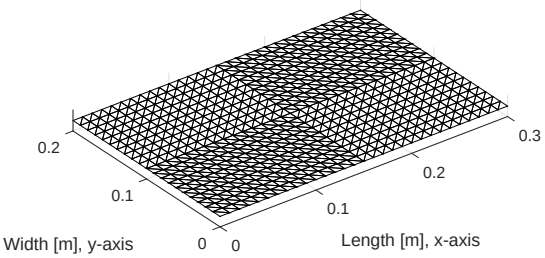

Figure 5.9: Plate with length, width and mesh structure

Before performing the time-history analysis, a frequency analyses is performed. The natural frequencies of the first five symmetric modes are presented in Table 5.2. It is ensured that the frequencies generated by the finite element code of the ROM are in sufficient agreement with the ones of Abaqus, such that any errors can be spotted prior to performing the time-history analysis. For completeness the frequencies computed from an analytic solution [43] (the Fourier method) are given as well. The frequencies of the three models are in good

agreement.

Table 5.2: Comparison frequency analysis

Mode	Frequency ROM [Hz]	Frequency Abaqus [Hz]	Frequency analytic [Hz]
1	43.79	43.82	43.81
4	151.79	152.00	151.65
8	287.33	288.30	286.46
11	368.61	370.14	367.34
12	395.24	396.27	394.29

The modes corresponding to the frequencies are displayed in Figure 5.10. The symmetric modes show a displacement in the center of the plate. These are the modes that contribute to the response at the center of the plate and thus they are used in the basis of the ROM.

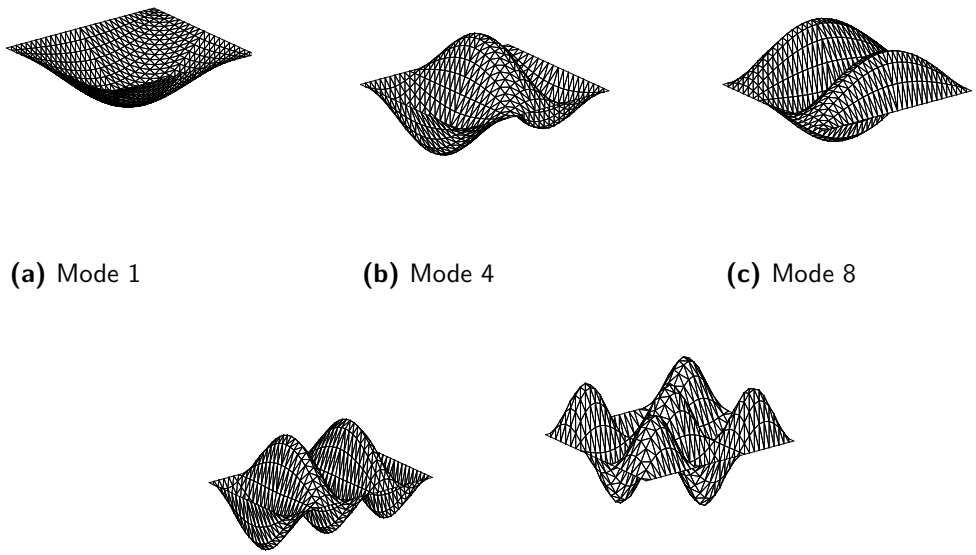

(a) Mode 1 **(b)** Mode 4 **(c)** Mode 8

(d) Mode 11 **(e)** Mode 12

Figure 5.10: First five symmetric modes

The plate is subjected to a uniform pressure load given by:

$$p = \lambda \sin(\omega t)$$

where $\lambda = 50$ N/m^2 and $\omega = 0.9\omega_1$.

The linear and nonlinear response of the ROM for a forced undamped vibration is shown in Figure 5.11. The presented displacement is the one at the center of the plate. In the linear

analysis just one mode in the basis is sufficient to obtain good agreement with Abaqus. The phenomenon of beats is observed in this case. In the nonlinear analysis two modes are needed in the basis to obtain agreement with Abaqus. The shape of the response is completely different from the linear case and the amplitude is much less. This implies that the plate stiffens.

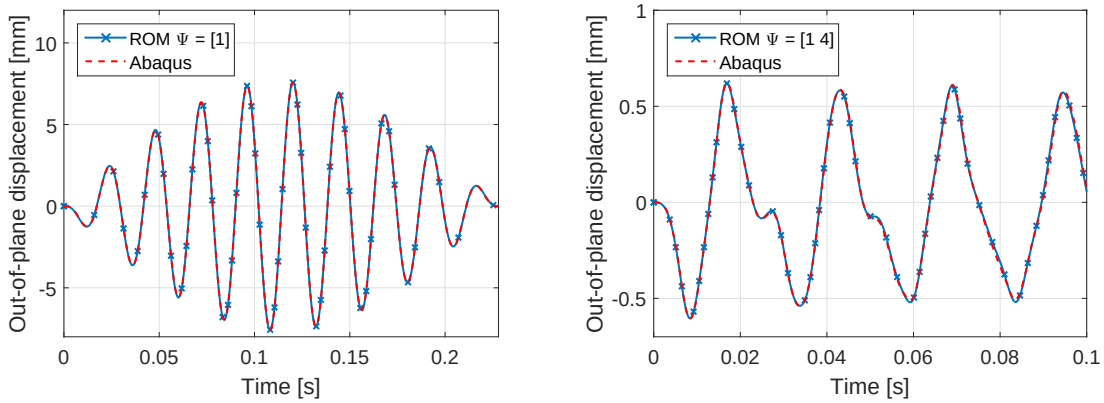

(a) Linear response **(b)** Nonlinear response

Figure 5.11: Forced undamped vibration of a simply supported plate

Table 5.3 quantifies the performance of the ROM in more detail. The ROM is run for five times with an increasing number of modes in the basis. The error at the highest peak of Figure 5.11b is considered. The table shows that the each additional mode does not necessarily decrease the error with Abaqus. Adding a second mode to the basis yields a nearly spot on agreement, whereas the addition of a third mode slightly increases the error. After adding a fifth mode, the same result as for two modes is obtained. Nevertheless, all error percentages are marginally small. The large advantage of the ROM is seen by considering the computational times of it compared to Abaqus. The ROM decreases the computational times drastically. The highest computational time of the ROM is 32.5 seconds in contrast to the 963 seconds of Abaqus. The ROM is thus nearly 30 times faster in this case. However, with two modes the smallest error is already obtained and in this case the computational time is 8.2 seconds. The ROM is then 117 times faster than Abaqus. Overall, the ROM shows an outstanding performance.

Table 5.3: Computational time and error percentage

Number of modes in the basis	Computational time ROM [s]	Error at maximum amplitude [%]	Computational time Abaqus [s]
1	7.0	3.2	963
2	8.2	-0.4	
3	11.4	-0.9	
4	18.5	-0.6	
5	32.5	-0.4	

The stress resultant for each element is computed through Equation 4.49, by directly substituting the computed displacements for $\mathbf{q}$.

A qualitative comparison of the stress resultants N_x and N_y is given in Figure 5.12 and Figure 5.13, respectively. It shows the stress resultants at the maximum amplitude of Figure 5.11b. A good agreement is observed between the ROM and Abaqus. Figure 5.12 shows the lowest values at the four corners of the plate and the highest values at the top and bottom center. Towards the center of the plate the values slightly decrease. This effect is more profoundly seen in Abaqus than in the ROM. The presented results of both the ROM and Abaqus are converged ones.

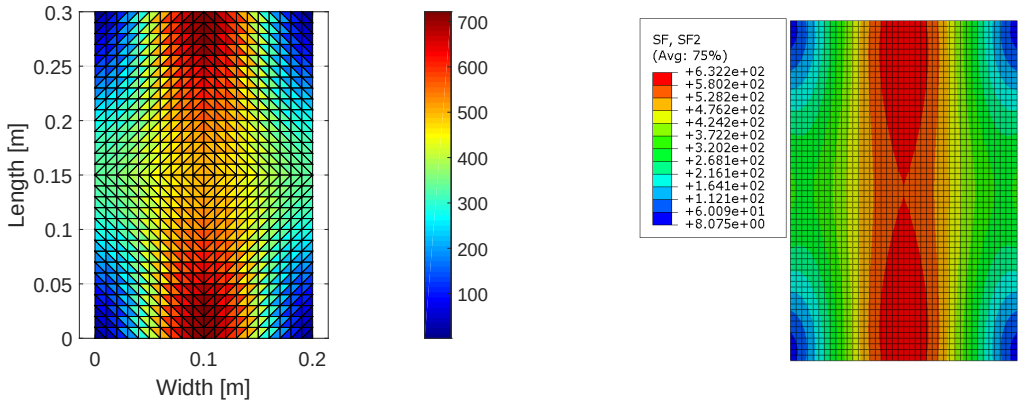

(a) ROM **(b)** Abaqus

Figure 5.12: Comparison of the stress resultant N_x

Figure 5.13 shows the lowest values along the top and bottom edge of the plate. Moving towards the center of the plate, the values increase. The observed difference between the ROM and Abaqus is that the ROM has slightly higher values at the left and right edges of the plate.

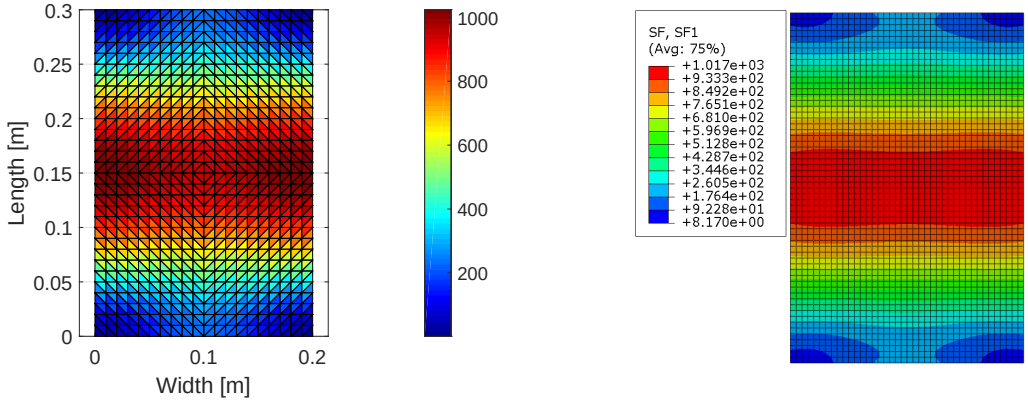

(a) ROM **(b)** Abaqus

Figure 5.13: Comparison of the stress resultant N_y

A quantitative comparison between the ROM and Abaqus is done in Figure 5.14. It shows the stress resultants at the center of the plate over time. The plots of the ROM are obtained by averaging the values of the four elements in the middle of the plate. Those of Abaqus

are obtained by averaging the values at the centroid of the four elements in the center of the plate. For both N_x and N_y the general trend and minimums are similar to that of Abaqus. The peak values of the ROM underestimate those of Abaqus. Five modes have been used in the basis. However, the addition of more modes does not improve the results. The agreement between the two models is said to be fair. The error may be the result of the fact that the displacement expansion is truncated after the second order terms.

An attempt was made to improve the results by computing the stress resultants in an alternative way. This is done by ignoring cubic and quartic terms when the displacement expansion is substituted into the expression for the stress resultant. One is left with the expression given by Equation 5.2.

$$\mathbf{N} = \mathsf{A}_m \left\{ \mathsf{B}_l \left(\mathbf{u}_\alpha \xi_\alpha \right) + \left[\mathsf{B}_l \mathbf{u}_{\alpha\beta} + \frac{1}{2} \mathsf{B}_{nl}(\mathbf{u}_\alpha) \mathbf{u}_\beta \right] \xi_\alpha \xi_\beta \right\} \tag{5.2}$$

This equation includes terms up to second order and is therefore in line with the displacement expansion of Equation 4.3. However, the stress resultants that Equation 5.2 produces are nearly identical to the one that includes cubic and quartic terms as well. No improvements were found and thus the cubic and quartic terms are negligibly small.

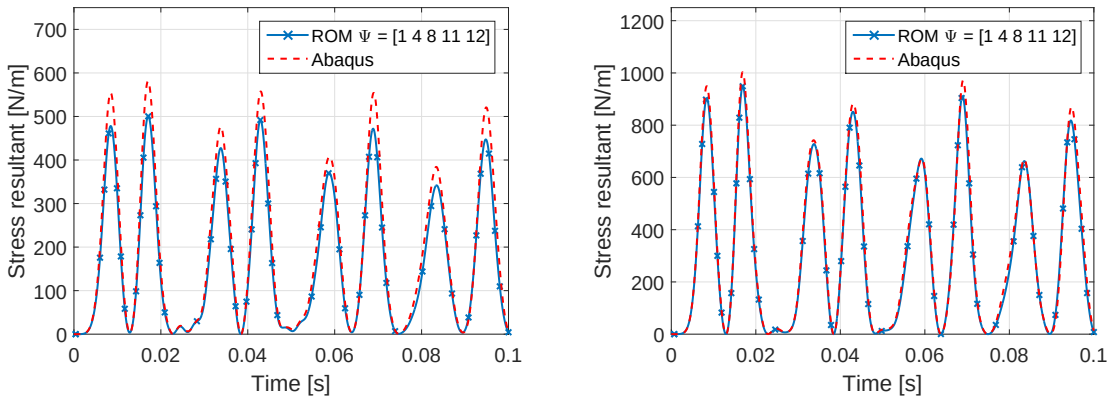

(a) Stress resultant N_x **(b)** Stress resultant N_y

Figure 5.14: Stress resultants for the nonlinear forced undamped response at the center of the plate

The moments (or stress couples) are computed in the same way as the stress resultants, except now the strain-displacement matrix for bending is used instead. Note that the stress resultants are nonlinear, whereas the moments are linear. The moment distribution over the plate is shown for M_x and M_y in Figure 5.15 and Figure 5.16, respectively. The distribution of the ROM is in good agreement with that of Abaqus. Values near the edges are low and increase towards the center of the plate where the moment is maximum. From the colour bars it is seen that the values are similar for both models.

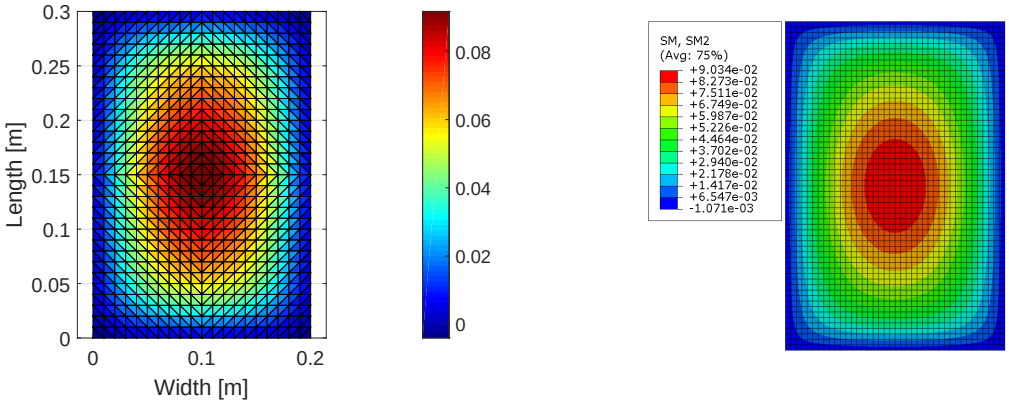

(a) ROM **(b)** Abaqus

Figure 5.15: Comparison of the moment M_x

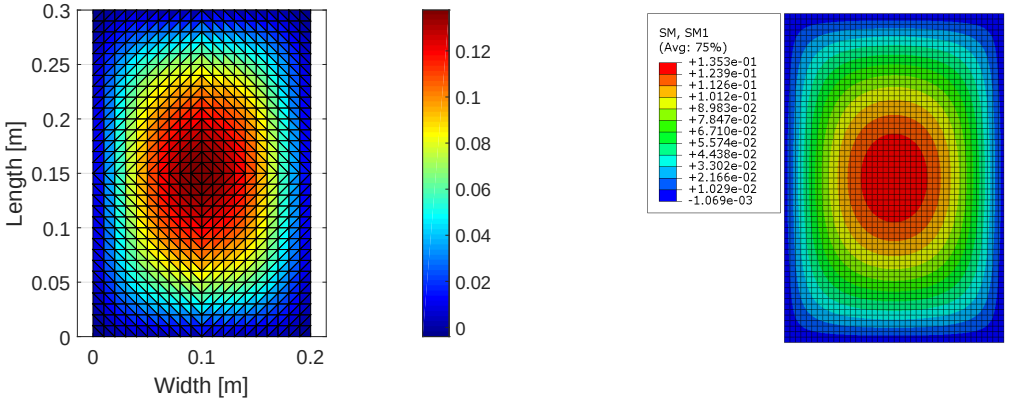

(a) ROM **(b)** Abaqus

Figure 5.16: Comparison of the moment M_y

The moments are quantitatively compared in Figure 5.17. The plots show the moments at the center of the plate over time. They are created by averaging in the same way as was done for the stress resultants. Five modes are used in the basis of the ROM. A good agreement is observed between the ROM and Abaqus for both the linear and nonlinear case.

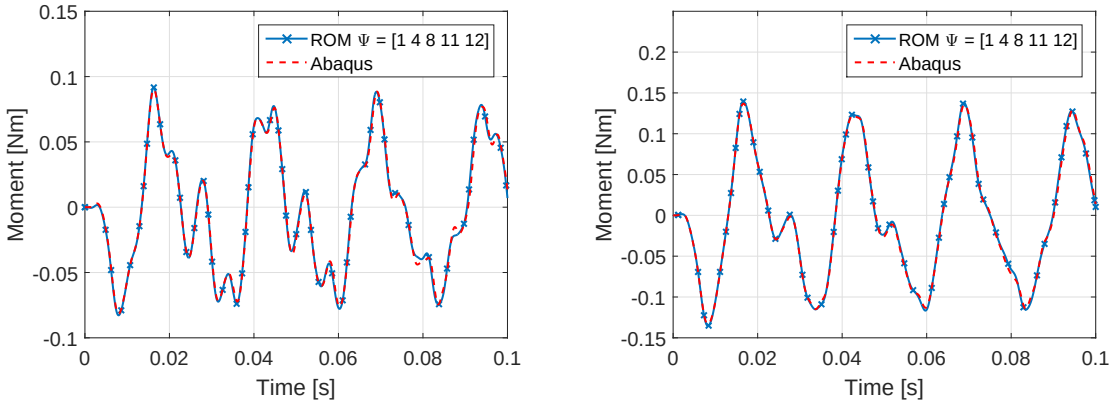

(a) Moment M_x **(b)** Moment M_y

Figure 5.17: Moments for the nonlinear forced undamped response at the center of the plate

The choice of the dimensions of the plate, considered in this section, was dominated by Abaqus. Convergence issues were encountered for large panels with the same thickness (e.g. 2×3×0.0005 m). The linear analysis always works without problems, however, the incorporation of geometric nonlinearity causes severe issues. To overcome the issue, attempts have been made to decrease the minimum time increment. Setting the minimum time step of 10^{-8} allows the analysis to proceed, however, the computational times of Abaqus then become too excessive, and infeasible. The other parameter that was adjusted is a convergence criterion in the general solution controls. This value is by default set to 0.5%. Increasing this value lets the analysis convergence much faster. Nevertheless, these controls are not to be altered, since it is unclear how this affects the accuracy of the solution. A possible reason for the convergence problem is thought to be that the displacements of the plate, subject to the harmonic load, are of the same order as the numerical accuracy of the software. Another issue encountered in Abaqus is that during mesh convergence studies, the analysis required very small step sizes for some of the finer meshes, while for the coarser meshes already good agreement was found with the ROM. No issues were encountered when running the ROM itself, for the cases that yielded issues in Abaqus. Only for stiffer systems (for example a clamped plate) the *ode*45 in Matlab showed highly oscillatory behaviour. This can be overcome by using a different integrator in Matlab specifically created for stiffer systems, such as *ode*23*s*.

Response of a composite plate

To demonstrate that the ROM also works for composite materials, an example is given. The plate has the same length and with as the example of the isotropic panel, which is 300 mm by 200 mm. Although the thickness is now 1 mm. The boundary conditions are the same as those for the isotropic plate, discussed above.

The layup and the material properties are borrowed from [44]. The layup is symmetric and balanced and is given as $[90/\text{-}45/45/0]_s$. It is a graphite/epoxy composite with the following properties: $E_L = 120.5$ GN/m^2, $E_T = 9.63$ GN/m^2, $G_{LT} = 3.58$ GN/m^2, $\nu_{LT} = 0.32$ and $\rho = 1540$ kg/m^3. Similar to the previous example, the plate is subject to a uniform pressure load with a sinusoidal amplitude. However, the plate is excited slightly above its first natural frequency. The load is made more complicated by adding a constant pressure load to the sinusoidal load. The applied pressure load is written as:

$$p = \lambda \left(1 + \sin\left(\omega t\right)\right)$$

where $\lambda = 100$ N/m^2 and $\omega = 1.1\omega_1$.

In Figure 5.18 the displacement at the center of the plate is plotted against time. In both the linear and nonlinear case one observes beats. Similar to all previous examples, the amplitudes of the response for the nonlinear case is lower than the linear case and more cycles are observed. This is due to the stiffening of the plate. Remarkable is that the nonlinear response of the ROM yields results in good agreement when two modes are used in the basis. The same number of modes are used in the basis for the linear analysis. However, after the maximum amplitude is reached (at about 0.05 s), the amplitude of the ROM is slightly larger compared to that of Abaqus. Typically, less modes are needed in the basis for the linear analysis compared to the nonlinear analysis to achieve agreement. Increasing the mesh density or adding more modes does however, not improve these results.

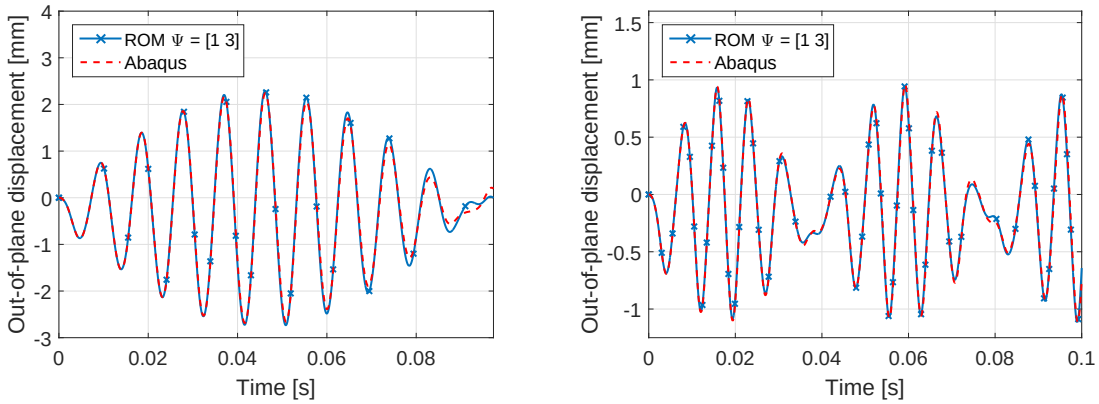

(a) Linear response **(b)** Nonlinear response

Figure 5.18: Forced undamped vibration of a simply supported composite plate

5.2.2 Comparison to literature

The ROM is compared to some cases of literature. First considered is a plate with the dimensions 2000×3000×0.5 mm. The plate is subject to a uniform pressure given by:

$$p = \lambda \cos\left(\omega t\right)$$

with $\lambda = 0.01$ N/m^2 and $\omega = 0.9\omega_1$.

The edges of the plate are simply supported and the stress condition are: all edges immovable. Referring to Figure 5.9, this implies that u is zero along the edges parallel to the x-axis and v is zero along the edges parallel to the y-axis. This is a case that has been solved with an approximate solution in [45]. Figure 5.19 shows the response of the ROM compared to that of Yamaki [45]. One mode is used in the basis of the ROM. This is done because the approximate solution also assumes a deflection in the shape of one mode. The response of the two methods is nearly identical. This is a typical example that yielded convergence issues in Abaqus, while here it is shown that the ROM works perfectly compared to the approximate analytic solution.

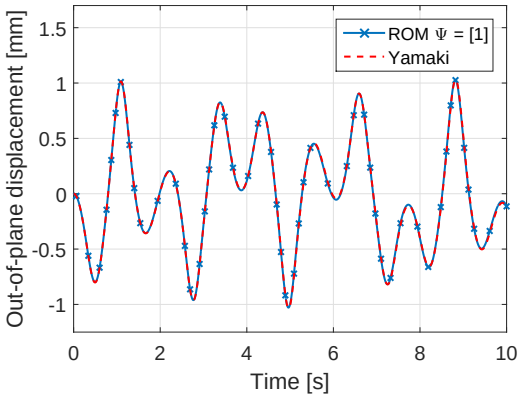

Figure 5.19: Nonlinear dynamic response

The last comparison to literature is done in Figure 5.20. The ROM is applied to a square plate, with the same boundary conditions as the previous example, and is compared to the methods of Yamaki [45], Timoshenko [46], Chu-Herrnann [47] and Wah [48]. The period ratio (linear period/nonlinear period) is plotted against the nondimensional amplitude. Similar as was done for the case of beams, the period ratio is obtained by running the ROM several times with varying initial conditions of displacement. Again this is only done by using one mode in the basis. The amplitude is made nondimensional by dividing it by the thickness of the plate. All methods are in good agreement. Only the solution of Wah shows a slightly stiffer behaviour than the others. Nevertheless, the ROM yields accurate results compared to the other methods.

5.3 Shells

In this section the reduced order model is applied to shells. Both a shell with isotropic material properties as well as composite shell are presented. The results are limited to vertical displacement responses at the center of the shell. The ROM is compared to results of Abaqus.

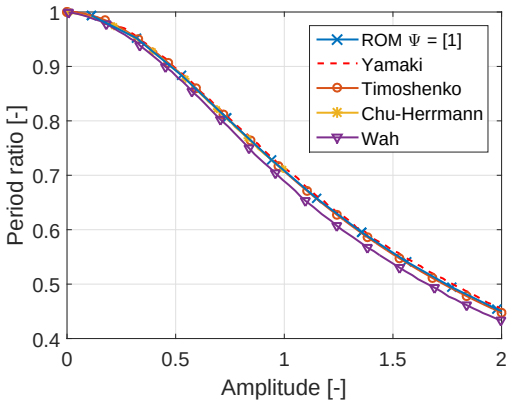

Figure 5.20: Period ratio versus amplitude for a square plate

5.3.1 Comparison to Abaqus

Response of an isotropic shell

Two different shallow cylindrical shells are considered. They both have the same dimensions except for the thickness. The shells are simply supported along all four edges. All three translational degrees of freedom are constrained. The properties used are taken from [49]. These are: $E = 21$ GPa, $\nu = 0.3$ and a length and width of 1 m. Furthermore the radius is given to be 17.895 m. The shell is presented in Figure 5.21. The z-axis is scaled up to show the curvature.

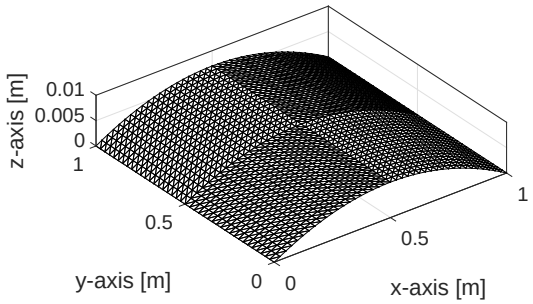

Figure 5.21: Shell with length, width and mesh structure

Note that [49] uses dimensionless values, however, in this thesis they are assumed to be dimensional. A thickness is not given and thus two different thicknesses are considered. These are 1 mm and 4 mm. The applied load is a uniform pressure acting on the outside (convex) part of the shell given by:

$$p = \lambda \sin(\omega t)$$

where in the following two examples $\omega = 0.9\omega_1$.

In Figure 5.22 the response is shown for the 1 mm thick shell where $\lambda = 4$ N/m^2. The presented response is the vertical displacement at the center of the shell. For the linear case five modes are needed to achieve a reasonable agreement with Abaqus. In the nonlinear case eight modes are used. In the linear case the peak values are in reasonably good agreement with those of Abaqus, whereas in the nonlinear case from 0.25 second and onwards, the peak values of the ROM are somewhat lower than those of Abaqus. The addition of the relatively large amount of modes in this latter case does not improve the results. Nevertheless, in both cases the general trend of the plots of the ROM is in agreement with Abaqus. Furthermore, it is seen that the peak values in the nonlinear case reach higher values than in the linear case. The nonlinearity is thus of the softening type in contrast to all earlier examples, which showed a hardening type of behaviour.

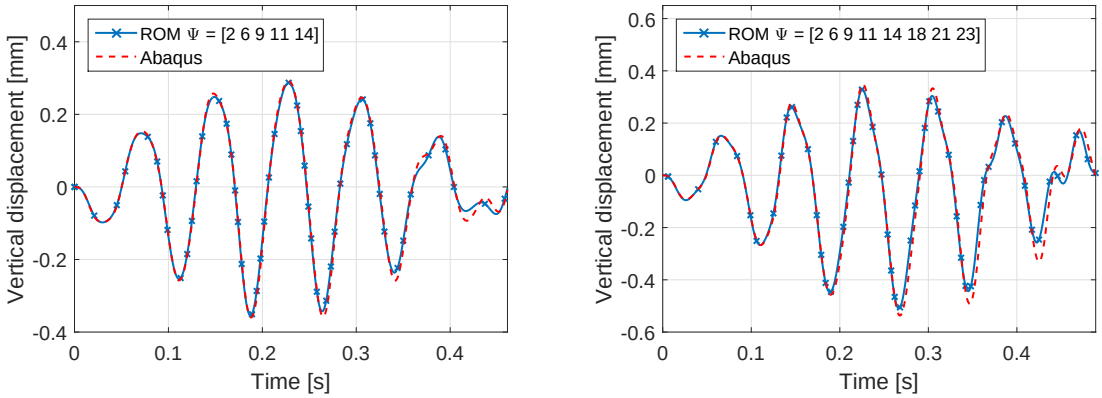

(a) Linear response **(b)** Nonlinear response

Figure 5.22: Forced undamped vibration of a simply supported shallow shell 1 mm thick

In Figure 5.23, the same example as the previous one is considered, however, the amplitude of the pressure load is increased to $\lambda = 10$ N/m^2 to demonstrate the performance of the ROM applied to shells, for larger loads. As expected the linear response is of the same shape as was the case in Figure 5.22a. The nonlinear response shows a very different behaviour in comparison to the lower load amplitude. Furthermore, it is seen that the ROM has difficulties to match Abaqus around 0.3 seconds. Attempts have been made to increase the number of modes to determine if a better agreement with Abaqus can be reached. However, the Matlab code is unable to cope with these large amounts of numbers and crashes. Overall, for the nonlinear response plots of the previous two examples, it can be stated that the ROM matches Abaqus quite well in first few cycles. However, larger errors in peak value occur as the time increases.

In the last example for the isotropic shallow shell, the thickness is increased to 4 mm. The load is of the same shape as the previous examples, however, $\lambda = 45$ N/m^2 and $\omega = 0.85\omega_1$. The vertical displacement at the center of the shell is plotted in Figure 5.24. The shape of both the linear and nonlinear response is similar. However, when comparing the linear and nonlinear case, it is observed that the softening type of nonlinearity is observed. Comparing the linear case of the ROM to Abaqus, a good agreement is found in the first few cycles. However, from 0.15 seconds and onward the peak values are slightly different. Remarkable is

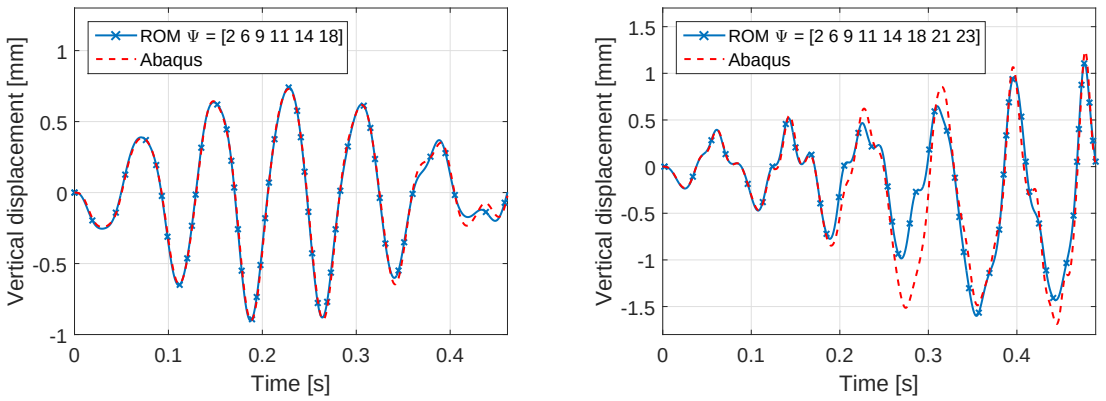

(a) Linear response **(b)** Nonlinear response

Figure 5.23: Forced undamped vibration of a simply supported shallow shell 1 mm thick

that the second beat of the ROM results appears to be the mirrored response of the first beat of the Abaqus results. This kind of behaviour has been found to be resolved by increasing the mesh density in Abaqus. However, increasing the mesh density more for this particular case leads to infeasible computational times.

For the nonlinear case a similar behaviour is observed. The first few cycles are in good agreement with Abaqus. Peak values are underestimated by the ROM. Again, the second beat of the ROM results appear to be mirrored to the first beat of the Abaqus results.

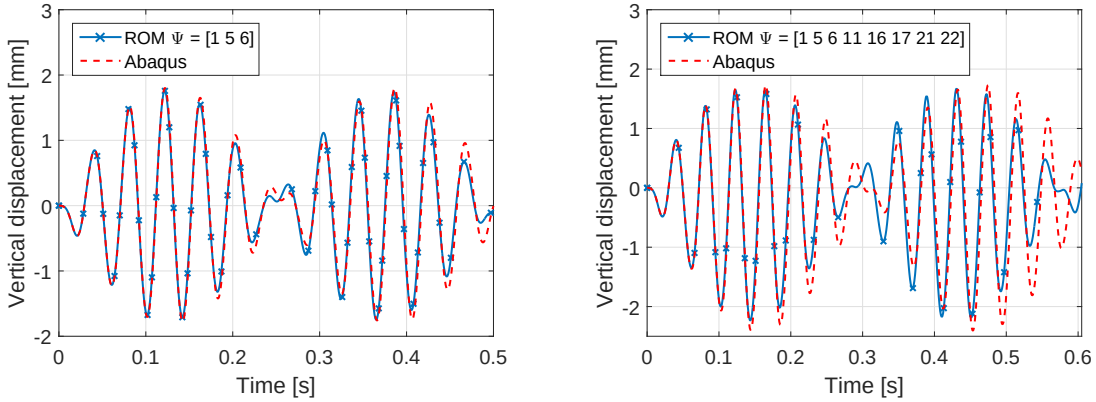

(a) Linear response **(b)** Nonlinear response

Figure 5.24: Forced undamped vibration of a simply supported shallow shell 4 mm thick

Response of a composite shell

In this last example, the ROM is applied to a composite cylindrical shallow shell. The shell is simply supported along all of its four edges. The material properties are borrowed from [44,49]. These are $E_L/E_T = 15.4$, $\nu_{LT} = 0.3$, $G_{LT}/E_T = 0.79$ an $\rho = 1630$ kg/m^3. The radius is given to be 10.695 [49], which is assumed to have the unit of meters. E_1 is assumed

to have the value 120.5 GPa, which is the same value as in the example of the composite plate in Section 5.2.1. In accordance with [49], the layup is selected to be a cross-ply. It is assumed to be symmetric cross-ply of eight layers with the stacking sequence $[90/0/90/0]_s$ and a total thickness of 1 mm. The load is applied on the outside (convex) part of the shell and is a uniform pressure load given by:

$$p = \lambda \sin(\omega t)$$

where $\lambda = 50$ N/m^2 and $\omega = 0.9\omega_1$.

Figure 5.25 shows the vertical displacement at the center of the shell for the linear and the nonlinear case of a forced undamped vibration. The agreement of the ROM with Abaqus is quite good for the linear case. However, after the maximum amplitude has been reached, the ROM has difficulties in capturing the peak values. Seven modes have been used in the basis. In the nonlinear case 11 modes are used in the basis and up to 0.055 seconds quite good agreement is observed between the ROM and Abaqus. Beyond this point, the shape of the response of the ROM follows that of Abaqus, however, the plots are offset from each other. The relatively large number of basis vectors result in high computational times, due to implementation of the code in Matlab (inefficient programming) and adding more basis vectors becomes infeasible. The addition of more basis vectors in the nonlinear case yielded an improvement of the results. It is noted that it has been attempted to have 11 basis vectors in the linear case as well. The results, however, did not improve compared to the case for 7 basis vectors.

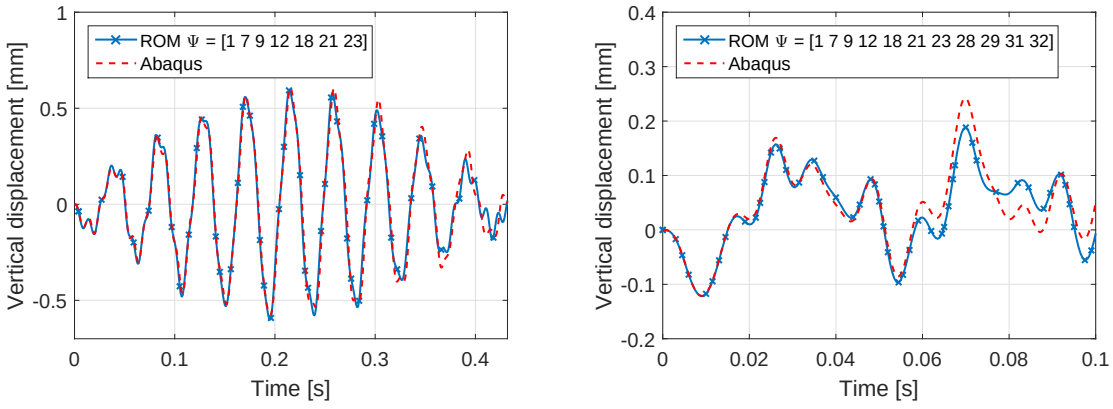

(a) Linear response **(b)** Nonlinear response

Figure 5.25: Forced undamped vibration of a simply supported composite shallow shell

5.4 Conclusion

In this chapter the reduced order model has been applied to beams, plates and shells. The ROM was used to analyse the response of a hinged-hinged beam. This was done for free vibrations, forced undamped vibrations and forced damped vibrations. The displacement results produced by the ROM are in nearly perfect agreement with results produced by

Abaqus. Additionally, the internal forces were compared for the forced undamped vibrations. Good agreement with Abaqus was observed. Noteworthy is that more modes were needed in the basis of the ROM to obtain agreement for the bending moments. A frequency ratio - amplitude plot was created using the ROM. These results were compared to that of some methods used in literature. A very good agreement was found.

In the second section the ROM was applied to simply supported plates for forced undamped vibrations. For the isotropic plate, a good agreement was found between the ROM and Abaqus in terms of displacement. Additionally, the stress resultants and moments were compared in a qualitative way through colour plots. Overall, the stress fields were similar. The quantitative comparison over time of the stress resultants at the center of the plate showed that the ROM results followed the general trend of Abaqus, but peak values of the ROM were lower. The addition more modes to the basis was not able to resolve this. The qualitative comparison of moments showed a good agreement, however, more modes were needed in the basis to obtain agreement as was also the case for beams. Application of the ROM to a composite plate showed fair agreement. Remarkable was that the nonlinear response was in better agreement than the linear response for the same number of modes in the basis. Additionally, the ROM was compared to literature. In terms of displacements the ROM was in good agreement with the presented literature. A period ratio - amplitude was created. Good agreement was found between several methods and the ROM.

Finally, the ROM was applied to isotropic and composite shells. For the isotropic shells, vertical displacements at the center of the shell followed the general trend of Abaqus, however, the agreements were not as good as was the case for beams and plates. Adding a relatively large number of modes in the basis did not improve the results. A similar behaviour was observed for the composite shell. For the nonlinear case a relatively large number of basis vectors were needed in the basis to obtain some agreement with Abaqus.

Overall, the large advantage of the ROM is the large decrease in computational time. For beams the computational times were of the order of seconds whereas Abaqus takes minutes. For plates the improvement in computational times was even more pronounced, with the ROM being 30 times faster or more, while retaining good accuracies. The shells, a high mesh density and a large number of basis vectors were needed to obtain some agreement with Abaqus. This yielded very high computational times due to the crude method of programming used in Matlab. More research is required to improve the ROM for shells.

Chapter 6

Conclusion

In this thesis, a Hamiltonian reduction method for nonlinear dynamics has been developed and applied. The method is an extension of the reduction method developed in [4] applicable to nonlinear static stability problems. The elements of this static reduction method, needed for the extension to dynamics, were presented in Chapter 2. In the static reduction method, a force subspace is defined as the span of predefined force vectors and is the product of a load matrix and an amplitude vector. The force vectors are called the perturbation loads. The pre-image of the force subspace is the displacement subspace, which is a nonlinear surface parametrised by a set of coordinates representing the displacement amplitudes. To simplify the nonlinearity, the force subspace is expanded in a Taylor series up to third order. The relationship between the displacement amplitudes and the load amplitudes represents the reduced order model. The reduction method for statics was based on the fact that the virtual work in the actual model must be equal to the virtual work in the reduced order model. The displacement was expanded in a Taylor series up to third order to derive three orthogonality conditions. In line with the displacement expansion, the load amplitude was expanded up to third order in terms of a reduced linear, quadratic and cubic operator. The static reduction method yields the two-dimensional, three-dimensional and four dimensional tensors, together with the first and second order displacement fields.

In Chapter 3 a review of Lagrangian and Hamiltonian mechanics and canonical transformations was given. The Hamiltonian is described in terms of a set of the position coordinates and the conjugate momenta, which are treated independently. The formulation describes the motion of a system in terms of $2n$ first order ordinary differential equations. These are the Hamilton's canonical equation of motion, which can be integrated. Furthermore, Hamilton's principle was derived in the Hamiltonian setting. It was used to derive the conditions that ensure a canonical transformation. If a transformation from one set of canonical coordinates to another is a canonical one, then the resulting system is also Hamiltonian. This fact is made use of in Chapter 4, where the reduced order model for nonlinear dynamics was derived. The essence of the model is based on the assumption that the lateral motion of a system (a beam or plate) can be described by a momentum subspace. In this thesis, it was assumed that the overall shape of the motion of the system is described by its eigenmodes (alternatively,

another suitable basis can be used). These are used in the momentum subspace, which is the product of a basis matrix and an amplitude vector. In nonlinear dynamics, the amplitude of the vibrations is finite and causes in-plane stretching of the structure. This is where the nonlinearity of the system is induced. The position of the system is expanded as a Taylor series of second order, in line with the static reduction method. Using the expansion for the displacement and the momentum subspace together with the conditions that ensure a canonical transformation, three constraint equations were derived. The equations were of identical form as those of the static reduction method. The dynamics was thus reduced to statics. The reduced order model for dynamics was constructed by computing a reduced Hamiltonian, which was then used in Hamilton's equations of motion. A reduced order model was derived for free vibrations, forced vibrations and damped vibrations. After integration, the amplitude and momentum of the reduced order model are substituted back into the displacement expansion and momentum subspace to obtain the response of the full finite element model. The chapter was completed with an elaboration on the finite element framework for beam and shell elements.

In Chapter 5, the reduced order model for dynamics was applied to beams, plates and shells. A comparison was made with Abaqus. For beams it was shown that good agreement is obtained in terms of displacements and internal forces. Furthermore, it was shown that by adding more modes in the basis of the ROM, the solution of the ROM approaches that of Abaqus. Additional modes were needed in the basis for the nonlinear case compared to the linear one. To obtain agreement for the bending moments, more modes were needed in the basis than for the case of displacements and axial forces. For plates, fairly good agreement with Abaqus was found. Displacements showed good agreement whereas stress resultants of the ROM reached lower peak values than Abaqus. To obtain agreement for the moments, again more modes were needed in the basis. Overall the stress fields looked similar to those of Abaqus. A comparison for beams and plates was done with literature for frequency ratio - amplitude and period ratio - amplitude, respectively. Very good agreement between various methods and the ROM was found. Additionally, the ROM for plates was compared to an approximate exact solution in terms of displacement, and here nearly spot on agreement was demonstrated. Lastly, the ROM was applied to shallow shells to compare vertical displacements. The results were less in quality compared to beams and plates. However, the ROM followed the general trend of the response plots of Abaqus.

The ROM for nonlinear dynamics has shown to be much faster than Abaqus, while retaining reasonable to good levels of accuracy. For beams it completed analyses within a few seconds, compared to minutes for Abaqus. For plates the ROM was at least 30 times faster. The existing reduction method developed in [2], required to add a large number of second order modes to the basis, to obtain accurate results. In the present thesis this is avoided, and having a relatively small number of modes in the basis already yields reasonable to good results. The new method is thus an extension of the static reduction method and an improvement of the reduction method for nonlinear dynamics based on the perturbation approach. The Hamiltonian reduction method for nonlinear dynamics allows one to save costly time.

Chapter 7

Recommendations

The reduction method presented in this thesis leaves room for extensions and improvements. These are elaborated upon in this chapter, together with recommendations on some of its potential applications.

It has been found that in the computation of the reduced tensors $\bar{\mathsf{L}}$, $\bar{\mathsf{Q}}$ and $\bar{\mathsf{C}}$ valuable time can be saved. Especially, the calculation of the four-dimensional reduced order tensor takes a relatively large proportion of the overall computational time of the code. This is because it is coded by means of four *for* loops. When adding more modes in the basis, the number of loops drastically increases. For systems with a small number of degrees of freedom, this does not cause issues. However, for systems with a large number of degrees of freedom, this results in unnecessarily long computational times. This can be improved by making use of the fact the the reduced tensors are symmetric in their indices for conservative systems. Of all permutations of each index, only one has to be computed and this value can be assigned to all other permutations of this index. Thus the computational times as presented in this thesis can be reduced further by means of smart coding.

In the expansion of the displacement up to second order, the nominal configuration was always assumed to be zero. More interesting dynamics can be studied by expanding about a different nominal configuration. For example, a nominal configuration near buckling can be chosen and one can study the dynamic behaviour of the system in the presence of buckling. This requires one to first perform a nonlinear static analysis preceding the application of the reduced order model for dynamics.

The damping model (Rayleigh damping) used in this thesis matches with that of Abaqus in linear analyses. However, for geometrically nonlinear analyses, Abaqus uses a more complicated damping model for the stiffness proportional part of damping. In the case of nonlinear analyses, the ROM in this thesis can only be compared to Abaqus for damped vibrations when mass proportional damping is considered. For future use, a more complicated damping model could be implemented such that the ROM can be compared to Abaqus in the case of nonlinear damped vibrations.

The materials used are limited to isotropic materials and symmetric composite laminates. In

future work one can extend this to the case of asymmetric laminates or even variable stiffness panels. Additionally, the work can be extended to include material nonlinearities as well.

Throughout the thesis the eigenmodes of the system have been used in the momentum subspace. Alternatively, the ROM allows one to use different vectors in the basis. One of these, as discussed in the literature review, can be the Ritz-Wilson vectors. Ritz-Wilson vectors take into account the shape of the load and could result in faster convergence and more accurate results. It is fully up to the user of the ROM to decide what type of basis is to be used.

The reduced order model was applied to beam and shell elements. These elements could be combined to create a hybrid structure. As an example, one can create a stiffened panel, where the panel is modelled using shell elements and the stringers are modelled by beam elements. Furthermore, it could be interesting to see how the ROM performs for larger structures. Using many beam elements, a tower could be built, or using the beam and shell elements together, full fuselage or wing panels could be modelled for instance. The reduced order model does not limit itself to the type of elements used in the present thesis. It could be applied in any finite element framework.

The aim the reduced order model is to save time while obtaining accurate solutions to problems of structural dynamics. The model is especially useful in problems where many iterative analyses are to be done. A typical example is a fatigue analysis. This type of analysis requires the application of many load cycles. The ROM allows to performs these analyses in a relatively short time. The effect of different load amplitudes on the performance of the structure, can be rapidly analysed. Another example is to obtain responses of a structure to random loadings. The ROM allows to quickly change the shape of the load, perform the analysis and extract the response. In this manner the average response of the structure to many random loads can be studied in a much faster fashion than by using a commercial finite element package.

Overall, the reduced order model can be applied to any field of engineering. One can think of analysing aircraft structures such as wing panels, or fuselage panels subject to gust or impact loads and structures for the automotive industry. Another example is structures subject to highly dynamic loads for the offshore industry, such as blast walls or the analysis of jackets that support topsides, which are subject to wave loads, wind loads or even earthquakes. The ROM allows to do many different analyses to eventually achieve the optimal design in a relatively short time.

References

[1] K. Liang, M. Abdalla, and Z. Gürdal. A Koiter-Newton approach for nonlinear structural analysis. *International Journal for Numerical Methods in Engineering*, 96(12):763–786, 2013.

[2] P. Tiso. *Finite element based reduction methods for static and dynamic analysis of thin-walled structures*. PhD thesis, TU Delft, Delft University of Technology, 2006.

[3] A.K. Noor. Recent advances and applications of reduction methods. *Applied Mechanics Reviews*, 47(5):125–146, 1994.

[4] K. Liang. *A Koiter-Newton arclength method for buckling-sensitive structures*. PhD thesis, TU Delft, Delft University of Technology, 2013.

[5] M.J. Patil and D.H. Hodges. On the importance of aerodynamic and structural geometrical nonlinearities in aeroelastic behavior of high-aspect-ratio wings. *Journal of Fluids and Structures*, 19(7):905–915, 2004.

[6] R. Palacios, J. Murua, and R. Cook. Structural and aerodynamic models in nonlinear flight dynamics of very flexible aircraft. *AIAA journal*, 48(11):2648–2659, 2010.

[7] V. Mukhopadhyay, J. Sobieszczanski-Sobieski, I. Kosaka, G. Quinn, and G.N. Vanderpaats. Analysis, design, and optimization of noncylindrical fuselage for blended-wing-body vehicle. *Journal of Aircraft*, 41(4):925–930, 2004.

[8] S.R. Idelsohn and A. Cardona. A reduction method for nonlinear structural dynamic analysis. *Computer Methods in Applied Mechanics and Engineering*, 49(3):253–279, 1985.

[9] N.F. Morris. The use of modal superposition in nonlinear dynamics. *Computers & Structures*, 7(1):65–72, 1977.

[10] P. Leger and E.L. Wilson. Modal summation methods for structural dynamic computations. *Earthquake engineering & structural dynamics*, 16(1):23–27, 1988.

[11] R.E. Cornwell, R.R. Craig, and C.P. Johnson. On the application of the mode-acceleration method to structural engineering problems. *Earthquake engineering & structural dynamics*, 11(5):679–688, 1983.

[12] H.L. Soriano and F. Venâncio Filho. On the modal acceleration method in structural dynamics. Mode truncation and static correction. *Computers & structures*, 29(5):777–782, 1988.

[13] V.N. Shah, G.J. Bohm, and A.N. Nahavandi. Modal superposition method for computationally economical nonlinear structural analysis. *Journal of Pressure Vessel Technology*, 101(2):134–141, 1979.

[14] E.L. Wilson, M-W. Yuan, and J.M. Dickens. Dynamic analysis by direct superposition of Ritz vectors. *Earthquake Engineering & Structural Dynamics*, 10(6):813–821, 1982.

[15] B.P. Jacob and N.F.F. Ebecken. Adaptive reduced integration method for nonlinear structural dynamic analysis. *Computers & structures*, 45(2):333–347, 1992.

[16] A. Przekop and S.A. Rizzi. Efficient modal basis selection criteria for reduced-order nonlinear simulation. In *Proceedings of the Seventh European Conference on Structural Dynamics*, 2008.

[17] B.F. Feeny. On proper orthogonal co-ordinates as indicators of modal activity. *Journal of Sound and Vibration*, 255(5):805–817, 2002.

[18] B.F. Feeny and R. Kappagantu. On the physical interpretation of proper orthogonal modes in vibrations. *Journal of sound and vibration*, 211(4):607–616, 1998.

[19] S.A. Rizzi and A. Przekop. System identification-guided basis selection for reduced-order nonlinear response analysis. *Journal of Sound and Vibration*, 315(3):467–485, 2008.

[20] M. Meyer and H.G. Matthies. Efficient model reduction in non-linear dynamics using the karhunen-loeve expansion and dual-weighted-residual methods. *Computational Mechanics*, 31(1-2):179–191, 2003.

[21] P. Krysl, S. Lall, and J.E. Marsden. Dimensional model reduction in non-linear finite element dynamics of solids and structures. *International Journal for numerical methods in engineering*, 51(4):479–504, 2001.

[22] J.J. Hollkamp, R.W. Gordon, and S.M. Spottswood. Nonlinear modal models for sonic fatigue response prediction: a comparison of methods. *Journal of Sound and Vibration*, 284(3):1145–1163, 2005.

[23] W.T. Koiter. *On the stability of the elastic equilibrium.* PhD thesis, Delft University of Technology, 1945.

[24] B. Budiansky. Dynamic buckling of elastic structures: criteria and estimates. *Dynamic stability of structures*, pages 83–106, 1966.

[25] E. Byskov and W. Hutchinson. Mode interaction in axially stiffened cylindrical shells. *AIAA Journal*, 15(7):941–948, 1977.

[26] L.W. Rehfield. Nonlinear free vibrations of elastic structures. *International Journal of Solids and Structures*, 9(5):581–590, 1973.

[27] J. Wedel-Heinen. Vibration of geometrically imperfect beam and shell structures. *International Journal of Solids and Structures*, 27(1):29–47, 1991.

[28] E.L. Jansen. A perturbation method for nonlinear vibrations of imperfect structures: application to cylindrical shell vibrations. *International Journal of Solids and Structures*, 45(3):1124–1145, 2008.

[29] P. Tiso and E. Jansen. A finite element based reduction method for nonlinear dynamics of structures. *Proceedings of the 46th AIAA/ASME/ASCE/AHS/ASC Structures, Structural Dynamics, and Materials Conference*, 2005.

[30] P. Tiso, E. Jansen, and M. Abdalla. A reduction method for finite element nonlinear dynamic analysis of shells. In *47th Structures, Structural Dynamics and Material Conference, Newport, Rhode Island*, 2006.

[31] A.K. Noor and J.M. Peters. Reduced basis technique for nonlinear analysis of structures. *AIAA journal*, 18(4):455–462, 1980.

[32] J.M.T. Thompson and A.C. Walker. The non-linear perturbation analysis of discrete structural systems. *International Journal of Solids and Structures*, 4(8):757–768, 1968.

[33] W. Greiner. *Classical Mechanics: Systems of Particles and Hamiltonian Dynamics*. Classical theoretical physics. Springer, 2009.

[34] H. Goldstein, C.P. Poole, and J.L. Safko. *Classical Mechanics*. Addison-Wesley, 3rd edition, 2002.

[35] L.N. Hand and J.D. Finch. *Analytical Mechanics*. Cambridge University Press, 1998.

[36] R.W. Clough and J. Penzien. *Dynamics of Structures*. Computers & Structures, Inc., 3rd edition, 2003.

[37] K. Modin and G. Söderlind. Geometric integration of Hamiltonian systems perturbed by Rayleigh damping. *BIT Numerical Mathematics*, 51(4):977–1007, 2011.

[38] C. Militello and C.A. Felippa. The first ANDES elements: 9-dof plate bending triangles. *Computer methods in applied mechanics and engineering*, 93(2):217–246, 1991.

[39] K. Alvin, M. Horacio, B. Haugen, and C.A. Felippa. Membrane triangles with corner drilling freedoms-I. The EFF element. *Finite Elements in Analysis and Design*, 12(3):163–187, 1992.

[40] S.R.R. Pillai and B.N. Rao. On nonlinear free vibrations of simply supported uniform beams. *Journal of sound and vibration*, 159(3):527–531, 1992.

[41] M. Sathyamoorthy. *Nonlinear Analysis of Structures*, volume 8. CRC Press, 1997.

[42] J.D. Ray and C.W. Bert. Nonlinear vibrations of a beam with pinned ends. *Journal of Manufacturing Science and Engineering*, 91(4):997–1004, 1969.

[43] E. Ventsel and T. Krauthammer. *Thin plates and shells: theory: analysis, and applications*. CRC press, 2001.

[44] W. Han and M. Petyt. Geometrically nonlinear vibration analysis of thin, rectangular plates using the hierarchical finite element method-ii: 1st mode of laminated plates and higher modes of isotropic and laminated plates. *Computers & structures*, 63(2):309–318, 1997.

[45] N. Yamaki. Influence of large amplitudes on flexural vibrations of elastic plates. *ZAMM-Journal of Applied Mathematics and Mechanics/Zeitschrift für Angewandte Mathematik und Mechanik*, 41(12):501–510, 1961.

[46] S. Timoshenko and D.H. Young. *Vibration Problems in Engineering*. D. Van Nostrand Company, Inc., 3rd edition, 1955.

[47] H.N. Chu and G. Herrmann. Influences of large amplitudes on free flexural vibrations of rectangular plates. *Journal of Applied Mechanics*, 3:532–540, 1956.

[48] T. Wah. Large amplitude flexural vibration of rectangular plates. *International Journal of Mechanical Sciences*, 5(6):425–438, 1963.

[49] K.A. Alhazza. *Nonlinear Vibrations of Doubly Curved Cross-Ply Shallow Shells*. PhD thesis, Virginia Polytechnic Institute and State University, 2002.

[50] C. Felippa. Introduction to Finite Element Methods (ASEN 5007) Fall 2015, Department of Aerospace Engineering Sciences , University of Colorado at Boulder. http://www.colorado.edu/engineering/CAS/courses.d/IFEM.d/. Accessed: 28-07-2015.

Appendix A

Derivations

A.1 Hamilton's principle

D'Alembert's principle for a set of particles states:

$$\sum_i (\mathbf{F}_i - m\ddot{\mathbf{x}}_i)\delta\mathbf{x} = \mathbf{0} \tag{A.1}$$

For convenience this is rewritten as:

$$\sum_i \mathbf{F}_i \cdot \delta\mathbf{x}_i - \sum_i m_i\ddot{\mathbf{x}}_i \cdot \delta\mathbf{x}_i = \mathbf{0} \tag{A.2}$$

One can write:

$$\begin{aligned} \ddot{\mathbf{x}}_i \cdot \delta\mathbf{x}_i &= \ddot{\mathbf{x}}_i \cdot \delta\mathbf{x}_i + \dot{\mathbf{x}}_i \cdot \delta\dot{\mathbf{x}}_i - \dot{\mathbf{x}}_i \cdot \delta\dot{\mathbf{x}}_i \\ &= \frac{\mathrm{d}}{\mathrm{d}t}\left(\dot{\mathbf{x}}_i \cdot \delta\mathbf{x}_i\right) - \dot{\mathbf{x}}_i \cdot \delta\dot{\mathbf{x}}_i \end{aligned} \tag{A.3}$$

Substituting Equation A.3 into Equation A.2 yields:

$$\sum_i \mathbf{F}_i \cdot \delta\mathbf{x}_i + \sum_i (m_i\dot{\mathbf{x}}_i) \cdot \delta\mathbf{x}_i - \sum_i m_i \cdot \frac{\mathrm{d}}{\mathrm{d}t}\left(\dot{\mathbf{x}}_i \cdot \delta\mathbf{x}_i\right) = \mathbf{0} \tag{A.4}$$

This equation represents the principle of virtual work for dynamics. Integrating between two time instances t_1 and t_2 gives:

$$\begin{aligned}
\int_{t_1}^{t_2} \sum_i \mathbf{F}_i \cdot \delta\mathbf{x}_i \mathrm{d}t + \int_{t_1}^{t_2} \sum_i (m_i \dot{\mathbf{x}}_i) \cdot \delta\mathbf{x}_i \mathrm{d}t - \int_{t_1}^{t_2} \sum_i m_i \cdot \frac{d}{dt} (\dot{\mathbf{x}}_i \cdot \delta\mathbf{x}_i)\, \mathrm{d}t = \mathbf{0} \\
\int_{t_1}^{t_2} \sum_i \mathbf{F}_i \cdot \delta\mathbf{x}_i \mathrm{d}t + \int_{t_1}^{t_2} \sum_i (m_i \dot{\mathbf{x}}_i) \cdot \delta\mathbf{x}_i \mathrm{d}t - \sum_i m_i \cdot (\dot{\mathbf{x}}_i \cdot \delta\mathbf{x}_i) \Big|_{t_1}^{t_2} = \mathbf{0} \\
\int_{t_1}^{t_2} \sum_i \mathbf{F}_i \cdot \delta\mathbf{x}_i \mathrm{d}t + \int_{t_1}^{t_2} \sum_i (m_i \dot{\mathbf{x}}_i) \cdot \delta\mathbf{x}_i \mathrm{d}t = \mathbf{0}
\end{aligned} \tag{A.5}$$

By Hamilton's principle the last term of Equation A.5 is equal to zero. The force is derivable from a scalar potential V:

$$\mathbf{F}_i = -\frac{\partial V}{\partial \mathbf{x}_i} \tag{A.6}$$

The kinetic energy T is defined as:

$$T = \frac{m_i}{2} \dot{\mathbf{x}}_i \cdot \dot{\mathbf{x}}_i \tag{A.7}$$

When taking the variation, this becomes:

$$\delta T = m_i \dot{\mathbf{x}}_i \cdot \delta\dot{\mathbf{x}}_i \tag{A.8}$$

Substituting Equation A.6 and Equation A.8 into Equation A.5 gives:

$$\int_{t_1}^{t_2} -\delta V \, \mathrm{d}t + \int_{t_1}^{t_2} \delta T \, \mathrm{d}t = 0 \tag{A.9}$$

which finally leads to Hamilton's principle:

$$\begin{aligned}
\int_{t_1}^{t_2} \delta(T - V) \mathrm{d}t = 0 \\
\int_{t_1}^{t_2} \delta L \, \mathrm{d}t = 0
\end{aligned} \tag{A.10}$$

A.2 Conditions for a canonical transformation

This section contains the derivations for the conditions that ensure a canonical transformation. The derivation is initially performed using index notation, after which the matrix notation is introduced. The following transformation is adopted:

$$q_i = q_i(\boldsymbol{\xi}, \boldsymbol{\pi}) \tag{A.11a}$$

$$p_i = p_i(\boldsymbol{\xi}, \boldsymbol{\pi}) \tag{A.11b}$$

Computing the derivatives $\dot{q}_i$ and $\dot{p}_i$:

$$\dot{q}_i = \frac{\partial q_i}{\partial \xi_j}\dot{\xi}_j + \frac{\partial q_i}{\partial \pi_j}\dot{\pi}_j \tag{A.12a}$$

$$\dot{p}_i = \frac{\partial p_i}{\partial \xi_l}\dot{\xi}_l + \frac{\partial p_i}{\partial \pi_l}\dot{\pi}_l \tag{A.12b}$$

From which one can write:

$$\begin{aligned}\dot{p}_i \cdot \delta q_i - \dot{q}_i \cdot \delta p_i = &\left(\frac{\partial p_i}{\partial \xi_l}\dot{\xi}_l + \frac{\partial p_i}{\partial \pi_l}\dot{\pi}_l\right) \cdot \left(\frac{\partial q_i}{\partial \xi_j}\delta\xi_j + \frac{\partial q_i}{\partial \pi_j}\delta\pi_j\right) - \\ &\left(\frac{\partial q_i}{\partial \xi_j}\dot{\xi}_j + \frac{\partial q_i}{\partial \pi_j}\dot{\pi}_j\right) \cdot \left(\frac{\partial p_i}{\partial \xi_l}\delta\xi_l + \frac{\partial p_i}{\partial \pi_l}\delta\pi_l\right)\end{aligned} \tag{A.13}$$

Expanding the brackets:

$$\begin{aligned}\dot{p}_i \cdot \delta q_i - \dot{q}_i \cdot \delta p_i = &\frac{\partial p_i}{\partial \xi_l} \cdot \frac{\partial q_i}{\partial \xi_j}\dot{\xi}_l \cdot \delta\xi_j + \frac{\partial p_i}{\partial \xi_l} \cdot \frac{\partial q_i}{\partial \pi_j}\dot{\xi}_l \cdot \delta\pi_j + \\ &\frac{\partial p_i}{\partial \pi_l} \cdot \frac{\partial q_i}{\partial \xi_j}\dot{\pi}_l \cdot \delta\xi_j + \frac{\partial p_i}{\partial \pi_l} \cdot \frac{\partial q_i}{\partial \pi_j}\dot{\pi}_l \cdot \delta\pi_j - \\ &\frac{\partial q_i}{\partial \xi_j} \cdot \frac{\partial p_i}{\partial \xi_l}\dot{\xi}_j \cdot \delta\xi_l - \frac{\partial q_i}{\partial \xi_j} \cdot \frac{\partial p_i}{\partial \pi_l}\dot{\xi}_j \cdot \delta\pi_l - \\ &\frac{\partial q_i}{\partial \pi_j} \cdot \frac{\partial p_i}{\partial \xi_l}\dot{\pi}_j \cdot \delta\xi_l - \frac{\partial q_i}{\partial \pi_j} \cdot \frac{\partial p_i}{\partial \pi_l}\dot{\pi}_j \cdot \delta\pi_l\end{aligned} \tag{A.14}$$

Terms are grouped:

$$\begin{aligned}\dot{p}_i \cdot \delta q_i - \dot{q}_i \cdot \delta p_i = &\left(\frac{\partial p_i}{\partial \xi_l} \cdot \frac{\partial q_i}{\partial \xi_j} - \frac{\partial q_i}{\partial \xi_l} \cdot \frac{\partial p_i}{\partial \xi_j}\right) \cdot \dot{\xi}_l \cdot \delta\xi_j + \\ &\left(\frac{\partial p_i}{\partial \pi_l} \cdot \frac{\partial q_i}{\partial \pi_j} - \frac{\partial q_i}{\partial \pi_l} \cdot \frac{\partial p_i}{\partial \pi_j}\right) \cdot \dot{\pi}_l \cdot \delta\pi_j + \\ &\left(\frac{\partial p_i}{\partial \xi_l} \cdot \frac{\partial q_i}{\partial \pi_j} - \frac{\partial q_i}{\partial \xi_l} \cdot \frac{\partial p_i}{\partial \pi_j}\right) \cdot \dot{\xi}_l \cdot \delta\pi_j + \\ &\left(\frac{\partial p_i}{\partial \pi_l} \cdot \frac{\partial q_i}{\partial \xi_j} - \frac{\partial q_i}{\partial \pi_l} \cdot \frac{\partial p_i}{\partial \xi_j}\right) \cdot \dot{\pi}_l \cdot \delta\xi_j\end{aligned} \tag{A.15}$$

$$\begin{aligned}\dot{p}_i \cdot \delta q_i - \dot{q}_i \cdot \delta p_i = &\left(\frac{\partial p_i}{\partial \xi_l} \cdot \frac{\partial q_i}{\partial \xi_j} - \frac{\partial q_i}{\partial \xi_l} \cdot \frac{\partial p_i}{\partial \xi_j}\right) \cdot \dot{\xi}_l \cdot \delta\xi_j + \\ &\left(\frac{\partial p_i}{\partial \pi_l} \cdot \frac{\partial q_i}{\partial \pi_j} - \frac{\partial q_i}{\partial \pi_l} \cdot \frac{\partial p_i}{\partial \pi_j}\right) \cdot \dot{\pi}_l \cdot \delta\pi_j + \\ &\left(\frac{\partial q_i}{\partial \xi_l} \cdot \frac{\partial p_i}{\partial \pi_j} - \frac{\partial p_i}{\partial \xi_l} \cdot \frac{\partial q_i}{\partial \pi_j}\right) \cdot \left(\dot{\pi}_j \cdot \delta\xi_l - \dot{\xi}_l \cdot \delta\pi_j\right)\end{aligned} \tag{A.16}$$

The following ordering for the matrix notation is introduced:

$$\frac{\partial \mathbf{p}}{\partial \boldsymbol{\xi}} = \begin{pmatrix} \frac{\partial p_1}{\partial \xi_1} & \frac{\partial p_1}{\partial \xi_2} & \cdots & \frac{\partial p_1}{\partial \xi_l} \\ \frac{\partial p_2}{\partial \xi_1} & \frac{\partial p_2}{\partial \xi_2} & \cdots & \frac{\partial p_2}{\partial \xi_l} \\ \vdots & \vdots & \ddots & \vdots \\ \frac{\partial p_i}{\partial \xi_1} & \frac{\partial p_i}{\partial \xi_2} & \cdots & \frac{\partial p_i}{\partial \xi_l} \end{pmatrix}$$

One can write:

$$\begin{aligned} \dot{p}_i \cdot \delta q_i - \dot{q}_i \cdot \delta p_i = & \left[\left(\frac{\partial \mathbf{p}}{\partial \boldsymbol{\xi}} \right)_{il} \cdot \left(\frac{\partial \mathbf{q}}{\partial \boldsymbol{\xi}} \right)_{ij} - \left(\frac{\partial \mathbf{q}}{\partial \boldsymbol{\xi}} \right)_{il} \cdot \left(\frac{\partial \mathbf{p}}{\partial \boldsymbol{\xi}} \right)_{ij} \right] \cdot \dot{\xi}_l \cdot \delta \xi_j + \\ & \left[\left(\frac{\partial \mathbf{p}}{\partial \boldsymbol{\pi}} \right)_{il} \cdot \left(\frac{\partial \mathbf{q}}{\partial \boldsymbol{\pi}} \right)_{ij} - \left(\frac{\partial \mathbf{q}}{\partial \boldsymbol{\pi}} \right)_{il} \cdot \left(\frac{\partial \mathbf{p}}{\partial \boldsymbol{\pi}} \right)_{ij} \right] \cdot \dot{\pi}_l \cdot \delta \pi_j + \\ & \left[\left(\frac{\partial \mathbf{q}}{\partial \boldsymbol{\xi}} \right)_{il} \cdot \left(\frac{\partial \mathbf{p}}{\partial \boldsymbol{\pi}} \right)_{ij} - \left(\frac{\partial \mathbf{p}}{\partial \boldsymbol{\xi}} \right)_{il} \cdot \left(\frac{\partial \mathbf{q}}{\partial \boldsymbol{\pi}} \right)_{ij} \right] \cdot \left(\dot{\pi}_j \cdot \delta \xi_l - \dot{\xi}_l \cdot \delta \pi_j \right) \end{aligned} \tag{A.17}$$

In matrix form:

$$\begin{aligned} \dot{\mathbf{p}}^t \delta \mathbf{q} - \dot{\mathbf{q}}^t \delta \mathbf{p} = & \left[\left(\frac{\partial \mathbf{p}}{\partial \boldsymbol{\xi}} \right)^t \cdot \left(\frac{\partial \mathbf{q}}{\partial \boldsymbol{\xi}} \right) - \left(\frac{\partial \mathbf{q}}{\partial \boldsymbol{\xi}} \right)^t \cdot \left(\frac{\partial \mathbf{p}}{\partial \boldsymbol{\xi}} \right) \right] \cdot \dot{\boldsymbol{\xi}}^t \delta \boldsymbol{\xi} + \\ & \left[\left(\frac{\partial \mathbf{p}}{\partial \boldsymbol{\pi}} \right)^t \cdot \left(\frac{\partial \mathbf{q}}{\partial \boldsymbol{\pi}} \right) - \left(\frac{\partial \mathbf{q}}{\partial \boldsymbol{\pi}} \right)^t \cdot \left(\frac{\partial \mathbf{p}}{\partial \boldsymbol{\pi}} \right) \right] \cdot \dot{\boldsymbol{\pi}}^t \delta \boldsymbol{\pi} + \\ & \left[\left(\frac{\partial \mathbf{q}}{\partial \boldsymbol{\xi}} \right)^t \cdot \left(\frac{\partial \mathbf{p}}{\partial \boldsymbol{\pi}} \right) - \left(\frac{\partial \mathbf{p}}{\partial \boldsymbol{\xi}} \right)^t \cdot \left(\frac{\partial \mathbf{q}}{\partial \boldsymbol{\pi}} \right) \right] \cdot \left(\dot{\boldsymbol{\pi}}^t \delta \boldsymbol{\xi} - \dot{\boldsymbol{\xi}}^t \delta \boldsymbol{\pi} \right) \end{aligned} \tag{A.18}$$

This yields the final conditions that ensure a canonical transformation, in matrix form:

$$\left[\left(\frac{\partial \mathbf{p}}{\partial \boldsymbol{\xi}} \right)^t \cdot \left(\frac{\partial \mathbf{q}}{\partial \boldsymbol{\xi}} \right) - \left(\frac{\partial \mathbf{q}}{\partial \boldsymbol{\xi}} \right)^t \cdot \left(\frac{\partial \mathbf{p}}{\partial \boldsymbol{\xi}} \right) \right] = \mathbf{0} \tag{A.19a}$$

$$\left[\left(\frac{\partial \mathbf{p}}{\partial \boldsymbol{\pi}} \right)^t \cdot \left(\frac{\partial \mathbf{q}}{\partial \boldsymbol{\pi}} \right) - \left(\frac{\partial \mathbf{q}}{\partial \boldsymbol{\pi}} \right)^t \cdot \left(\frac{\partial \mathbf{p}}{\partial \boldsymbol{\pi}} \right) \right] = \mathbf{0} \tag{A.19b}$$

$$\left[\left(\frac{\partial \mathbf{q}}{\partial \boldsymbol{\xi}} \right)^t \cdot \left(\frac{\partial \mathbf{p}}{\partial \boldsymbol{\pi}} \right) - \left(\frac{\partial \mathbf{p}}{\partial \boldsymbol{\xi}} \right)^t \cdot \left(\frac{\partial \mathbf{q}}{\partial \boldsymbol{\pi}} \right) \right] = \mathbf{I} \tag{A.19c}$$

Appendix B

Finite Element Expressions

B.1 Beam element

B.1.1 Shape functions

The shape functions used for the beam element are given by [2, 50]:

$$\begin{cases} N_{u_1} = \frac{1}{2}(1-\xi) \\ N_{u_2} = \frac{1}{2}(1+\xi) \\ N_{w_1} = \frac{1}{4}(1-\xi)^2(2+\xi) \\ N_{w_2} = \frac{1}{4}(1+\xi)^2(2-\xi) \\ N_{\theta_1} = \frac{1}{8}L(1-\xi)^2(1+\xi) \\ N_{\theta_2} = -\frac{1}{8}L(1+\xi)^2(1-\xi) \end{cases} \tag{B.1}$$

B.1.2 Strain and curvature expressions

The explicit expressions for the axial strain and curvature are defined as [4]:

$$\begin{aligned} \epsilon = \frac{1}{L}\int_0^L \left(u_{,x} + \frac{1}{2}w_{,x}^2\right) \mathrm{d}x = \\ \frac{1}{L}(u_2-u_1) + \frac{1}{2}\left[\frac{6}{5L^2}(w_1-w_2)^2 + \frac{2}{15}(\theta_1-\theta_2)^2 + \frac{1}{5}\theta_1\theta_2 + \frac{1}{5L}(\theta_1+\theta_2)(w_1-w_2)\right] \end{aligned} \tag{B.2}$$

$$\chi = w_{,xx} = -\frac{1}{L^2}\left[3w_1 - 3w_2 - \frac{6w_1x}{L} + \frac{6w_2x}{L} + (2L-3x)\theta_1 + (L-3x)\theta_2\right] \tag{B.3}$$

B.1.3 Derivatives of axial strain

The **b** vector and **s** matrix are defined as [4]:

$$\mathbf{b} = \frac{\partial \epsilon}{\partial q} = \begin{bmatrix} -\frac{1}{L} \\ \frac{6}{5L^2}(w_1 - w_2) + \frac{1}{10L}(\theta_1 + \theta_2) \\ \frac{2}{15}(\theta_1 - \theta_2) + \frac{1}{10}\theta_2 + \frac{1}{10L}(w_1 - w_2) \\ \frac{1}{L} \\ -\frac{6}{5L^2}(w_1 - w_2) - \frac{1}{10L}(\theta_1 + \theta_2) \\ -\frac{2}{15}(\theta_1 - \theta_2) + \frac{1}{10}\theta_1 + \frac{1}{10L}(w_1 - w_2) \end{bmatrix} \tag{B.4}$$

$$\mathsf{s} = \frac{\partial^2 \epsilon}{\partial q^2} = \begin{bmatrix} 0 & 0 & 0 & 0 & 0 & 0 \\ 0 & \frac{6}{5L^2} & \frac{1}{10L} & 0 & -\frac{6}{5L^2} & \frac{1}{10L} \\ 0 & \frac{1}{10L} & \frac{2}{15} & 0 & -\frac{1}{10L} & -\frac{1}{30} \\ 0 & 0 & 0 & 0 & 0 & 0 \\ 0 & -\frac{6}{5L^2} & -\frac{1}{10L} & 0 & \frac{6}{5L^2} & -\frac{1}{10L} \\ 0 & \frac{1}{10L} & -\frac{1}{30} & 0 & -\frac{1}{10L} & \frac{2}{15} \end{bmatrix} \tag{B.5}$$

B.2 Shell element

B.2.1 Geometric coordinates and element area

For the three-node triangular flat shell element the nodal geometric coordinates (x_1, y_1), (x_2, y_2), and (x_3, y_3) are defined as:

$$x_{ij} = x_i - x_j \tag{B.6}$$

$$y_{ij} = y_i - y_j \tag{B.7}$$

with $i, j = 1, 2, 3$. Using these coordinates the element area is calculated from:

$$\mathcal{A} = \frac{y_{21}x_{13} - x_{21}y_{13}}{2} \tag{B.8}$$

B.2.2 Linear strain-displacement matrix

The linear strain-displacement matrix B_l, is obtained from [39], and is defined by:

$$\mathsf{B}_l = \frac{1}{2\mathcal{A}} \begin{bmatrix} \mathsf{B}_1 & \mathsf{B}_2 & \mathsf{B}_3 \end{bmatrix} \tag{B.9}$$

with

$$\mathsf{B}_1 = \begin{bmatrix} y_{23} & 0 & & \frac{y_{23}(y_{13}-y_{21})}{6} \\ 0 & x_{23} & [\mathbf{0}]_{3\times 3} & \frac{x_{32}(x_{32}-x_{12})}{6} \\ x_{32} & y_{23} & & \frac{x_{31}y_{13}-x_{12}y_{21}}{3} \end{bmatrix} \tag{B.10}$$

$$\mathsf{B}_2 = \begin{bmatrix} y_{31} & 0 & & \frac{y_{31}(y_{21}-y_{32})}{6} \\ 0 & x_{13} & [\mathbf{0}]_{3\times 3} & \frac{x_{13}(x_{12}-x_{23})}{6} \\ x_{13} & y_{31} & & \frac{x_{12}y_{21}-x_{23}y_{32}}{3} \end{bmatrix} \tag{B.11}$$

$$\mathsf{B}_3 = \begin{bmatrix} y_{12} & 0 & & \frac{y_{12}(y_{32}-y_{13})}{6} \\ 0 & x_{21} & [\mathbf{0}]_{3\times 3} & \frac{x_{21}(x_{23}-x_{31})}{6} \\ x_{21} & y_{12} & & \frac{x_{23}y_{32}-x_{31}y_{13}}{3} \end{bmatrix} \tag{B.12}$$

B.2.3 Isoparametric coordinates

The triangular coordinates system is introduced for which holds [2, 50]:

$$\zeta_1 + \zeta_2 + \zeta_3 = 1 \tag{B.13}$$

The relation between the Cartesian coordinate system and the isoparametric coordinates is given by:

$$\begin{bmatrix} 1 \\ x \\ y \end{bmatrix} = \begin{bmatrix} 1 & 1 & 1 \\ x_1 & x_2 & x_3 \\ y_1 & y_2 & y_3 \end{bmatrix} \begin{bmatrix} \zeta_1 \\ \zeta_2 \\ \zeta_3 \end{bmatrix} \tag{B.14}$$

The relation between the partial derivatives in the Cartesian coordinate system and the isoparametric coordinate system then becomes:

$$\begin{bmatrix} \frac{\partial}{\partial x} \\ \frac{\partial}{\partial y} \end{bmatrix} = \begin{bmatrix} \mathbf{T}_x \\ \mathbf{T}_y \end{bmatrix} \begin{bmatrix} \frac{\partial}{\partial \zeta_1} \\ \frac{\partial}{\partial \zeta_2} \\ \frac{\partial}{\partial \zeta_3} \end{bmatrix} \tag{B.15}$$

in which:

$$\mathbf{T}_x = \frac{1}{2\mathcal{A}} \begin{bmatrix} y_{23} & y_{31} & y_{12} \end{bmatrix} \tag{B.16}$$

$$\mathbf{T}_y = \frac{1}{2\mathcal{A}} \begin{bmatrix} x_{32} & x_{13} & x_{21} \end{bmatrix} \tag{B.17}$$

B.2.4 Shape functions

The displacements components u, v and w are interpolated using linear shape functions given as [2]:

$$\begin{bmatrix} u \\ v \\ w \end{bmatrix} = \begin{bmatrix} \zeta_1 & 0 & 0 & & \zeta_2 & 0 & 0 & & \zeta_3 & 0 & 0 & \\ 0 & \zeta_1 & 0 & [\mathbf{0}]_{3\times3} & 0 & \zeta_2 & 0 & [\mathbf{0}]_{3\times3} & 0 & \zeta_3 & 0 & [\mathbf{0}]_{3\times3} \\ 0 & 0 & \zeta_1 & & 0 & 0 & \zeta_2 & & 0 & 0 & \zeta_3 & \end{bmatrix} \mathbf{q} \tag{B.18}$$

B.2.5 Constant matrices

The constant matrices K_{xx}, ,K_{yy} and K_{xy} used to form the B_{nl}, are finally defined as [2]:

$$\mathsf{K}_{xx} = \mathbf{B}_w^t \mathbf{T}_x^t \mathbf{T}_x \mathbf{B}_w + \mathbf{B}_v^t \mathbf{T}_x^t \mathbf{T}_x \mathbf{B}_v \tag{B.19}$$

$$\mathsf{K}_{yy} = \mathbf{B}_w^t \mathbf{T}_y^t \mathbf{T}_y \mathbf{B}_w + \mathbf{B}_u^t \mathbf{T}_x^t \mathbf{T}_x \mathbf{B}_u \tag{B.20}$$

$$\mathsf{K}_{xy} = \mathbf{B}_w^t \left(\mathbf{T}_x^t \mathbf{T}_y + \mathbf{T}_y^t \mathbf{T}_x \right) \mathbf{B}_w \tag{B.21}$$

with:

$$\mathbf{B}_w = \begin{bmatrix} 0 & 0 & 1 & 0 & 0 & 0 & 0 & 0 & 0 & 0 & 0 & 0 & 0 & 0 & 0 & 0 & 0 & 0 \\ 0 & 0 & 0 & 0 & 0 & 0 & 0 & 0 & 1 & 0 & 0 & 0 & 0 & 0 & 0 & 0 & 0 & 0 \\ 0 & 0 & 0 & 0 & 0 & 0 & 0 & 0 & 0 & 0 & 0 & 0 & 0 & 0 & 1 & 0 & 0 & 0 \end{bmatrix} \tag{B.22}$$

$$\mathbf{B}_u = \begin{bmatrix} 1 & 0 & 0 & 0 & 0 & 0 & 0 & 0 & 0 & 0 & 0 & 0 & 0 & 0 & 0 & 0 & 0 & 0 \\ 0 & 0 & 0 & 0 & 0 & 0 & 1 & 0 & 0 & 0 & 0 & 0 & 0 & 0 & 0 & 0 & 0 & 0 \\ 0 & 0 & 0 & 0 & 0 & 0 & 0 & 0 & 0 & 0 & 0 & 0 & 1 & 0 & 0 & 0 & 0 & 0 \end{bmatrix} \tag{B.23}$$

$$\mathbf{B}_v = \begin{bmatrix} 0 & 1 & 0 & 0 & 0 & 0 & 0 & 0 & 0 & 0 & 0 & 0 & 0 & 0 & 0 & 0 & 0 & 0 \\ 0 & 0 & 0 & 0 & 0 & 0 & 0 & 1 & 0 & 0 & 0 & 0 & 0 & 0 & 0 & 0 & 0 & 0 \\ 0 & 0 & 0 & 0 & 0 & 0 & 0 & 0 & 0 & 0 & 0 & 0 & 0 & 1 & 0 & 0 & 0 & 0 \end{bmatrix} \tag{B.24}$$